TÉCNICO LISBOA

Hydrogen based solutions to help electrical grid management

Application to the Terceira Island case

Luiz Carlos Santos de Jesus

Thesis to obtain the Master of Science Degree in

Energy Engineering and Management

Supervisor: Prof. Rui Manuel Gameiro de Castro

Examination Committee

Chairperson: Prof. Edgar Caetano Fernandes

Supervisor: Prof. Rui Manuel Gameiro de Castro

Member of the Committee: Dr. António Setas Lopes

December 2021

I declare that this document is an original work of my own authorship and that it fulfils all the requirements of the Code of Conduct and Good Practices of the *Universidade de Lisboa*.

To my mother, Roberta Santos.

Acknowledgements

Tomo esta chance para reconhecer e profundamente agradecer à Direção-Geral do Ensino Superior por me terem garantido bolsas de estudo sem as quais possivelmente não conseguiria ter continuado o meu percurso académico.

Gostaria de agradecer também ao meu supervisor, professor Rui Castro, pelo acompanhamento que fez ao longo deste processo, o seu feedback honesto e prático, e o seu empenho em auxiliar-me.

Agradeço à minha companheira Inês que partilhou estes anos comigo, inspirando o melhor de mim, e, acima de tudo, agradeço a toda a minha família, Roberta, Rogéria, Marli, Carlos e Nilda, por todo o apoio que me deram e todo o trabalho que tiveram para que conseguisse construir o meu caminho e chegar aqui.

Abstract

The need for decarbonization has become an urgent objective being pursued across borders and sectors. The energy sector has been one example to follow, with the penetrations of renewable energy sources increasing year after year and already having an impact on carbon emissions. Despite their benefits, as these penetration levels grow, grid stability has been affected. Part of this instability is caused by the different type of connection to the grid used by most renewable energy sources. These converter connected technologies do not contribute to the grid's inertia the same way synchronous generators do.

Focusing on the behaviour of the system's frequency, a Matlab/Simulink based model of the Portuguese Terceira Island is created to assess the potential benefits of using hydrogen technologies to provide grid services. Two different scenarios are analyzed, the system's frequency response to large imbalances and to steady-state imbalances stemming from load and wind power forecasting errors. The results reflect on how the frequency behaviour is affected by the amount of system's inertia, synchronous generators characteristics and the presence of electrolyzers and fuel cells, with new metrics being introduced to compare the frequency's reaction to each.

Keywords

Renewable Energy Sources; Hydrogen Technologies; Frequency Control; Large imbalances; Steady-state imbalances

Resumo

A necessidade de descarbonização tornou-se um objetivo urgente a ser perseguido, transcendendo fronteiras e setores. O setor de energia tem sido um exemplo a seguir, com a penetração de fontes de energia renovável aumentando ano após ano e já tendo um impacto nas emissões de carbono. Apesar de seus benefícios, à medida que esses níveis de penetração vêm aumentando, a estabilidade da rede elétrica tem sido afetada. Parte dessa instabilidade é causada pelos diferentes tipos de conexão à rede usados pela maioria das fontes de energia renováveis. Estas tecnologias conectadas por conversores não contribuem para a inércia da rede como fazem os geradores síncronos.

Focando-se no comportamento da frequência do sistema, é criado um modelo, com bases em Matlab/Simulink, da portuguesa Ilha Terceira, para avaliar os potenciais benefícios da utilização de tecnologias de hidrogénio na prestação de serviços de rede. Dois cenários diferentes são analisados, a resposta da frequência do sistema a grandes desequilíbrios e a desequilíbrios de estado estacionário causados por erros de previsão de carga e potência eólica. Os resultados refletem como o comportamento da frequência é afetado pela quantidade de inércia no sistema, características dos geradores síncronos e presença de eletrolisadores e células de combustível, com novas métricas sendo introduzidas para comparar a resposta da frequência a cada um.

Palavras-chave

Fontes de Energia Renovável; Tecnologias de Hidrogénio; Controlo de Frequência; Grandes perturbações; perturbações de Estado Estacionário

Table of Contents

List of Figures

List of Tables

List of Abbreviations

HFO	- Heavy Fuel Oil
EAE2030	- Estratégia Açoriana para a Energia 2030
RES	- Renewable Energy Sources
VRES	- Variable Renewable Energy Sources
EU	- European Union
IEA	- International Energy Association
SDS	- Sustainable Development Scenario
ESO	- Electricity System Operators
FR	- Frequency Response
RoCoF	- Rate of Change of Frequency
FN	- Frequency Nadir
FCR	- Frequency Containment Reserve
aFRR	- automatic Frequency Restoration Reserve
mFRR	- manual Frequency Restoration Reserve
DG	- Distributed Generation
AEC	- Alkaline Electrolyzer
PEMEC	- Proton Exchange Membrane Electrolyzer
SOEC	- Solid Oxide Electrolyzer
AFC	- Alkaline Fuel Cell
PEMFC	- Proton Exchange Membrane Fuel Cell
DMFC	- Direct Methanol Fuel Cell
PAFC	- Phosphoric Acid Fuel Cell
MCFC	- Molten Carbonate Fuel Cell
SOFC	- Solid Oxide Fuel Cell
EEI	- Electrolyzer Equivalent Inertia
IEP	- Impact of Electrolyzer Power
IIC	- Impact of Inertia Constant

Chapter 1

Introduction

This chapter presents the topics addressed and methods used in the work. Establishing the research question to be answered and finally explaining the document’s structure.

1.1. Motivation

Renewable energy power sources have been the leading effort to decarbonize the energy sector, having not just a direct impact on sustainability through the substitution of carbon-based power sources, but also through allowing the process of electrification to develop across many sectors. The need for this decarbonization stems from the already noticeable climate changes, brought upon by the increased concentration of greenhouse gases in the atmosphere that is expected to keep growing at unsustainable rates if no adjustments are made. This environmental problem has become one of the most widespread discussions of today, garnering and infusing attention to and from all sectors. For these reasons renewable energy sources have been adopted at increasing rates and are showing positive results in this process. With their large uptake and the increasing electricity demand, the energy sector is in a clear transition period. This transition is, at the surface level, simply based on substituting carbon-based power sources by renewable ones, but, even just at a technical level, the different characteristics of these technologies makes this transition much more complex than it seems.

The electricity system is based on a constant balance between power demand and supply, whose state can be evaluated through the system's frequency, the frequency shared by all connected machines. Deviations from the frequency's nominal value can have negative implications and even damage grid systems. The differences in connection to the grid between technologies, with traditional thermoelectric power centrals being synchronously connect and wind and solar sources being converter connected, has caused changes to an important frequency stability parameter, the inertia constant. The system's inertia is a determining factor in its frequency response to power imbalances. With this parameter being supplied traditionally by the kinetic energy of the connected rotating masses of synchronous generators, the substitution of these power sources with others that do not contribute to it, has led to its decrease. Additionally, with the traditional electricity sector having been based on a direct line between a controllable fuel-based power source and the demand, the introduction of dispersed power sources that, in their essence, are not controllable, has led to both, a heterogeneity across space and time, and additional uncertainty. These challenges have the potential to slow, and in extreme cases even stop, the penetration of renewable energy sources. Because of that many options are currently being researched to tackle these barriers. The study presented here was done with the purpose of adding on that research by presenting and testing a plausible solution.

1.2. Objective and research questions

Motivated to contribute to a solution focused on reestablishing system frequency stability, this work combines this system need with the also increasingly more pursued topic of a hydrogen society. Despite being abundant in the universe it is not naturally available, and thus hydrogen is considered an energy vector, meaning a vessel used to store energy from an energy source and be converted back into another form of energy. Hydrogen technologies are not new, and the idea of a hydrogen-based energy sector has been discussed for 50 years now. Despite for a long time not growing in its role as an energy vector, hydrogen has been gaining traction, fueled by this same need for decarbonization. Being presented now as not necessarily a competitor to the already established energy vector that is electricity,

it has been pursued as a complementary measure. Two technologies that could be considered the pillars of the hydrogen energy vector are electrolyzers and fuel cells. Both are electrochemical devices, but while electrolyzers use electricity to generate hydrogen, fuel cells use hydrogen to generate electricity. These are considered for many applications, and here they will be seen as manageable loads and suppliers, focused on responding to the system's needs. Electrolyzer systems focused on providing grid services will, functioning from the side of power demand, control their load according to the deviation of the system's frequency, in the same way, fuel cell systems will adapt their power output to balance out supply deficits.

Being inserted in a large number of research efforts focused on these two topics, system frequency stability and hydrogen technologies, both separately and together, the purpose of the work presented here is three-fold. Firstly, to contribute to the understanding of the effects of lowering system inertia and of increasing uncertainty of power sources. Secondly, to present a model of an isolated power system composed of synchronous generators, electrolyzers and fuel cells, and promote one possible application of these technologies that can be an additional path for their growth and development. And lastly, to evaluate the performance of this solution from the perspective of the system's frequency stability, additionally developing a novel measure to connect the effects of the hydrogen technologies with the grid inertia constant. With that in mind along this report the following questions will be answered:

- What are the impacts on system frequency stability of system inertia, and power load and supply uncertainty?
- Can hydrogen technologies provide benefits to the frequency stability? If so, how can we measure them?

1.2.1. Island description

To answer these questions a model based on Azores' Terceira Island was created. The Azores archipelago is located in the Atlantic Ocean. This Portuguese archipelago has 9 islands divided into three main groups, according to their location, the eastern group composed by Santa Maria and São Miguel islands, the central group formed by Terceira, Graciosa, São Jorge, Faial and Pico and the western group constituted by Flores and Corvo. Terceira island is the second largest and the second most populated island of the Autonomous Region of the Azores. It has an average population of 55 000 people that grows substantially during the summer due to tourism. Commerce and residential consumers represent nearly 80% of electricity consumption with industrial being responsible for most of the remainder.

Each of the island has its own isolated, independent electrical micro-system. Despite their potential for the presence of RES their energy systems depend mainly on the use of fossil fuels, which not only is detrimental to the environment but has also led to higher electricity prices due to the additional costs of transportation. To diversify the generation sources and take advantage of the privileged amount of renewable energy potential in the last 15 years both a wind farm and a geothermal central have been built. While other forms of electricity generation are present in the island, their capacity and impact will

not be considered in this study, due to either their smaller size and presence [67], and to keep the study focused on the considered most relevance grid elements.

Islands like Terceira, others in the Azores archipelago and many others around the world, but particularly in Europe, are serving as testing grounds for different technology that aims at increasing renewable penetration but maintaining reliability while lowering emissions.

1.2.1.1. Synchronous Generation Sources

Thermoelectric Central of Belo Jardim

The Terceira Island has been very dependent of its fuel oil (HFO) electricity generation, being responsible for 99 percent of electricity generated up until the opening of the Serra do Cume wind park in 2008. The thermoelectric central of Belo Jardim, in Santa Cruz, runs mainly of HFO, emitting particulates, sulphur dioxide (SO_2), nitrous oxides (NOx) and carbon dioxide (CO_2) [66]. Today it still holds 78 percent of its total capacity, but the share of electricity produced has been lowered to 60 percent [67] due to the addition and priorities of wind and geothermal generation. The total of 61,116 MW of production capacity are split between ten groups with unequal capacities and installation dates that go from 1984 to 2004. This central started its activity in 1984 with the finished construction of groups 1 and 4 and since then has progressively grown from the 3,128 MW of each of those groups. Group 3 added 3,000MW in 1986, and group 2 another 2,860 MW in 1990. Groups 7 and 8 finished in 1997 have 6,100MW each. Two other increments of 6,100MW came with groups 6 and 5, respectively in the years 2000 and 2003. The most recent additions were groups 9 and 10 in 2004 with 12,300MW each.

Geothermal Central of Pico Alto

After a long research process, that lasted 10 years, studying the island's potential for geothermal generation, in 2017 the Geothermic Central of Pico Alto, in Praia da Vitória, was inaugurated. With 3.5 MW of capacity, it is projected to grow up to 10 MW in the future if the resource availability is proven [68]. The addition of a geothermal central in Terceira is a crucial step for the evolution of RES as it is a renewable resource capable of providing stable and controllable production.

1.2.1.2. Wind Parks of Serra do Cume

The wind farms in the island are located in Serra do Cume and are split between two companies, EDA and CAEN. The first one, owned by EDA, was built in 2008 with five ENERCON E 44/900 wind turbine models, each with 900 kW totaling 4.5 MW. In 2011 the park was upgraded, doubling the number of turbines, of the same model, and reaching a total of 9MW. The second wind park used four more turbines of the same model, increasing the island's wind capacity by 3.6MW in 2013.

1.2.1.3. Future of the island

With the wind park and the geothermal plant the presence of renewable power and the share of electricity being produced by this sources has grown considerably in the last decade. This is a positive signal of the island's efforts to become more sustainable and self-sufficient. The island's government plans to progress in this trajectory, setting their intentions clear for their energy sector in the Estratégia Açoriana para a Energia 2030 (EAE2030), the Azores energy strategy for 2030 [1]. In this strategic plan the following goals were highlighted:

- Reinforcement of energy security
- Reduction of energy costs
- Reduction of greenhouse gases emissions

Reinforcing energy security is described as lowering the probability of fault events and insurance of continuous sources of energy in the island. The plans to achieve this goal resolve around four focus points: the diversification of supply sources, the increase of system inertia, where the option of energy storage was mentioned, the reduction of consumption and the local production of energy. These efforts are complementary to each other in a way where their combined pursuit is expected to bring better results than the sum of each individual initiative. The reduction of energy costs is an objective set as a means to guarantee energy access to all population and promote the growth of business activities in the island. The reduction of greenhouse gases is not isolated but inserted together with other environmentally focus objectives whose goal is to maintain environmental stability and enhance quality of life in the island. To pursue their ambitions four guidelines were introduced and ranked:

1. Energy sufficiency - while in the middle of an energetic transition it is important to maintain high standards for quality of life.
2. Energy efficiency – the use of resources can be lowered through the improvement of processes or the development of new sources.
3. Electrification - change from other energy vectors that are intrinsically linked with bigger environmental impacts or limited by efficiency into electricity
4. Decarbonization – reduction of emission of greenhouse gases, in particular by changing away from responsible sources into alternative renewable energy sources.

These measures set the path that will be followed and the tools that will be used in the island to promote a sustainable energy sector. To measure the performance of these measures and mark clear intentions a set of targets were established in this strategy plan:

- 50 percent reduction in the use of butane gas compared to the values of 2010.
- 25 percent increase in energetic efficiency of land transportation compared to the values of 2010.
- 28 percent increase of energetic efficiency in buildings compared to the values of 2010.
- 40 percent increase in energetic efficiency in businesses compared to the values of 2010.
- 80 percent renewable electricity.
- 33 percent increase in overall energy efficiency compared to the values of 2010.
- 41 percent reduction in greenhouse gases emissions compared to the values of 2010.

This strategy and the targets set span across many disciplines in the energy sector and will demand action from a varied group of players. The work presented here fits in with the overall ambition and will be able to contribute to several objectives.

1.2.2. Thesis overview

The model created to simulate the island used load and wind speed data as inputs, together with developed models of synchronous generators and hydrogen-based technologies, electrolyzers and fuel cells. This model will then be used to perform two different sets of simulations that will reflect on the system's short term frequency response to large disturbances and the frequency variations along a day. The first set thus focusing of the impact of system inertia and the second on steady-state imbalances caused by uncertainty in load and power sources. Each set will have comparison simulations that compare the frequency's response with and without the addition of hydrogen technologies. Based on the simulation results, some conclusions will be drawn regarding the contribution of hydrogen systems to enhance the frequency response.

1.3. Structure

Here the work is presented following a path that starts with an introduction and review of the topics at hand based on the research leads, evolving into a description of the model created, and the testing and analyzing of the results obtained from the proposed solution.

Beginning in Chapter 2 by describing the need and the evolution of renewable energy sources brought upon by the transition to a sustainable energy sector, and their impact on system frequency stability. From there a description of the studied frequency control services is made, including a depiction of their future outlook. Finally, the research trends tackling this problem are presented and the potential options for the hydrogen-based solution are covered in detail, highlighting the ones most appropriate for this purpose, and then reporting on the grid and hydrogen technologies modeling approaches present in research.

Following, Chapter 3, describes thoroughly the modeling approach used in this study, explaining the model's structure, detailing each component, the multiple configurations used, and additionally describing the model's limitations, while also introducing the novel metric used to measure the impact of the proposed solution on system frequency stability.

Ultimately, Chapter 4, presents the two different scopes of simulation test sets, one focused on the frequency stability during the small period after a large imbalance, and the other on the impact of steady-state imbalances on this system parameter. Plus, it presents and discusses the results obtained from each scenario and configuration, with Chapter 5 highlighting the contributions and limitations of this work, adding closing remarks and pointing to possible future developments.

Chapter 2

State of the Art

Description the evolution of renewable energy sources and their impact on system frequency stability. Explanation of frequency control services. Overview of hydrogen technologies and modelling approaches.

2.1. Renewable energy sources and their impact

The urgency to transition into more sustainable ways is part of the fabric of today's society. From an individual level the public has been made more aware of their impact on the environment, how it connects with the bigger picture and the consequences that come with it. At a governmental level multiple plans have been drawn and targets have been set as signals of strong commitment to this transition. The energy sector has been a reference in this struggle and the electricity production industry is leading the way, with the penetration levels of Renewable Energy Sources (RES) growing year after year and, in some cases, even exceeding expectations.

There is a variety of renewable energy and power sources from different natures each with different characteristics. In Widén et al (2015) [2] the definition used for renewable energy is “any form of energy from solar, geophysical or biological sources that is replenished by natural processes at a rate that equals or exceeds its rate of use.” This definition englobes solar energy, hydro power, wind, wave, and tidal power, as well as geothermal heat and bioenergy [2]. Each can be used in different ways, and some are still under development. Aside from their renewable status there has been another distinguishing factor, from the nature of most of these that is currently gaining attention, and that is their variability. Solar, wind, wave and tidal energy are variable in time and have a non-dispatchable nature, that is, their output cannot be controlled or predicted without uncertainty. This variable nature is something the grid systems are not used to, coming from more easily controlled generation, but must adapt to as the levels of penetration of RES grows. Research studies point in multiple directions that are not mutually exclusive. Some of the evolution and the current status of RES is presented here, with the use of research to help explain the driving motivations behind the use of RES and the limitations that have been found, or might be present in the close horizon, to hinder and limit growth. At the end of this chapter some of the current options being researched to promote and stabilize the growth of RES are reviewed.

2.1.1. Reasons for going renewable

The transition to renewable sources of energy has its roots in sustainability but with the growth of the industry and society’s change in acceptance, many other reasons for the increased uptake of these technologies have arisen. These motivations span across environmental, economic, social, and political arenas.

The study Simões et al. (2011) [3] performed in 2010 did an analysis of the potential long-term benefits of the Portuguese short-term transition to RES. In this analysis the authors looked at this transition from different perspectives and covered multiple scenarios. They highlighted the fact that changes like this are motivated by more than just the need of cleaner electricity but also the desire of governments to be more energetically independent from others. The scenarios studied covered both positive and negative perspectives for future development and the possibilities of introducing RES at different stages of the supply chain. While it did not cover possible electricity supply security requirements that have the potential of being a bottleneck in the growth of RES

technologies, the authors concluded that the pursuit of RES is feasible and beneficial from both an economic and an environmental perspective, while also contributing to lower reliability on other countries.

Bañol et al (2020) [4] highlighted the considerable positive environmental impact already noticed in the European Union (EU). The growth of EU's renewable sector has resulted in the avoidance of an estimated $436\ Mt$ of gross CO_2 emissions between 2005 and 2015, with the replacement of carbon-based systems with RES in the energy sector being responsible for 76 percent of those. Just in 2012 these technologies were estimated to have averted 3.1 gigatons of $C0_2$ equivalent emissions worldwide, 20 percent of the global emissions.

Additionally, the attention and efforts put into developing and implementing wind and solar technologies have resulted in dramatic drops in cost, making those technologies competitive with fossil fuel-based generation in certain areas of the world [5]. The result has been a global increase in solar and wind capacity from 80 to 790 GW between the years of 2006 and 2016. The decrease of costs has the potential to turn perspectives and move from considering transitioning to RES as a burden to considering it an opportunity.

The European Council, in 2014, had set the following targets for 2030: reduction of greenhouse gas emissions by 40%, in comparison with the values of 1990 and a share of 27 percent of renewable energy in gross final energy demand [6]. Currently, as a result of positive developments and additional urgency, there is a discussion to increase these targets to a 55 percent greenhouse gas emissions reduction and a higher share of 40 percent of renewables in the energy mix [55]. The political positioning of countries regarding sustainability can be the builder or a destroyer of bridges.

For these reasons the growth of RES has been steady and its penetration is expected to continue growing in the future, especially in countries that need to comply with CO_2 emission limits, those that are searching for energy independency and those who can consider the environmental needs a priority.

2.1.2. Current state of penetration

The investments made on RES have been, at national levels, the leading signal of environmental consciousness, spanning from efforts to limit polluting processes, to the political framework that is set up to promote cleaner options. While the conversation of an energy transition has been had for many decades, the biggest changes have been noticed from 2010 to the current day due to the achievement of lower costs in solar PV and wind power. Figure 1 shows the global evolution of the share of renewables in power generation from the year 2000 until 2019 according to the International Energy Association (IEA) and while the growth has been remarkable, when looking at the values needed to accompany the IEA's Sustainable Development Scenario (SDS) up until 2030, the big challenge that lies ahead can be seen.

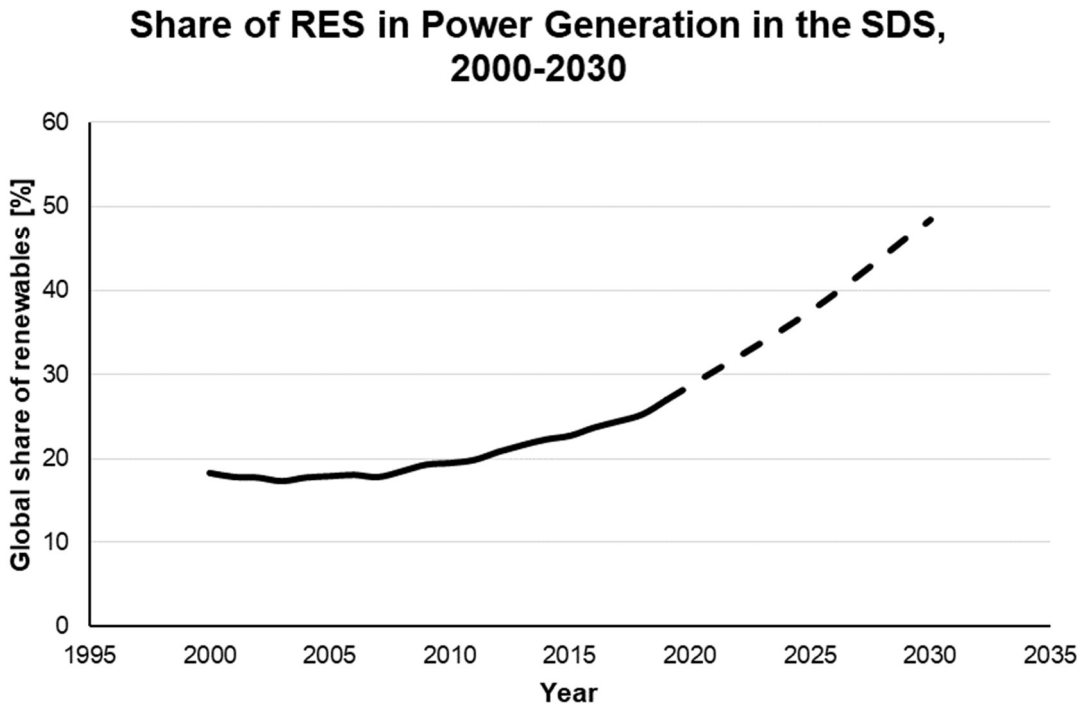

Figure 1 - World's share of renewables in power generation from 2000 to 2030 according to the Sustainable Development Scenario, figure adapted from [56].

In 2019 the emissions made by the power sector were lowered by 1.3 percent mainly resulting from a 5.6 percent increase in generation from low-carbon technologies and a decrease of 3.1 percent in non-abated coal [56] Maintaining and promoting the decarbonization of the power sector is a key for transitioning into clean energy, as not only is this sector responsible for 41 percent of CO_2 emissions [56], but there is also a foreseen increase of end-uses where energy is supplied in the form of electricity. The combination of these factors will enlarge the demand for decarbonization of this sector. Despite those pressures the recent trends are not fitting the SDS, which determined the need for average power sector emissions falls of 4 percent until the year 2030.

According to IEA's 2019 Renewables report [57], the growth of renewable capacity in the world had a steady increase until 2018, with the trend stopping due to a change in China's PV policy. Despite the rate of growth being paused the amount of net capacity added in 2018 was similar to that of 2017, 178 GW, and those additions represented 75 percent of all the net power capacity growth. In the next year the electricity being generated by these sources saw a growth of 6.5 percent, with two thirds of that growth being sourced by wind and solar PV. This growth resulted in renewables being responsible for a record 27 percent of electricity generated in 2019 [58]. For the following years IEA forecasted the annual capacity additions to continue growing, being fueled mainly by the North America, Europe and Asia-pacific regions. They couldn't have predicted a global pandemic. While the current crisis can be an obstacle for transition and innovation, and its effects will also be felt on the energy sector, in its 2020 Renewables report [58] the IEA reported the resilience of renewable capacity installation during this pandemic period, forecasting the

capacity to keep on growing in record numbers in multiple areas of the globe, predicting it will surpass coal and gas capacity by 2024 [9.15], with an expected addition of 1 123 GW of new solar and wind capacity between 2020 and 2025. This resilience shows the commitment of governments and their people to pursue the mitigation of climate change and to keep track of the SDS, which stated that the annual growth of renewable power must be around 7 percent.

These efforts have not been homogeneous across the globe and the results, combined with the usual factors, economic development for example, have reflected that. In 2020's report [56], EIA forecasted an increase in renewable capacity in Europe of one-third between 2019 and 2024 with six countries being the leaders of that growth: Germany, Spain, France, the Netherlands and Turkey [57]. In the same report the worldwide disparities were referenced by highlighting the fact that of the $9000\,TWh$ total renewable electricity generation available by 2024, 75 percent will belong to just six market: China, Europe, the United Stated, Brazil, India and Japan. While these markets are also the ones with the largest emissions, and thus are socially seen as considerably more responsible, their dominance might lead to an increase in disparities between them and less developed regions. To promote an accelerated development across regions the following challenges must be addressed by governments: policy and regulation uncertainty; high investment risks in developing countries; and system integration of wind and solar electricity in some countries [56].

2.1.3. The consequences of renewables

The nature of Variable Renewable Energy Sources (VRES) entails that their electricity production capabilities will be dependent on both time and location, varying across different timescales of minutes, hours, days and even years. There have been many studies analyzing the variability of some of these sources, focusing on data analysis for pattern detection, improving forecasting and on measuring and controlling its effects. To continue thriving the RES sector must understand the variability of each resource and the resulting limitations of technologies [5]. While there isn't a consensus on the scale of these impacts, most research studies indicate that as levels of penetration increase, additional challenges will arise.

Widén et al., 2015 [2], present an overview of the research on the topics of variability and forecasts and provide concise conclusions. In the study the authors look at the varied approaches used for studying the variability of RES. They comment on the fact the timescales used in the look-at studies are determined according to the phenomenon being examined while they believe it is important to also study them in a standard set timescale to better understand their behavior, specifically with the growth of their dimension. The same thought is shared in relation to the methods used, where more studies should try to diversify the methods applied to each source and apply them across multiple sources. In the same way forecasting efforts should share common metrics to facilitate the implementation process for utilities and other players. As a closing note the lack of shared data is emphasized by the authors as an important thing to correct for the sake of better and more complex research.

Apart from the individual volatility of these energy sources, it is increasingly more relevant to consider and research the coupling of multiple intermittent sources and their effects combined with load volatility. In the relationship between different sources there might be complementing aspects that balance each other and help avoid large variances, and by including load volatility the result will be the amount of load the system operators will have to match with other forms of generation. The unpredictability coming from both fronts can result in a profile that is very inconsistent and hard to handle, studying the combination of elements is key to predict and understand extreme cases.

The curtailment of power is also one of the growing issues that is being covered in research. With the constant possibility of forecasting errors in a system where there is direct line connecting production to consumption, the increase of RES can lead to excess electricity generation in certain parts of the day or the year. This excess generation must be thrown out resulting in wasted cheap electricity that is then compensated to the producers. In [7] the study [8] was mentioned to have estimated an annual curtailment value in the range of 14 to 22 percent in an United Kingdom power system with high penetrations of solar PV. To better understand the potential impact of high shares of wind and solar PV power on the system of Great Britain, Villamor et al. (2020) [7] created a model to simulate its unit commitment and economic dispatch, testing it on multiple scenarios of high renewable penetration. The results brought light to how curtailment can be connected to avoiding system instability, with the authors pointing to how increasing flexibility in the balancing grid services can lead to a 75 to 88 percent decrease in curtailment. Joos et al. (2018) [9] tackled the question of increased cost due to the penetration of renewables. In the data analyzed, from Germany and Britain, an increase of 62 percent in system operation costs could be seen, mainly due to congestion management costs. These costs were mainly incurred by power curtailment and by redispatch of gas power plants, respectively in Germany and Britain. This limiting factor can be grouped with the concerns of the growth of RES possibly lowering system stability. RES do not share the same type of connection to grid that power plants with synchronous generators do. These traditional power plants not only produce electricity, but they also help maintain the system in a stable state. With their substitution the stability of the system can be compromised. Mokolo et al. (2021) [10] evaluated the impact of lower stability measurements stemming directly from the implementation of high percentages of renewable sources. In this research the negative impacts of high penetrations of RES were apparent, using the system's response to power imbalances as a measurement. Possible solution pathways for solving this problem were described in detail as well as their current state of development in research. Again, the author called upon the availability and analysis of data as one of the keys to better understand this problem and help develop better solutions. Using Great Britain as a current example REF[9] referred to how, due to the increase in instability, certain limits might be put on the maximum share of RES that are allowed on any given moment.

For all the benefits of RES there are also challenges that must be acknowledged, analyzed, and solved. As there is not one root for the challenges being noticed, the solutions also can be

approached from multiple angles. Some of the current research on possible alternatives to be implemented are presented here.

2.1.4. Possible solutions

Almost all research studies on the topic of high penetration of RES point to the need of additional measures to not only help avoid the degradation of system stability but also evolve the current electricity system into a new era with more homogeneous availability, security and also lower prices. With these multiple objectives in mind a large part of authors seems to agree that the most feasible and beneficial options are energy storage and smarter grid systems.

One of the most developed options currently are the battery energy storage systems. Koller et al. (2015) [11] performed a review on the possible grid application for a $1\ MW$ Li-ion battery energy storage system from Zurich. The study covered the applications of primary frequency control, peak shaving and islanded operation with the results being positive for the three application cases. The use of this type of technology has been widely accepted from a technical standpoint with the main limitations being the worries of a short lifespan caused by continued ramping up or down and the economic viability of these projects. Currently there are several similar pilot projects being launched in small islands to serve as a testing ground for this technology while promoting renewable investments in islands to achieve green and self-dependent grids [59].

Hydrogen is another technology that could cater to these needs brought upon by RES generation, serving simply as a consumer, through the use of electrolyzers, or as a storage option, by the combination with fuel cells. Hydrogen technology could be used as an energy transferring option, on a shorter weekly scale or even on a seasonal one. In a similar way the mentioned hydrogen technologies have the potential to serve as a grid management tool, acting from both the supply and the demand sides. Chen et al. (2021) [12] performed a techno-economic analysis on the use of hydrogen-based energy storage systems, comparing it with a traditional battery storage system, to mitigate the variability of RES. The study was performed for two distinct locations and reflected on the possible effects of the renewable source's variability on economic potential. The results were favorable for the hydrogen energy storage system.

Another approach that has been gaining traction is the concept of overbuilding. This solution consists of increasing renewable capacity as much as possible to a point where it could cover the load by itself in any situation. The trade-offs of this solution are the amount of capacity that would inevitably be unused or curtailed. Solomon et al. (2016) [13] performed a study that followed a similar concept. The results pointed to the possibility of achieving 85 percent electricity penetration from wind and solar with an energy wastage of 20 percent of the annual demand. In the study this hypothesis also included large amounts of storage and an increase in capacity reserves.

This session covered the benefits, the status, and the future challenges of the energy sector's transition into a more sustainable future. This future includes the use of RES, in some cases as the main form of electricity generation, but it must also contain energy security and system

stability. The work presented here is focused on maintaining grid stability, in specific through the analysis of the grid's frequency, and the use of hydrogen technology. The following sections will introduce the topic of grid management and explore the many options of hydrogen technologies that could be suited for these purposes.

2.2. Grid Management

The electric power system is constituted by the production, transmission, and consumption of power in real time. Power is produced and consumed at the same time and lay at different sides of a scale that must stay balanced [14]. The measurement used to assess the status of the scale is the grid frequency; that is the frequency at which all the synchronous generators and demand units are rotating at [15]. The system has a nominal frequency that is set for the synchronous region, a region that is tied together during normal operation and operates at a synchronized frequency [14], for Europe this value is 50 Hz. An imbalance between power produced and consumed will lead to a change in system frequency. The change will be a reflection of the imbalance, if the amount of production is larger than the demand the frequency will rise and if the demand is greater than the production the system frequency will fall.

While systems can sustain small deviations, larger ones, caused for example by a fault in a large generator, are much more detrimental and can be threats to equipment and, in extreme cases, lead to potential blackout. Because of that the frequency of the system must be kept inside a strict interval. The ones responsible for that are the electricity system operators (ESO), who work every second to maintain the system frequency as close as possible to its nominal value [15]. To perform they have at their disposal frequency response (FR) services, a set of generation and demand units available to alter their power output or input in response to grid frequency changes. The work presented here is focused on frequency control services, but they are part of a larger set of ancillary services which also include voltage control, spinning reserve, standing reserve, black start capacity, remote automatic generation control, grid loss compensation and emergency control actions [16].

2.2.1. Imbalance Characteristics

The services mentioned above are present to provide the system stability which [16], quoting [60], described as the "ability of an electric power system, for a given operation condition, to regain a state of operating equilibrium after being subjected to a physical disturbance, with most system variables bounded so that practically the entire system remains intact".

In traditional electric systems the generation was almost completely performed by synchronous generators in central power plants, whose rotating speed is directly related to the grid frequency, resulting in a tandem configuration, illustrated in Figure 2, where load is shared according to the different plant conditions [14]. Due to these connections a sudden change in load, which will lead to a subsequent change in frequency, is resisted by generators who release the kinetic energy in their rotors [14], this is referred to as rotational inertia [14-16]. The amount of inertia present in a system is dependent on the amount of rotating masses within the system. The higher the inertia

the better the system will initially contain frequency deviations, acting in particular during the first 5-10 seconds after a disturbance. With a similar effect, loads that are frequency dependent also evoke a damping effect created by their variation according to the system's frequency.

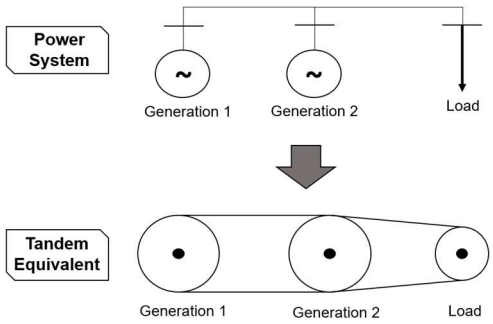

Figure 2 - Mechanical equivalent of the power system's operation, adapted from [14].

To evaluate deviations and system's response a couple of measures are looked at, one is the rate of change of frequency ($RoCoF$), defined as the frequency deviation during the first $500\ ms$ after a disturbance [16], and the others being the frequency nadir, the maximum value of frequency deviation, and steady-state frequency deviation, the value of frequency after achieving a steady state [17].

2.2.2. Frequency Control Response

After a disturbance that deviates the frequency outside the normal operational window the system, together with its inertial response, will begin an active response that is divided into two stages. In the first stage the Frequency Containment Reserve (FCR) is activated. This is an initial automatic response whose goal is to bring stability back to the system, by limiting frequency deviation and thus avoiding great damages. This occurs during the first 30 seconds after a disturbance and is guided by a droop control that adjusts the power released by the generator [14, 17]. As can be seen in Figure 3 the frequency when stabilized will settle at a value different from the nominal.

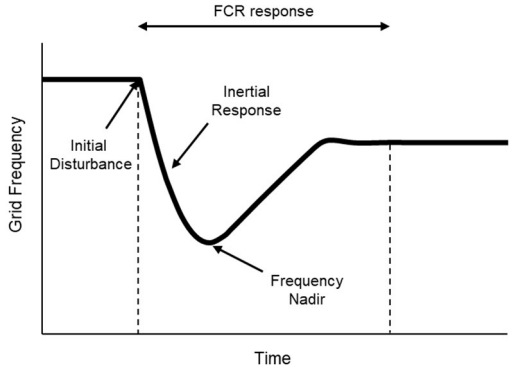

Figure 3 - Representation of a frequency containment reserve response to a large disturbance.

The secondary control loop response, named automatic Frequency Restoration Reserve ($aFRR$) which acts on a considerably larger time frame, of up to 15 minutes, will be activated to bring back

the frequency to its nominal level. Additionally, there is the service of manual Frequency Restoration Reserve ($mFRR$), which can be activated by the responsible ESO in case of long-lasting imbalances [16,17]. This is done through the use of standby power sources to avoid the dangers of continued frequency deviations from its nominal value [17]. This work is focused mainly on the primary response.

2.2.3. Future

RES and other distributed generation sources (DGs) that are electronically connected do not share the inertia-providing characteristics of synchronous generators, that is why the increase in their penetration, in conjunction with their intermittency and higher uncertainty, has brough new challenges to ESOs. Coupling their presence with the unpredictability of growing amounts of load has led to increased requirements for system flexibility. Recent research and regulation efforts have been focused on defining the effects of the increased penetration of RES, in particular in isolated and island grids, and on the different option to combat the decrease of reliability without hindering the growth of RES popularity.

Ulbig et al. (2014) [18] perform a thorough analysis on how the closing of synchronous power plants and larger presence of RES have resulted in inertia variances that did not have to be considered in the past, both spatial heterogeneity and time variance resulting from the distributed presence of converter-connected units and their variability. The analysis performed highlighted the larger grid frequency instability events resulting from lower inertia and how faster control reserves might help contain such situations. The search of technologies to be integrated in the system as a counterbalance to the expected decrease in inertia has led many in the direction of what is called synthetic inertia. Often also referred to as virtual inertia, this area of research is focused on the development of technologies or processes to serve a similar purpose that of the rotating masses' kinetic energy. Due to its more recent growth of attention, there is not yet a universal definition that limits what can and cannot be described as synthetic inertia. As an example of the lack of an universal definition, [10] references the following definitions of synthetic inertia: "the controlled response from a generating unit to mimic the exchange of rotational energy from a synchronous machine with the power system" and "the facility provided by a power park module or HVDC system to replace the effect of the inertia of a synchronous power generating module to a prescribed level of performance". Clearly these refer to the same phenomenon but each one describes it differently, focusing on different characteristics and thus demonstrating the lack of consensus on what constitutes a synthetic inertial response. Eriksson et al. (2018) [19] tackles this gap, reviewing the current views on the topic and providing a clear definition, comparing it and differentiating it from another usually compared term, fast frequency response. The definition is declared from the perspective of a transmission system operator, describing synthetic inertia as "the controlled contribution of electrical torque from a unit that is proportional to the RoCoF at the terminals of the unit." At the same time, a definition for fast frequency response is given as "the controlled contribution of electrical torque from an unit which responds quickly to changes in frequency in order to counteract the effect of reduced inertial response",

thus indicating pointing to the separating line between these two being mainly on the reference metric considered. These definitions are not centered on a specific technology or process and thus leaves the door open to include a great number of research leads. Two large groups have been taking part in this discussion, one focused on providing this virtual inertia through the use of storage technologies that can act fast, and the other on generating this phenomenon through the adjustment of converter connected power sources, in particular solar and wind power. Tielens et al. (2016) [20] presents a review of converter connected inertia sources, touching on the use of wind turbines, highlighting the functioning of this mechanism, its benefits and some of its challenges. Wind turbines, despite having rotors, are not usually considered to have inertia due to the decoupling of their rotational speed from the grid frequency, but certain control techniques can give them the option to change their power output in response to the system frequency. Morren et al. (2006) [21] depicts a combination of fuel cells and wind turbine to perform frequency control services. In this combination the fuel cells are used as the substitute mechanism for inertia. This combination is tested with results highlighting the sensitivity of this setup's feasibility and benefits.

With technology pushing the evolution of this sector, the surrounding structure has also been forced to adapt with markets increasingly seeking more flexible technological options and processes. Lobato et al. (2008) [22] presents a thorough overview of the ancillary services in Spain, covering the management structure behind their supply, the technical details demanded from participants and detailing the organization of the markets for these services. The study also briefly touches on the tools and algorithms used for optimization by the agents. According to this review, in similar markets, the primary reserve is automatically activated in response to imbalances. It is performed by the generators in a mandatory and non-remunerated regimen. To be eligible the generators must be capable of altering their output by 1.5 percent of their rated power within a window of 15 seconds, for changes of $100mHz$, and 30 seconds, for changes of 200 mHz. The generators are permitted a response dead band with a maximum value of 10mHz. Anshehri et al. (2019) [23] details the current and expected FCR market shared by Germany, the Netherlands, Austria, Switzerland, Belgium, and France. At this moment there is one auction per week where generators, loads and storage technologies are involved, with offers having to stand for 1-week windows. The bids have a 1MW minimum, being limited to 1 MW steps and must be equal for up and down reserve. The prices of this market have currently been going down due to the increased competition brought on by the entry of new players. In the upcoming years it is expect for this market to undergo some changes. More regions are planned to be included, and a different structure is to be introduced, with auctions once per day for day-ahead orders. In this reshaped market the offers for up or down reserve can be separated and exclusive, additionally they are made and performed for 4-hour slots and the remuneration is expected to change to a marginal clearing price strategy. The technical requirements presented until now don't have any changes but it is expected for them to become more velocity demanding. These changes facilitate the entrance of new players as they introduce more flexibility and, at the same time, are expected to raise prices, due to the change from pay-as-bid to marginal clearing price. The solutions

presented here are capable of performing under tighter requirements and the changes expected in the FCR market will make their participation more economically feasible.

2.3. Hydrogen Technology

The concept of a hydrogen society has been in discussion since the decade of 1970 [24], but its realization has always been held back by the large inertia, caused by the great amount of implementation actions needed for it to be feasible and the lack of incentive behind this change. Despite the hurdles in front of hydrogen's large-scale introduction, currently it has been gaining traction, which can be seen with the development of technology and the public policy attention received from multiple countries around the world [25, 61, 62].

Many hydrogen-based technologies and processes are currently being studied, tested, and implemented. These are being developed for applications across multiple sectors in efforts to stabilize and accelerate the decarbonization process. Part of this focus has been on the energy sector, with hydrogen technologies working to complement and provide alternatives that promote sustainability. This work is indirectly focused on one of those alternatives, as already discussed the stabilization of electrical grids can be a key factor on the continuation of RES investments. This can be done through the use of electrolyzers and fuel cells that will help manage the grid frequency through by changing their power consumption and production, respectively. The current state of the art of these technologies is presented here in this section, covering their operation principles, the main alternatives for each, their characteristics, and their development status. The suitability of each presented technology is discussed and the most suitable one for this application is chosen.

2.3.1. Electrolyzers

Water electrolysis is a process where, with the use of an electric current, water is split into hydrogen and oxygen [26,27]. The electrochemical reaction of water electrolysis, equation 1, to form H_2 and O_2 is endothermic, requiring an outside energy source.

A typical electrolyzer consists of an anode and a cathode that are immersed in an electrolyte, when the electrical current is applied hydrogen is produced at the cathode while oxygen generated will be at the anode side [28]. The general water electrolysis process is illustrated in Figure 4, adapted from [28].

$$H_2O \rightarrow H_2 + \frac{1}{2}O_2 \qquad \Delta H = -288\ kJ.mol^{-1} \tag{1}$$

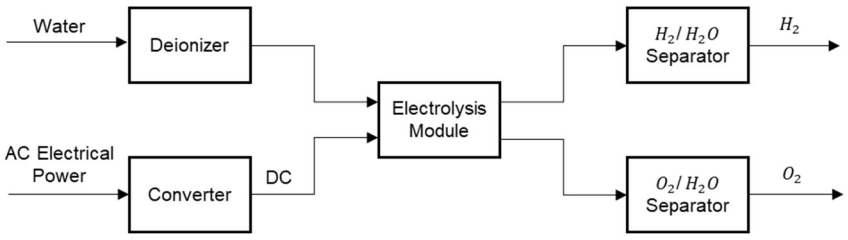

Figure 4 - Water electrolysis process diagram, adapted from Nikolaidis et al.(2017) [28]

The exact reaction differs according to the technology used, having different carriers. Currently there are three main types of electrolyzers: alkaline (AEC), proton exchange membrane (PEMEC), and solid oxide electrolyzers (SOEC). The three have different characteristics and are at different stages of development, here follows a description of each of these technologies.

Alkaline Electrolyzer (AEC)

The electrolytes used in this technology are alkali aqueous solutions that can be separated in two categories, according to the alkali solution used, the first being potassium hydroxide (KOH) and the second one sodium hydroxide ($NaOH$), with concentrations of 20 – 40 percent [29, 30]. The electrodes are usually made of nickel materials [30] and the diaphragm used to separate the two electrodes is composed of asbestos [29, 30]. Additionally, the diaphragm, which usually has a thickness of 3 mm [29], must be airtight, and the pressures at both sides of it must be balanced to avoid hydrogen or oxygen penetration in it, due to the risk of explosion [30]. This diaphragm is the reason these electrolyzers have a maximum operational temperature of 80°C [29, 30]. The electrolysis can be performed at atmospheric pressure as well as higher pressures, up to 30 bar.

Pressure plays an important role in the electrolysis process as while using higher pressures leads to a lower energy demand in the compression stage for storage, it also results in less pure hydrogen due to increased membrane permeability [26]. The specific energy demand for this electrolyzers ranges from 4.1− 5.5 kWh/Nm^3H_2 [26, 30], depending on the pressure and other characteristics. As can be seen in equation 2 and 3, hydrogen and hydroxide are generated at cathode, from where the hydroxide is moved to the anode part generating oxygen [29].

$$\text{Anode: } 4OH^- \rightarrow O_2 + 2H_2O + 4e^- \quad (2)$$

$$\text{Cathode: } 2H_2O + 2e^- \rightarrow 2OH^- + H_2 \quad (3)$$

The hydrogen generated has a purity of 99% [26, 28-30] but is mixed in an alkali fog that must be removed, for that an external separation unit is used. This whole process of alkaline electrolyzers has an efficiency of 50 – 60 percent, with the maximum values for current density being in the range of 0.1− 0.3 $\mathrm{A/cm^2}$ [26,29,30]. This is currently the electrolyzer technology that is most used for large scale applications [29], with prices around 1000 − 1200 €/kW [30], despite that, the low flexibility of this technology, in terms of startup quickness and loading response, is the reason why they are not the most viable for implementation with RES. It has an expected lifetime of up to 30 years, with expected replacements in periods of 7 to 15 years [26]. The research for the development of this technology is mostly focused on the search for an alternative diaphragm material because of the health hazards caused by asbestos [29].

Proton Exchange Membrane Electrolyzer (PEMEC)

This technology, instead of a liquid electrolyte, uses a gas tight thin polymer membrane. This membrane has a much lower gas permeability than that of asbestos [30]. The electrodes in this technology, until now, have demanded the use of noble metals, most commonly platinum. The hydration needs of the membranes have been the reason to limit the cell temperature at close to

80°C [26, 29]. The range of pressures applied is larger than that of AEC and the specific energy demand is about 6-8 kWh/Nm^3 [26], with higher values being reached in large-scale production cases. In PEMECs water is introduced at the anode where, though an oxidation reaction, it is split into oxygen, electrons and protons, hydrogen cations (H^+). The protons will travel though the membrane into the cathode where they are reduced to form hydrogen. These reactions are explicit in equations 4 and 5.

$$Anode: 2H_2O \rightarrow O_2 + 4H^+ + 3e^- \quad (4)$$

$$Cathode: 4H^+ + 4e^- \rightarrow 2H_2 \quad (5)$$

The hydrogen has a very high purity, 99.99 percent [26, 29], and due to the lower gas permeability of the PEM, when compared with asbestos, the hydrogen generated does not require the process of post purification, thus the final efficiency of this technology lies in the range of 67−82 percent [26, 30], using current densities that are much higher than AEC, close to 3 A/cm^2 [26,29,30].

This technology is currently entering the commercialization and is being revered for its higher efficiency, flexibility and fast response while also being more environmentally friendly than AEC. On the other hand, the higher costs of this technology, 1860 − 2320€$/kW$, are still holding it back. Its short time start-up and response makes it appropriate for implementation with RES. The current research on this technology is mostly focused on finding alternative cheaper materials for the electrocatalysts.

Solid Oxide Electrolyzer (SOEC)

The Solid Oxide Electrolyzers (SOEC) enter the realm of steam electrolysis, functioning at higher temperatures, sometimes reaching 1000 °C. The cathode and anode are, respectively, made of a cermet made of nickel and yttrium stabilized zirconia (YSZ), and perovskite, while the solid electrolyte is made of YSZ. In this technology steam and recycled hydrogen are introduced at the cathode where water is reduced, producing hydrogen and oxide anions. While the hydrogen then moves out into an external separation unit to be separated from the water, the oxide anions pass though the solid electrolyte to the anode, where, by recombining, they form oxygen [26,29,30], as expressed in equations 6 and 7.

$$\text{Anode: } O^{2-} \rightarrow 0.5O_2 + 2e^- \quad (6)$$

$$\text{Cathode: } 2H_2O + 2e^- \rightarrow H_2 + O^{2-} \quad (7)$$

Currently the temperature used in this technology varies between 750 − 950 °C and the pressure between 10 − 30 bar [26,29,63]. Higher temperatures lead to higher electrolyzer efficiencies, in this technology part of the electrical energy demand is substituted by thermal energy, reducing it by close to 25 percent [26, 63], resulting in efficiencies closer to 90 percent [26, 20, 30, 9.18]. The current densities in this technology vary between 0.3 and 1.0 A/cm^2. The hydrogen produced has a purity level of 99.9 percent.

SOEC technology is currently still in early development, with only laboratory scale models. The use of higher temperatures makes it very attractive for combinations with applications where heat is generated but not used. The higher efficiency makes it a very promising option for the future, but at this moment it is still not competitive with prices always above 2000 $€/kW$. The high temperatures, despite its advantages, also limit the opportunity for a cyclic or intermittent operation mode due to degradation of the materials, thus making the coupling of this technology with RES not viable.

Comparison of electrolyzers

The characteristics of all electrolyzers described are presented succinctly in Table 1 - Overview of electrolyte technologies, adapted from [26, *29, 30]*. In the study performed by Schmidt et al. (2017) [31] predictions for the development of electrolyzer technologies are made by experts from academic and industry backgrounds, the consensus was that in 2020 AEC would be the preferable technology but that by 2030 that would change in favor of PEMEC. SOEC while having great potential, due to its higher efficiencies, are still considerably behind in development and expected to have higher costs.

While AEC have the lower costs due to their longer development, the gap between them and PEMEC is going to get smaller as cheaper options for materials and processes are found. The flexibility, the rapid response time, combined with the higher efficiency are the factors that differentiate PEMEC and make them more appropriate for coupling with RES.

Table 1 - Overview of electrolyte technologies, adapted from [26, 29, 30]

Specification	Units	AEC	PEMEC	SOEC
Electrolyte	-	Aq. Potassium Hydroxide (20 - 40%)	Polymer Membrane	Yttrium Stabilized Zirconia (YSZ)
Cathode	-	$Ni, Ni-Mo$ alloys	$Pt, Pt-Pd$	Ni/YSZ
Anode	-	$Ni, Ni-Co$ alloys	$RuO2$, $IrO2$	Perovskite
Technology Maturity	-	mature	commercial	demonstration
Cell Temperature	$°C$	60-80	50-80	650-1000
Cell Pressure	bar	<30	<200	<30
Efficiency	%	50 - 60	67 - 82	81 - 86
Current Density	A/cm^2	0.1 - 0.4	0.6 - 3.0	0.3 - 1.0
Cell Voltage	V	1.8 - 2.4	1.8 - 2.2	0.7 - 1.5
Power Density	W/cm^2	<1.0	<4.4	-
System Specific Energy Consumption	Wh/Nm^2	4.5 - 7.0	4.5 - 8	2.5 - 3.5
Partial Load Range	%	20 - 40	0 - 10	-
Cell Area	m^2	<4	<300	-
Hydrogen Production Rate	Nm^3/hr	<760	<40	<40
Lifespan	hr	<90000	<20000	<40000
Purity of Hydrogen Produced	%	>99.5	99.999	99.9
Cold Start-up Time	min	15	<15	>60
System Response	-	seconds	milliseconds	seconds
Capital Cost	$€/kW$	1000 - 1200	1860 - 2320	>2000

2.3.2. Fuel Cells

Fuel cells are electrochemical devices that convert the chemical energy of fuel, mainly hydrogen, and an oxidizing agent, often oxygen, into electricity, with water and heat being the only by-products. They can continuously generate electricity as long as fuel and oxidant are supplied.

The hydrogen oxidation occurs in the anode and the oxygen reduction reaction occurs in the cathode, in the majority of fuel cells. The electrons are extracted at the anode and flow through an external circuit, generating electricity, in the direction of the cathode, where they are used in the oxygen reduction. The protons cross the electrolyte and react in the cathode with oxygen, generating water and heat. A fuel cell can then be described as a multi-component device that has two electrodes separated by an electrolyte, as is illustrated in Figure 5. Additionally, electrocatalyst may be used to lower the activation energy, but they are not mandatory.

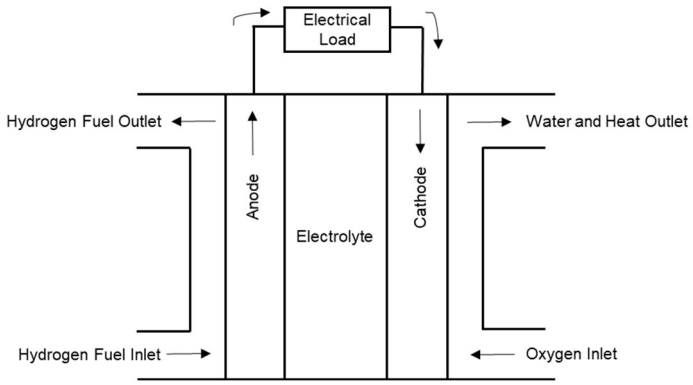

Figure 5 - Fuel cell diagram, adapted from Akinyele et al., 2020 [32].

There are different types of fuel cells, that are categorized by the type of fuel used, the type of electrolyte and based on the operation temperature. Here six categories of FC technologies that are present in the market will be presented, the proton exchange FC, alkaline FC, direct methanol FC, phosphoric acid FC, molten carbonate FC, and solid oxide FC. This section is based mostly on the review of fuel cell technologies performed by Akinyele et al., 2020 [32].

Alkaline Fuel Cells (AFC)

The AFC uses an aqueous alkaline electrolyte, composed of potassium hydroxide (KOH), and function with pure hydrogen and oxygen. The anode and cathode use nickel (Ni) and silver (Ag), with Ni also being used as a catalyst. The hydrogen and oxygen are supplied, correspondently, to the anode and cathode. The direct current is generated by the exchange of ions promoted by the KOH. The anode and cathode reactions are expressed in equations 8 and 9.

$$\text{Anode: } H_2 + 2OH^- \rightarrow 2H_2O + 2e^- \quad (8)$$

$$\text{Cathode: } 0.5O_2 + H_2O + 2e^- \rightarrow 2OH^- \quad (9)$$

The temperature of this technology has lowered with time, from 100 – 250 °C to 70 °C, and the efficiency has reached values of 60 percent in some applications. The power range of these fuel

cells is between 5 – 150 kW. The electrolyte used, KOH, brings the problems of corrosion and carbon dioxide poisoning that lowers its conduction power.

Proton Exchange Membrane Fuel Cell (PEMFC)

These fuel cells use, as a solid electrolyte, a polymetric membrane that is very thin and permeable. The electrodes use platinum. In this technology hydrogen is supplied at the anode where it is separated into electron and hydroxide protons. While the protons cross the membrane to the cathode side, the electrons are forced to flow through an external circuit, generating a direct current. In the cathode, the electrons and hydroxide protons react with oxygen and form water, this process is expressed in equations 10 and 11.

$$\text{Anode: } H_2 \rightarrow 2H^+ + 2e^- \tag{10}$$

$$\text{Cathode: } 0.5O_2 + 2H^+ + 2e^- \rightarrow H_2O \tag{11}$$

These are low temperature fuel cells, operating at close to 80°C. At the moment the efficiency of this technology is around 40 – 60 percent. They have a flexible operation range that can be suited to the load demands, while also being flexible in terms of capacity, currently ranging from 5 – 250 kW, with the great advantage of having a high-power density, >1000 W/kg. The use of a solid electrolyte leads to cheaper manufacturing, but the need of platinum catalysts has increased its costs considerably.

Direct Methanol Fuel Cell (DMFC)

This technology is, in general, very similar to the PEMFC, using some of the same materials at the electrodes, Nafion membrane and platinum (Pt). Contrary to other fuel cell technologies, the direct methanol fuel cells, does not use hydrogen as a fuel, instead they extract the hydrogen from the mixture of liquid pure methanol and steam that is introduced at the anode side. From there, the reaction results in the methanol transforming into CO_2 and hydrogen ions. The remaining process is very similar to the PEMFC, the protons pass though the electrolyte while the electrons go through an external circuit and they meet again in the cathode where, by reacting with oxygen they form water. The anode and cathode reaction of the direct methanol fuel cell are expressed in equations 12 and 13:

$$\text{Anode: } CH_3OH + H_2O \rightarrow CO_2 + 6H^+ + 6e^- \tag{12}$$

$$\text{Cathode: } 1.5O_2 + 6H^+ + 6e^- \rightarrow 3H_2O \tag{13}$$

Direct Methanol Fuel Cells are another example of low temperature system, ranging between 60−130 °C. The technology shows the lowest efficiency of all fuel cells studied here, with only 35 percent, despite that, the cheaper cost of methanol, the reduced risk of explosions and low weight have made DMFC a considered option for smaller applications, lower than 5kW.

Phosphoric Acid Fuel Cell (PAFC)

The electrolyte used in this technology is liquid phosphoric acid (H_3PO_4) with platinum being the material of the electrodes. The transport of charges is equal to the already presented PEMFC and DMFC and are expressed in equations 14 and 15.

$$\text{Anode: } H_2 \rightarrow 2H^+ + 2e^- \tag{14}$$

$$\text{Cathode: } 0.5O_2 + 2H^+ + 2e^- \rightarrow H_2O \tag{15}$$

The temperature ranges set it in the medium range, operating at around 150−220°C. The efficiency from fuel to electricity is relatively low, at 35 – 40 percent, but if combined with combined heat and power it can reach 85%. They have a simple structure and are currently used in plants of 50 kW to 11 MW. The largest economic drawback is related to the need of corrosion resistant components driven by the effects of the electrolyte.

Molten Carbonate Fuel Cell (MCFC)

The MCFC uses molten carbonate salt as the electrolyte and the electrodes are $Ni - 5Cr$ and NiO, for the anode and cathode respectively. At high temperatures the salts melt and form carbonate ions, CO_3^{2-}, that will migrate from the cathode to the anode where they will combine with hydrogen to form water, carbon dioxide and electrons. These electrons are moved from the anode to the cathode though an external circuit generating direct current. The electrolyte is replenished by the reaction combining oxygen, CO_2 and electrons to from carbonate ions. These reactions are made explicit in equations 16 and 17.

$$\text{Anode: } H_2 + CO_3^{2-} \rightarrow H_2O + CO_2 + 2e^- \tag{16}$$

$$\text{Cathode: } 0.5O_2 + CO_2 + 2e^- \rightarrow CO_3^{2-} \tag{17}$$

These are high temperature fuel cells, working at the temperature of 650 °C. The use of higher temperature leads to an increase in reaction kinetics, replacing the need for platinum catalysts. Without the inclusion of co-generation applications, the efficiency of MCFC is around 60 percent but if it is used in that context, it can have and efficiency of 80 percent. They are currently used in decentralized co-generation scenarios with electrical power around 0.1 – 2 MW. On one side lower risk of CO poisoning and the fact that it does not need an external reformer, by taking advantage of internal reforming, are strong advantages of these fuel cells, while the durability issues caused by the high temperature are the most considerable drawbacks.

Solid Oxide Fuel Cell (SOFC)

SOFC use yttria-stabilized zirconia (YSZ) as their electrolyte, a nonporous solid ceramic. As the anode and cathode, it uses, respectively, nickel-yttria-stabilized zirconia (Ni–YSZ) and lanthanum strontium manganite (LSM). In the case of SOFC, oxygen is fed to the cathode and its ions are moved to the anode by the effect of the solid electrolyte, while the electrons go through an external circuit. At the anode, the reaction involving oxygen ions and hydrogen results in the formation of water. These reactions are presented in equations 18 and 19.

$$\text{Anode: } H_2 + O_2^- \rightarrow H_2O + 2e^- \quad (18)$$

$$\text{Cathode: } 0.5O_2 + 2e^- \rightarrow O^{2-} \quad (19)$$

This fuel cells are part of the high temperature group, operating at temperatures of 800−1000 $°C$. The high temperatures show an opportunity to include them with co-generation applications, in which cases it could achieve efficiency values of 85 percent, otherwise it still has efficiencies higher than 60 percent. It is also used in distributed co-generation application, with a power capacity of 100 – 250 kW, and just like MCFC this technology can also take advantage of the internal reforming process while also suffering from high temperature corrosion problems

Comparison of Fuel Cells

The information gathered for all fuel cells is compiled in *Table 2*. Due to the early stage and the non-linear nature of the behavior of some of these options, the prices of these technologies is still based on broad estimates, with Akinyele et al. pointing to DMFC having the highest costs and SOFC and AFC having the lowest ones. At the same time PAFC are reported to have the longest life span.

Similar to electrolyzer systems, fuel cells specifically for conjugating with RES must be flexible in their operation range and in their response quickness. Madurai et al. (2021) [33], and Virij et al. (2020) [34], recommended characteristics such as high-power density, precise power, low working temperature, longevity, efficiency, good dynamic performance, and comparative ability to quickly regulate the changes in power demand. The technology that exhibits a performance closest to these characteristics is the PEMFC, with a power density of 4.2 – 35 kW/m^3, an operational temperature ranging between 50 – 100 $°C$, an efficiency that can reach 60 percent, a life span of possibly 20 000 hours and the ability to function in a dynamic setting. This is corroborated by the study performed by Inci et al. (2019) [35].

Table 2 - Overview of fuel cell technologies, adapted from [9, 28, 38]

SPECIFICATION	UNIT	PEMFC	AFC	DMFC	PAFC	MCFC	SOFC
FUEL	-	H_2	H_2	$CH_3OH + H_2O$	H_2	H_2, CO	H_2, CO
OXIDIZER	-	O_2, air	O_2, air	O_2, air	O_2, air	CO_2,O_2, air	O_2, air
MOST COMMON ELECTROLYTE	-	Perflourosulfonic acid membrane (Nafion by DuPont)	Potassium hydroxide (KOH)	Perflourosulfonic acid membrane (Nafion by DuPont)	Liquid phosphoric acid (H_3PO_4)	Molten carbonate salt	Yttria stabilized zirconia
ION TRANSFERRED	-	H^+	OH^-	H^+	H^+	CO_3^{2-}	O^{2-}
MOST COMMON ANODE CATALYST	-	Pt	$Pt\ or\ Ni$	Pt/Ru	Pt	Ni	Ni/YSZ
TEMPERATURE	$°C$	50-100	60 - 250	70-100	150 - 220	600-800	600-1000
EFFICIENCY	%	40 - 60	35-60	35 - 40	35-45	45-57	50-65
CELL VOLTAGE	V	1.1	1	0.2 - 0.4	1.1	0.7 - 1.0	0.8 - 1.0
ENERGY DENSITY	kWh/m^3	112.20 - 770.00	-	29.9 - 274	-	25.00 - 40.00	172.00 - 462.09
POWER DENSITY	kW/m^3	4.20 - 35.00	1	0.6	0.8 - 1.9	1.05 - 2.6	4.20 - 19.25
SPECIFIC ENERGY	kWh/kg	0.1 – 0.45	-	0.1403 – 0.960	-	0.012 – 0.367	-
SPECIFIC POWER	kW/kg	>1	-	-	0.120	0.012 – 0.0367	0.00105 – 0.00167
ENERGY COST	$€/kWh$	70 - 13 000	-	3067 - 3190	-	146 - 175	180 - 333
POWER COST	$€/kW$	1230 - 4609	~ 1800	12 300 - 102 500	1 107 - 2460	1640 - 3440	395 - 6560
LIFESPAN	h	2000 - 20 000	8000	>4500	>50000	7000 - 8000	> 10 000
POWER RANGE	kW	0.001 – 100	1 – 100	1 – 100	200 – 10 000	500 – 10 000	1-2000

2.4. Research and Models

The analysis in this study is performed through the modeling of the technologies presented above, in particular by creating a model capable of simulating an electrical grid's response to power imbalances, together with electrolyzer and fuel cell systems to be added to said grid. This section covers some of the research studies in these areas, presenting the publications, their scope, some of the models used and their conclusions.

2.4.1. Grid

The modeling of electrical grids, despite being a large and experienced field of study, has many different forms displayed in research that vary across the focus of the particular study and complexity levels. While being a topic in and of itself, it is also the basis for many studies akin to this one who set out to test hypothesis for different elements or parameters of grids. In the same way, the size and configuration of the grid is a significant aspect that has sparked an interest in the most recent past, part of it being owed to the referred energy transition.

Daniela et al. (2016) [14] provide a report extensively covering the functioning of the frequency control services in a detailed way. The report's scope spans from an introduction of synchronous generators and the importance of frequency stability, to a complete model capable of simulating the response to large power imbalances. The usual techniques used in system's simulation and relevant components are presented in an academic way, providing a great introduction to the topic. In a more complex analysis [23] shows the process of modeling a generator, using dump tests, and then applying it to model an island's grid. The grid model was then used to design and test a stabilizing scheme for the frequency stabilizing system, that was operational and showing positive results in combating frequency variations caused by wind power generations.

The modeling of grids and grid systems is the basis for the deeper analysis necessary to evolve the energy sector which is in a stage of evolution propelled by many forces, from sustainability to digitalization. That growth and adaptation is reflected in the research being done, one of the trends in this field's research is the impact of systems inertia on grid stability, the possible trends affecting inertia levels, and methods to combat instability. A thorough analysis is done on the concept of system inertia [20], defining it in a detailed way, from the methods used for its estimation in traditional systems to the more novel concepts of virtual inertia and the expected future of the field. In an effort to examine the impact of virtual inertia on the system, [10] produce a simple model which includes a synchronous generator's governor and turbine dynamic response, its droop control, renewable power and load inputs, together with a virtual synchronous generator. This grid model is accompanied by the introduction of an inertia monitoring process focused on its optimization. The approach taken here puts an emphasis on the fact that in the future, frequency monitoring will have to be accompanied by inertia monitoring and that in the same way there are reserves in charge of maintaining the system's frequency, an equivalent structure might be necessary for system inertia. Ulbig et al (2014) [18] presents data connecting the increase in inverter connected RES to the increased time variability of system's inertia and describes a mathematical model that describes the system's dynamic behavior after an imbalance, using it to

simulate its response to power imbalances and test its stability under a range of inertia constant values. The results, obtained under the consideration of idealized system control dynamics, show the increased instability of grid frequency, leaving the authors to suggest the addition of faster frequency control options. Daly et al. (2015) [36] tackles this challenge by proposing unit commitment and economic dispatch strategies that take this element into consideration. The main metric used in this study to assess system stability is the rate of change of frequency following a large disturbance. The authors highlight the importance of implementing inertia related policy and opening the doors for other systems that can help system stability and serve as dedicated inertia providing technologies. Homan et al. (2021) [15] looked at historical frequency data from Great Britain to understand the evolution of frequency volatility and noticed considerable growth in the years of 2017 and 2018. It is then focused on how grid stability is impacted by the quickness of the reserve's response. The conclusion was that in the future the system's reserve must be largely comprised of fast-acting systems, giving the example of batteries.

Guinot et al. (2015) [37] tackled the possibility of introducing an electrolysis-based hydrogen system in the primary frequency regulation mechanism. Based on the French regulation structure the study performed and economic analysis of the potential benefits of participating in these services from the perspective of a hydrogen production plant operator, concluding that it was not a viable operation method. Matute et al. (2019) [38] created a similar study focused on the economic feasibility of an electrolyzer-based system to provide grid services, although the topic was approached considering a much larger system, in the range of multiple MW. The question posed in this study was on how large a fleet of fuel cell electrical vehicles would have to be to make a similar project feasible through the sale of hydrogen. The results indicated the need of more than a thousand fuel cell electric vehicles, and considerably high hydrogen prices. The work of Virji et al. (2020) [34] describes the application of an electrolyzer system in the island of Hawaii for grid management purposes. Building on a previous work of grid modeling, the authors create and validate a hydrogen electrolyzer system model to test its technical and economic benefits. The study reflects the subjects of correct sizing according to the renewable power production available in the island, the setting of a sensitivity window and its impacts on electrolyzer longevity and system stability, and on the focus on different remuneration schemes. These studies show how the introduction of hydrogen technologies has the ability to be beneficial from both a technical and an economic standpoint if a correct design is made.

2.4.2. Hydrogen

The focus of those studies are the uses of hydrogen technology for grid services, and thus they are more focused on their overall performance than on technology specifics. That understanding is only possible due to complex and detailed research on the characteristics and parameters of these technologies. The development of electrolyzer and fuel cell models are currently an evolving research field. The different studies span across a multitude of software, have varied focus, and follow different methods. Here some of the research efforts will be summarized, noting trends and the ones chosen will be highlighted.

The long history of these technologies has led to a deep understanding of their static behavior, with very detailed models already developed being capable of accurately predicting their performance. A large

number of studies in this field is now focused on the modeling of their dynamic behavior and the accurate estimation of the influence of their parameters. These studies span from empirical [39], to mechanistic [40], to mathematical [41,42], from one-dimensional [41] to two or three-dimensional [43], and from static [44] to dynamic [45].

The main studies used for the development of the electrolyzer, and fuel cell models presented here divide the fuel cell in many subsystems with one of those being dedicated voltage modeling, the element of focus here. In Abdin et al. (2015) [46] a detailed model of a PEM electrolyzer is presented. In this model an anodic, a cathodic, a membrane and a voltage subsystem are created in Simulink and connected to each other to model the behaviors of each component and the impact of its properties more profoundly. The model was validated using published data and multiple tests were performed to explore the impact of external factors and material characteristics. Hernández-Gomez et al. (2020) [47] with the objective of highlighting dynamic operation issues and works focused on it, present a summary of models of the electrical domain. As a main conclusion it is highlighted the relationship between dynamic models and empirical modeling and how their inherent connection limits the acceleration of the development of a standard dynamic behavior model. It also covers the study of electrolyzer efficiency. Guilbert et al. (2018) [45] showcases an equivalent electrical model for the dynamic behavior of a PEM electrolyzer, that was compared with experimental results. Simulink was the environment used and the final model consisted of a voltage source with resistances and capacitances that was capable of accurately following both the initial and the most prolonged transient periods. Blal et al. (2019) [43] developed and tested multiple PEM fuel cell models with different parameters and compared them to each other and experimental results to see which better represented the behavior of a PEM fuel cell. The effects of temperature, humidity, limiting currents and many other parameters on fuel cell performance were simulated, presented and compared against other research's experimental tests.

Chapter 3

Methods

Models developed and used. Description of components and overall structure.

With the purpose of analyzing the potential benefits of introducing a hydrogen system in Terceira's Island grid, as a frequency management tool, models were created to test the system's behavior under a varied set of circumstances., using the Matlab/Simulink platform. The grid model will include generation and load sources modeled after the island's characteristics. Two sets of tests will be performed, one focusing on the short-term impact of a large disturbance and on the system's capability to contain it, and the other on the influence of steady-state imbalances along a day and how their effects can be mitigated by the use of hydrogen-based technology in frequency control services. In both sets of tests, the performance of the system without the addition of hydrogen-based systems will be compared to that of a system with the addition of hydrogen-based systems.

The grid model will thus have three configurations according to the test being performed.

1. The simple system – includes load, wind power and synchronous generation. The synchronous generators are the only ones responsible for keeping the system's frequency stable.
2. The electrolyzer system – has the same elements of the simple system but with the addition of an electrolyzer plant that will participate in the frequency control services.
3. The electrolyzer and fuel cell system – includes the addition of electrolyzers and fuel cells that will both participate in the frequency control services.

For all tests and configurations, the structure of this model can be divided into three connected phases:

1. Input – data from the loads and generation sources is introduced and operations are made to determine the state of equilibrium in the system.
2. Deviation – the impact of a possible imbalance in the inputs is modeled and the resulting frequency deviation is estimated.
3. Response – In the case of a frequency deviation the system responds to it using the frequency control reserves to bring balance to the system, and, in the process, altering the forecasted operation point.

In each of these phases different model elements are active. This section will follow the process of the model functioning and explain each of its components and their connections.

3.1. Inputs

3.1.1. Load

The load data used here is from the year 2012 and contains the island's power demand along a day with a resolution of 30 minutes. The data set contained load data for three days of a month from each season, in particular for a Wednesday, a Saturday and a Sunday, of the moths of May, August, October and December. Despite the sample being small the fact it is diverse, having points from different days of the week and month, is a valuable tool for analysis.

For the first test sets this load values were not directly used as, due to the nature of the test, the load profile was considered to not be relevant. The initial response to a large disturbance happens quickly, less than 30 seconds, and no information was found in similar studies that alluded to the relevance of

the amount of load or generation at the time of the disturbance. For those reasons, the load value for those tests was simply set at $30\ MW$.

For the second set of tests the load profile is very important not only for its intrinsic role but also for the development of the model. In these tests the load data was used as an input but also for the definition of a forecasted generation power profile. Due to the smaller time scale of the grid interactions the data was interpolated to have 0.1 seconds time steps. In this model, using wind speed data and load data as forecasts of their expected values in the simulation day, the forecast for the needed power generation profile of synchronous generators is created. This process is explained more extensively in the following section, regarding the model of synchronous generators. When actually starting the simulation day, variations are added to the load data in an effort to replicate the steady-state imbalances that are always present as a result of uncertainty. The size of error is extremely dependent on the location and methods used. The range of these variations was chosen following the research values of steady-state imbalances caused by load and wind power forecast errors using state of the art methods [2, 48]. The value assumed here was of 1 percent and was implemented through the use of a random number generator as expressed in equation 20.

$$P_{load} = P_{load\ forecast} * \left(1 + rand(-0.01; 0.01)\right) \tag{20}$$

3.1.2. Synchronous generation

As an input into the grid model, the synchronous generation, both from the Belo Jardim thermoelectric central and Pico Alto geothermal central, are grouped together and used as a single element. This constitutes the pooling of their capacity, their inertia and their FCR bids.

The synchronous generator's model is created using the artificial load data. Their scheduled power is defined using the load and wind power data as forecasts. Due to the priority given to wind energy in this model, the term artificial load was introduced, referring to the amount of load that is still unanswered after the wind generation at that moment has been considered. The artificial load is thus the amount of load that will be handled by the synchronous generators and hydrogen systems, this concept is expressed in equation 21 and Figure 6.

$$P_{artificial} = P_{load\ forecast} - P_{wind\ forecast} \tag{21}$$

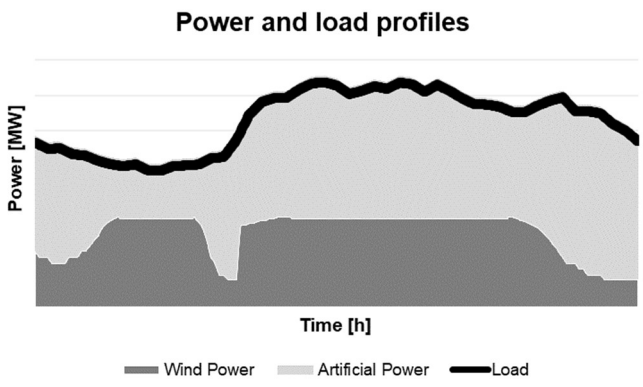

Figure 6- Load and power supply diagram, displaying the concept of artificial power.

In a simple system configuration, the forecasted synchronous power will be equal to the artificial load, equation 22.

$$P_{sinc\ forecast} = P_{artificial} \tag{22}$$

On other configurations, the forecasted synchronous load will take into consideration the load and power generation of the electrolyzer and the fuel cells systems. In those cases, the forecasted synchronous power will be expressed by equations 23 and 24, where $P_{electrolyzer\ n}$ and $P_{fuel\ cell\ n}$ represent the set nominal operation points of the electrolyzer and fuel cell systems, respectively.

$$P_{sinc\ forecast} = P_{artificial} + P_{electrolyzer\ n} \tag{23}$$

$$P_{sinc\ forecast} = P_{artificial} + P_{electrolyzer\ n} - P_{fuel\ cell\ n} \tag{24}$$

During simulations the synchronous generators will initially supply their forecasted power. When there is an imbalance between generation and demand the frequency control reserves will be activated to correct that imbalance. In most of the tests performed, for both test sets, the synchronous generators are part of that reserve. The synchronous generators' dynamic response in this work is modeled in a simplified way through the use of a ramp up limiting block to mimic their limited rate of change, saturation blocks to limit their output inside their operation range and a transport delay block to represent the reaction time of the machine's response. The block diagram applied in this model is presented in Figure 7, where the Droop Control block refers to the power adjustments made as a response to frequency deviations and will be explained in more detail ahead in Section 3.3; this approach was presented in a similar study performed by [34].

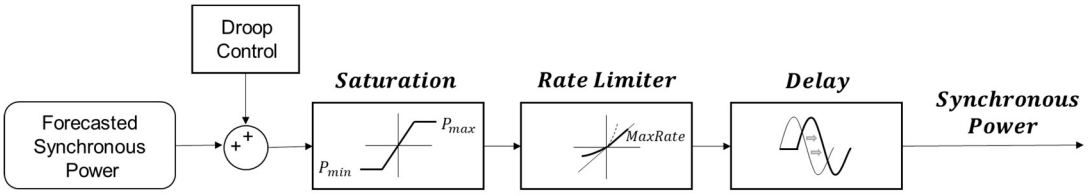

Figure 7 - Synchronous generators dynamic behavior diagram.

The values used for these parameters' blocks were taken from research studies where similar models were created, in particular [34, 49]. The maximum power limit was set at the available synchronous capacity and the minimum power limit was set at 10 percent of the maximum, although none of these limits were ever reached. The maximum rate defined for the synchronous generators was of 3 percent of its total capacity for both positive and negative slopes [16] and the turbine's time delay considered was 0.4 seconds, following [34].

3.1.3. Wind generation

To create the wind power generation model to be introduced, wind speed data at Terceira Island was gathered using the SOLCAST platform [64]. The data represented the wind speed at 10 meters high, to calculate the power that can be generated it is necessary to estimate the wind speed at rotor height. For that transformation the standard is to follow Prandtl's law, expressed in equation 25, where an estimation of the wind speed at hub height, h, is made taking into consideration defined roughness classes that are

connected to the surrounding landscape, with a scale that ranges from the surface of the water to tall city buildings. To the terrain's roughness class a specific roughness length is associated, z_0. By looking into the site's terrain the roughness class selected was equivalent to a 1.5, with the resulting value for z_0 being 0.055 meters. The remaining variables in equation 25 are the wind speed at hub height, $u(z_h)$, the height of measurement, z_1, and the measured wind speed, $u(z_1)$.

$$u(z_h) = u(z_1) * \frac{\ln\left(\frac{z_h}{z_0}\right)}{ln\left(\frac{z_1}{z_0}\right)} \tag{25}$$

According to the wind conditions wind turbines change their operation mode, having four distinct areas that are delimited by the wind speed. In the first one, at wind speed lower than cut in speed, the turbine is turned off due to the low electricity generation potential. For wind speeds higher than cut in speed and lower than rated speeds the turbine will work in its most efficient mode trying to extract the most energy possible from the wind. When wind speeds reach or surpass the rated wind speed the power output will be maximum and constant for the range in between rated and cut out speed. If cut out wind speed is reached the turbine will stop its operation to avoid damage. To calculate the wind power being generated at the Serra do Cume wind park at each moment of the studied days equation 26 was used. In equations 26, C_p refers to the turbine's power coefficient, a design dependent parameter that presents how efficient is the transformation of the energy from the wind to electricity, ρ represents the wind density, R is the radius of the turbine's rotation area and u is the instantaneous speed of the wind.

$$\begin{cases} P = 0 & u < u_{cut\ in} \\ P = \frac{1}{2} * Cp * \rho * (\pi R^2) * u^3 & u_{cut\ in} < u < u_{rated} \\ P = P_{rated} & u_{cut\ out} < u < u_{rated} \\ P = 0 & u > u_{cut\ out} \end{cases} \tag{26}$$

The values characteristic of the ENERCON E 44/900 wind turbine model were taken from the manufacturer's datasheet [65]. The turbine's power coefficient curve, with the values taken from that datasheet, is presented in Figure 8, the remaining model characteristics are presented in Table 3. The resulting wind power curve for a single turbine that was used in the model, as a basis for the wind power generation in the island, is presented in Figure 9.

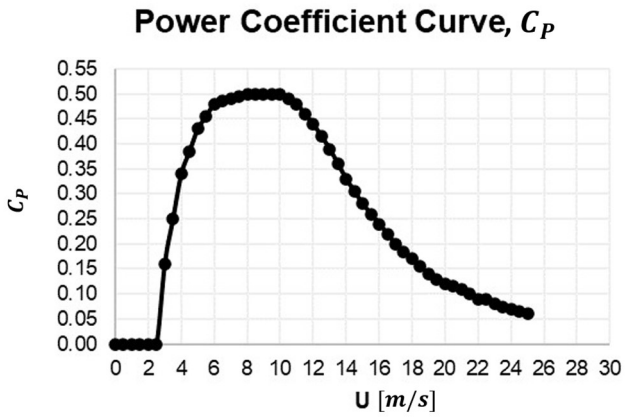

Figure 8 - Power coefficient curve of ENERCON E 44/900 wind turbine.

Table 3 - ENERCON E 44/900 wind turbine data [65].

Characteristic	Measurement	Units
Rotor Height	55	m
Rotor Diameter	44	m
Number of Blades	3	–
Rated Power	0.9	MW
Cut-in Speed	3	m/s
Rated Speed	16.5	m/s
Cut-out Speed	34	m/s

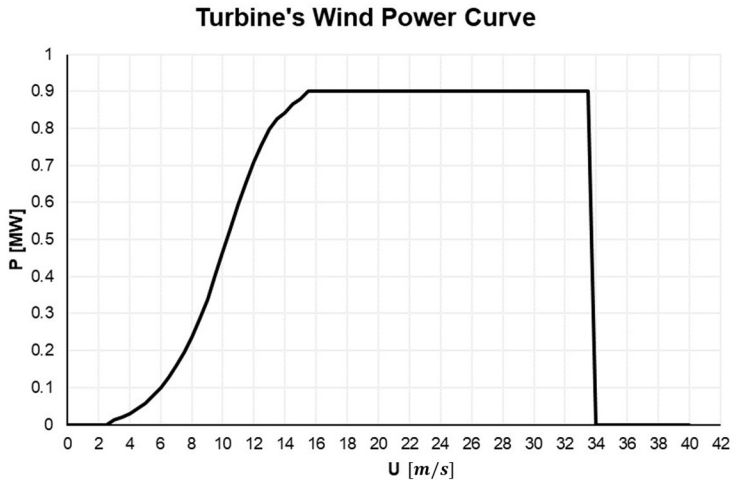

Figure 9 - Power output curve of ENERCON E 44/900 wind turbine.

3.1.4. Hydrogen Systems

The models used for the work presented here followed the ones presented in [39] for the electrolyzer model and in [50] for the fuel cell model. [39] sets out to review the available research and present a consensual model for PEM electrolyzer cell voltage modeling. It also covers, although more briefly, dynamic, and empirical models, the effects of temperature, the two-phase flow phenomenon and lists the software used in the considered research studies. Abdin et al. (2016) [50] is presented as a continuation of [46] in an effort to promote the development of hydrogen technology with the purpose of sustainability. The authors set out to progress beyond empirical dependency developing a model with parameters that are, as much as possible, connected to physical phenomena. The steady-state one dimensional model was validated using data from other studies and the relevance of various parameters was examined.

In the models of the hydrogen systems, according to the research standards present in the research, the following assumptions were made [40, 43, 46, 50]:

1. The model is one dimensional.
2. Current is uniformly distributed.
3. Temperature is uniform through the cell and the stack.
4. The humidified reactant gases are in equilibrium with liquid water.

5. Water activity at the membrane and the water activity at the anode and cathode are in equilibrium.
6. The flows are laminar and incompressible due to small pressure gradient and low Reynolds number.
7. All gases are considered ideal gases.
8. Electrode and membrane properties are homogeneous and isotropic.

Electrolyzer

The model used is a voltage model that based on the overpotentials of each cell calculated a cell's polarization curve. From there, with the assumptions of constant temperature and uniform distribution across all of the cells, the stack's power profile was estimated.

As presented in Section 2.3.2 PEM electrolyzers consist of an electrolytic membrane with an anode and a cathode on each side. For the electrolyzer to perform and produce hydrogen the DC electric power source's voltage must be higher than the thermodynamic reversible potential applied. The reversible cell potential, E_0, represents the minimum potential difference between the electrodes necessary for the water splitting reaction to occur, in a situation where the thermal energy contribution is covered and under reversible conditions. The value of E_0 can be calculated through the Gibbs free energy of the reaction, ΔG_R, the amount of energy necessary for the nonspontaneous process to take place, together with the Faraday constant, F, and n, the number of moles of electrons involved [5.3.1]. The expression used can be seen in equation 27.

$$E_0 = \frac{\Delta G_R}{nF} \tag{27}$$

Given the fact that no other source of energy is used, the electricity must provide the complete amount of energy necessary for the water splitting process. This is referred to as the thermoneutral voltage at standard state and it takes into consideration ΔH_R, the entire energy needed for the reaction to occur.

$$E_{th} = \frac{\Delta H_R}{nF} \tag{28}$$

The open circuit voltage represents the voltage necessary when the cell is in a thermodynamic equilibrium, taking into consideration the variation away from reversible voltage that happen at different operating points and is calculated through the use of the Nernst equation 29.

$$V_0 = E_{th} + \frac{RT_{el}}{2F} \ln\left(\frac{p_{H_2}\sqrt{p_{O_2}}}{p_{H_2O}}\right) \tag{29}$$

Here T_{el} is the electrolyzer cell temperature and p_{H_2}, p_{O_2} and p_{H_2O} represent the partial pressures of the H_2, O_2 and H_2O, respectively, all considered constant in this model. R is the universal gas constant and F is the Faraday constant.

The amount of energy necessary for the complete water splitting process is larger than the circuit open voltage due to the irreversible losses that ensue in the cell. These losses are caused by different

mechanisms and are generally divided into three groups and referred to as overpotentials, the activation overpotentials, the concentration overpotential and the ohmic overpotential. The polarization curve of an electrolyzer is the most used representation of its performance. The polarization curve exhibits the relationship between the cell's current and its voltage. Equation 30 is widely used to represent the polarization curve, where V_{cell} is the cell voltage and V_{act}, V_{conc} and V_{ohm} are the activation, the concentration and the ohmic overpotential, respectively. Figure 10 quantitatively expresses graphically the effect of these overpotentials.

$$V_{cell} = V_0 + V_{act} + V_{conc} + V_{ohm} \tag{30}$$

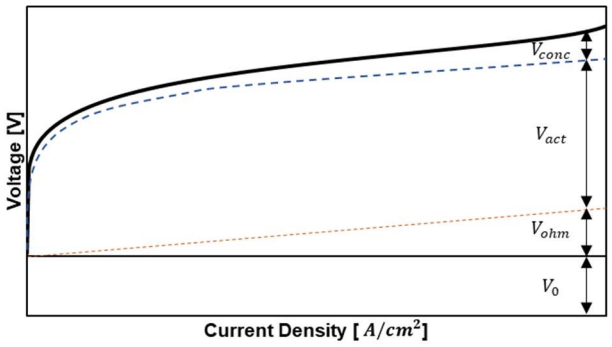

Figure 10 - Typical PEM electrolyzer polarization curve, with the separate ohmic, concentration and activation overpotentials.

Activation Overpotential

The activation overpotential is connected to the electrochemical kinetic behavior as part of the potential is sacrificed in an activation process of the electrochemical reactions. The reaction implies a change away from thermodynamic equilibrium that will reduce the speed of the reactions taking place at the electrode surface [39]. Part of the voltage applied is lost in transferring electrons into and away from the electrodes. This phenomenon is usually described using the Butler-Volmer equation 31.

$$V_{act} = \frac{RT_{el}}{n\alpha_{an}F}\sinh^{-1}\left(\frac{i}{2i_{0,an}}\right) + \frac{RT}{n\alpha_{ca}F}\sinh^{-1}\left(\frac{i}{2i_{0,ca}}\right) \tag{31}$$

Here R is the universal gas constant, T_{el} is the electrolyzer's temperature, n is the number of electrons involved in the reaction, F is the Faraday's constant, α_{an} and α_{ca} are the anodic and cathodic charge transfer coefficients, $i_{o,an}$ and $i_{o,ca}$ are the exchange current densities at the anode and cathode, and i is the cell's current density. The values used in the model presented here for these parameters are presented in *Table 4*. Activation losses are particularly present in low current density and high voltage operation.

Concentration Overpotential

At the other end of the polarization curve, at high current densities, concentration overpotentials gain a significant impact on the cell performance. These losses, often also referred to as diffusion losses, are caused by the limits of mass transport. The membrane surface will become congested with oxygen bubbles [46] that limit the access of reactants, and thus slow down the reaction rate [39, 46]. The equation 32 used to represent this overpotential is based on the i_{lim} value, the maximum current density

of the electrolyzer [39]. The remaining variables are the universal gas constant, R, the electrolyzer temperature, T_{el} and the number of electrons transferred, n, with i being the cell's current density. The values for these parameters are presented in Table 4.

$$V_{conc} = -\frac{RT_{el}}{nF}\ln\left(1 - \frac{i}{i_{lim}}\right) \tag{32}$$

The concentration overpotential is not always considered by authors due to its limited impact range, specially when considering it is most present in very high current density values, that are seldomly reached, despite that it will was introduced in the models used here.

Ohmic Overpotential

The ohmic overpotential is mainly a result of the materials resistance to the flux of protons, it is thus dependent on the material characteristics. There are other ohmic losses related to electron transport but they are not as influential. In the expression used (33), i is the current density at the cell and the resistance is constituted by the membrane thickness, δ, and by its conductivity, σ.

$$V_{ohm} = \frac{\delta}{\sigma} i \tag{33}$$

The membrane's conductivity is dependent on its hydration and electrolyzer temperature, equation 34, where λ represents the membrane water content. The values used for the membrane's thickness and water content are disclosed in *Table 4*.

$$\sigma = (0.005139\lambda - 0.00326)exp\left[1268\left(\frac{1}{303} - \frac{1}{T_{el}}\right)\right] \tag{34}$$

The ohmic overpotential displays a linear nature that can be better noticed in the middle range of current density where neither activation nor concentration overpotentials are dominating.

The polarization curve of an electrolyzer cell modeled here is presented in Figure 11, showcasing the cell's relationship between current density and voltage. As can be seen the curve shows the expected profile, with the each of the 3 specific overpotential zones being well defined, and the voltage values correspond to current research range values [39, 46, 47, 51].

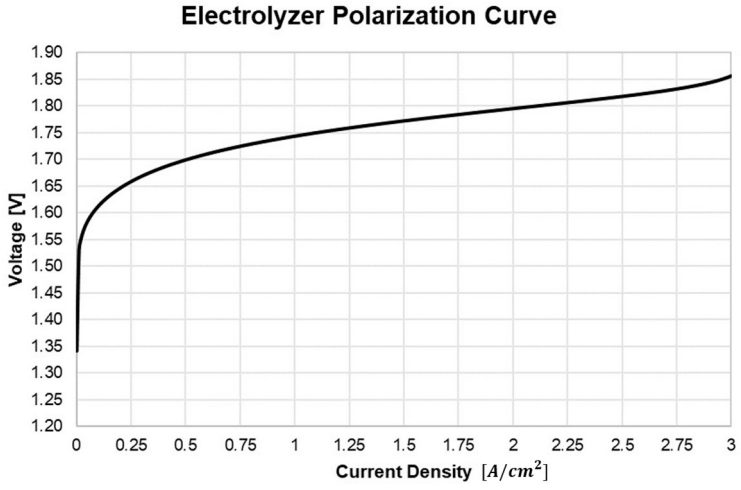

Figure 11 - Electrolyzer cell polarization curve created with electrolyzer model.

Table 4 - Electrolyzer cell model data [39].

Electrolyzer Model Data		
T_{ref}	298.15	K
T_{el}	350	K
R	8.314	$J/mol.K$
F	96485	C/mol
p_{H_2}	$30 * 10^5$	Pa
p_{O_2}	$30 * 10^5$	Pa
p_{H_2O}	$30 * 10^5$	Pa
α_{an}	0.5	-
α_{ca}	0.5	-
$i_{0,an}$	$2 * 10^{-5}$	A/cm^2
$i_{0,ca}$	$1 * 10^{-1}$	A/cm^2
i_{lim}	3	A/cm^2
δ	$50 * 10^{-4}$	cm
λ	20	-
E_0	1.229	V
E_{th}	1.481	V
n	2	-

Fuel cell

The PEM fuel cell model follows very similar principles to those of the PEM electrolyzer. In the same way, a cell's polarization curve is modeled and then the stack power profile is obtained from considering no variation along the stack. Fuel cells also have a reversible cell potential, E_0, and an open circuit voltage, V_{th}, presented in equation 35, that now represent the voltage that would be obtained if no losses were present in a situation where thermal energy is provided and one where it is not.

$$V_{th} = E_0 + (T_{fc} - T_{ref})\frac{\Delta s^0}{nF} \tag{35}$$

In the same way open-circuit voltage, equation 36, is equivalent to the amount of electricity released at a different state from standard operation conditions.

$$V_0 = V_{th} + \frac{RT_{fc}}{2F}\ln(p_{H_2}\sqrt{p_{O_2}}) \tag{36}$$

In fuel cells the overpotentials will limit the amount of power that can be produced. Identically to PEM electrolyzers the overpotentials that are most predominant are the activation, the concentration and the ohmic overpotentials, the expressions used to model these are expressed bellow in equations 37-40.

$$V_{cell} = V_0 - V_{act} - V_{conc} - V_{ohm} \tag{37}$$

$$V_{act} = \frac{RT_{fc}}{\alpha_{an}F} * ln\left(\frac{i}{i_{0,an}}\right) + \frac{RT_{fc}}{\alpha_{ca}F}\ln\left(\frac{i}{i_{0,ca}}\right) \tag{38}$$

$$V_{conc} = \frac{RT_{fc}}{2F}\ln\left(1 - \frac{i}{i_{lim}}\right) + \frac{RT_{fc}}{4F}\ln\left(1 - \frac{i}{i_{lim}}\right) \tag{39}$$

$$V_{ohm} = \frac{\delta}{\sigma}i \tag{40}$$

In these equations R is the universal gas constant, T_{fc} represents the fuel cell's temperature and F is the Faraday's constant. Additionally, α_{an} and α_{ca} represent the charge transfer coefficients of the fuel cell's anode and cathode, $i_{0,an}$ and $i_{0,an}$ are the exchange current densities at the electrodes. In the concentration overpotential $i_{\lim}$ refers to the cell's limiting current and in the ohmic overpotential δ and σ are the membrane's thickness and conductivity. In all equations 37 – 40, i represents the cell's current density.

The fuel cell cell's polarization curve is presented in Figure 12, showcasing its relationship between the voltage reached and the current density. Again, the area of impact of each overpotential is well defined, following closely the behavior of experimental and model results presented in research [40, 43, 50].

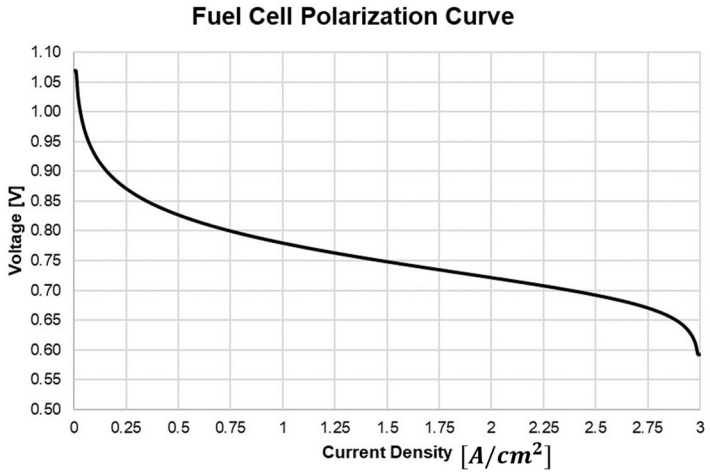

Figure 12 - Fuel cell, cell polarization curve created with fuel cell model.
Table 5 - Fuel cell model data [50].

Fuel Cell Model Data		
T_{ref}	298.15	K
T_{fc}	350	K
R	8.314	$J/mol.K$
F	96485	C/mol
p_{H_2}	$1 * 10^5$	Pa
p_{O_2}	$1 * 10^5$	Pa
α_{an}	0.7	$-$
α_{ca}	1.7	$-$
$i_{0,an}$	$3{,}5 * 10^{-2}$	$A/cm2$
$i_{0,ca}$	$1 * 10^{-1}$	$A/cm2$
i_{lim}	3	$A/cm2$
δ	$50 * 10^{-4}$	cm
λ	20	
E_0	1.229	V
p_{H_2O}	$1 * 10^5$	Pa

3.2. Deviation

The different components presented above will interact from their respective sides, generation and consumption, and the power balance, ΔP, will be determined. This operation is expressed in equation 41, where P_{gen} and $P_{T\ load}$ represent the generation and total load power respectively, expressed in equations 42 and 43.

$$\Delta P = P_{gen} - P_{T\ load} \tag{41}$$

$$P_{gen} = P_{sinc} + P_{wind} + P_{fuel\ cell} \tag{42}$$

$$P_{T\ load} = P_{load} + P_{electrolyzer} \tag{43}$$

ΔP will be the input for the calculation of the frequency deviation which will be determined, taking into account the system's characteristics, through the application of the equation of motion, here explained in detail.

3.2.1. Equation of Motion

The equation of motion, often also referred to as the swing equation, is used as the representation of synchronous machine's dynamic behavior [19]. As expressed in Section 2.2 this response is connected to the kinetic rotational energy stored in the rotating masses of synchronous generators, expressed here in equation 44 [18–20, 52], where J is the mass's moment of inertia and f_m is the machine's rotating frequency.

$$E_{kin} = \frac{1}{2} J (2\pi f_m)^2 \tag{44}$$

The inertia constant, H, studied here is measured in seconds and represents the amount of time the rotor's kinetic energy can supply its rated power. In that sense, with S_B being the generator's rated power, H can be calculated by equation 45. The research values considered for the inertia constant of synchronous generators are in the range of $3 - 9\ s$ according to the consulted studies [10, 20, 53, 54].

$$H = \frac{E_{kin}}{S_B} = \frac{J\ (2\pi f_m)^2}{2 S_B} \tag{45}$$

A synchronous system's response to a power imbalance is modeled with the equation of motion as a change in rotational frequency, $w_m = 2\pi f_m$. The machine's change in kinetic energy caused by a deviation from power balance is expressed in equation 46 [18], where H is the machine's inertia constant, S_B is its rated power, f_m is its rotating frequency, $\frac{df_m}{dt}$ is the rate of change of said frequency and P_m and P_e are the mechanical and electrical powers of the generator.

$$\dot{E_{kin}} = J(2\pi)^2 f_m \left(\frac{df_m}{dt}\right) = \frac{2HS_B}{f_m}\left(\frac{df_m}{dt}\right) = (P_m - P_e) \tag{46}$$

The naturally occurring system response to a large power imbalance is the result of pooling the individual responses of all the machines in the grid. Each machine's frequency will approach the system's

frequency as their individual dynamic response reaches an end, $f_m \longrightarrow f$. The individual inertia and rated power contributions can be lumped together to define the system's characteristics and simplify the calculations of its response. The systems inertia, H_{sys}, is determined by the amount of inertia each of the active producers provides in relation to its weight in the system's total power. The negative impact of converter connected RES on system inertia can be clearly seen here as their power will substitute other power provider's but not their inertia.

$$S_{B_{sys}} = \sum_{\forall i} S_{B_i} \tag{47}$$

$$H_{sys} = \frac{\sum_{\forall i} H_i S_{B_i}}{S_{B_{sys}}} \tag{48}$$

The complete system's reaction to a power imbalance can thus be analyzed by considering the system's inertia, its total power and studying the frequency changes caused by imbalances between its total load and its power generation. The system's dynamic response can thus be modeled by the use of equation 49, where f is the systems measured frequency and f_0 is its nominal frequency. P_{gen} and P_{load} are respectively the power being generated and the power being consumed, and H_{sys} and $S_{B_{sys}}$ are the system's inertia constant and its total power capacity.

$$\frac{df}{dt} = \left(P_{gen} - P_{load}\right) \frac{f_0}{2H_{sys}S_{B_{sys}}} \tag{49}$$

The implementation of this relation in the Simulink environment was done by applying the Laplace transform, resulting in equation 50, with Δf representing the change in frequency caused by the power imbalance presented as ΔP and s being the Laplace variable.

$$\Delta f = \Delta P \frac{f_0}{2H_{sys}S_{B_{sys}}s} \tag{50}$$

3.2.2. Load Damping

In electrical systems some of the loads are dependent on the grid frequency. These loads have a positive impact on grid stability as they will act as a damping mechanism, lowering their individual load when the system's frequency goes under its nominal value and vice-versa. This effect is referred to as load damping and is usually expressed in terms of a percentage, representing the amount of change in load according to a one percent change in frequency. Usual values for load damping are around or lower than 1 percent, which would mean a one percent value change in frequency will lead to one percent change in load [14, 20, 53].

This phenomenon is expressed in equation 51, where D is the load damping coefficient, Δf is the frequency deviation from its nominal value and ΔP is the resulting change in load. Here the load damping coefficient was not expressed in terms of percentage but directly in terms of load change per frequency deviation, with the value chosen for D in this model being $0.6\ MW/Hz$.

$$\Delta P = D\ \Delta f \tag{51}$$

This was applied in the grid model through a feedback loop that is connected to the system's frequency and the load. The block diagram application is expressed in the diagram of Figure 13.

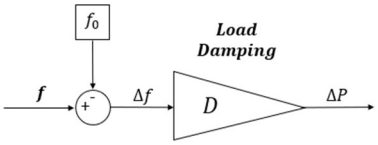

Figure 13 - Load damping block diagram.

3.3. Response

In the event of a considerable frequency deviation the system's reserves will be activated. As covered in Section 2.2 the system reserves can be explained as a capacity amount that is dedicated to balancing the system's frequency. In this model the system reserves refer to, according to the configuration being used, the synchronous or hydrogen system's capacity that is kept available to respond to power imbalances in the system. The reserves in this model are made to mimic the FCR in functioning and purpose.

In the model presented here the available reserve is simply the sum of each of the system's contributions with no limitations being enforced and no prioritization of technologies. The starting point for the size of reserve is that of usual reserve values in islanded grids, around 20-30 percent of peak load [66]. Additionally, no minimum qualifications are considered for system's participation in an effort to test a diverse set of scenarios.

The actual response to a frequency deviation is made separately by each technology. The electrolyzer system will work from the demand side, changing the amount of load it uses, while the synchronous generators and fuel cell systems will work from the supply side, altering the amount of power they produce. They will all use the same mechanism although with different bid values. They will apply a droop control mechanism, the standard for FCR. In droop control the change in operation point is performed through the engagement of a linear relationship between frequency deviation and power. In this way a frequency deviation will lead the reserve's system to slide along a drooped line, as can be seen in Figure 14. The slope of this line is defined by the droop control characteristic, which in this model is set according to the bid and the value set for maximum frequency deviation, the calculation of this parameter is expressed in equation 52, with P_{bid} corresponding to the capacity that was allocated for FCR, usually defined by the bid made, and Δf_{lim} to the set maximum frequency deviation, the point where the complete bid must be activated. This droop control characteristic is also referred to as the frequency bias [14]. While in the tests performed, the value of P_{bid} is changed between tests and according to the technology, the value of Δf_{lim} is equal in all the simulations, having been set to $200\ mHz$, a value used in similar studies [14, 23]. The signal of the frequency bias is defined according to the side the technology is working from, either supply or demand, with supply side reserves having a negative droop and demand side reserves having a positive droop.

$$B = \pm \frac{P_{bid}}{\Delta f_{lim}} \tag{52}$$

Figure 14 demonstrates the different behaviors of supply side reserves and demand side reserves. In this figure f_0 represents the nominal frequency, Δf_{lim} is the maximum frequency deviation limit, P_n is the set power point and P_{bid} is the bid capacity. As illustrated the supply side reserve, with their negative droop, will lower their output power in the case of a frequency increase and vice-versa, while the demand side reserves will perform an equivalent action but from another perspective, increasing their power consumption for increased system frequency and lowering it for a decrease in frequency.

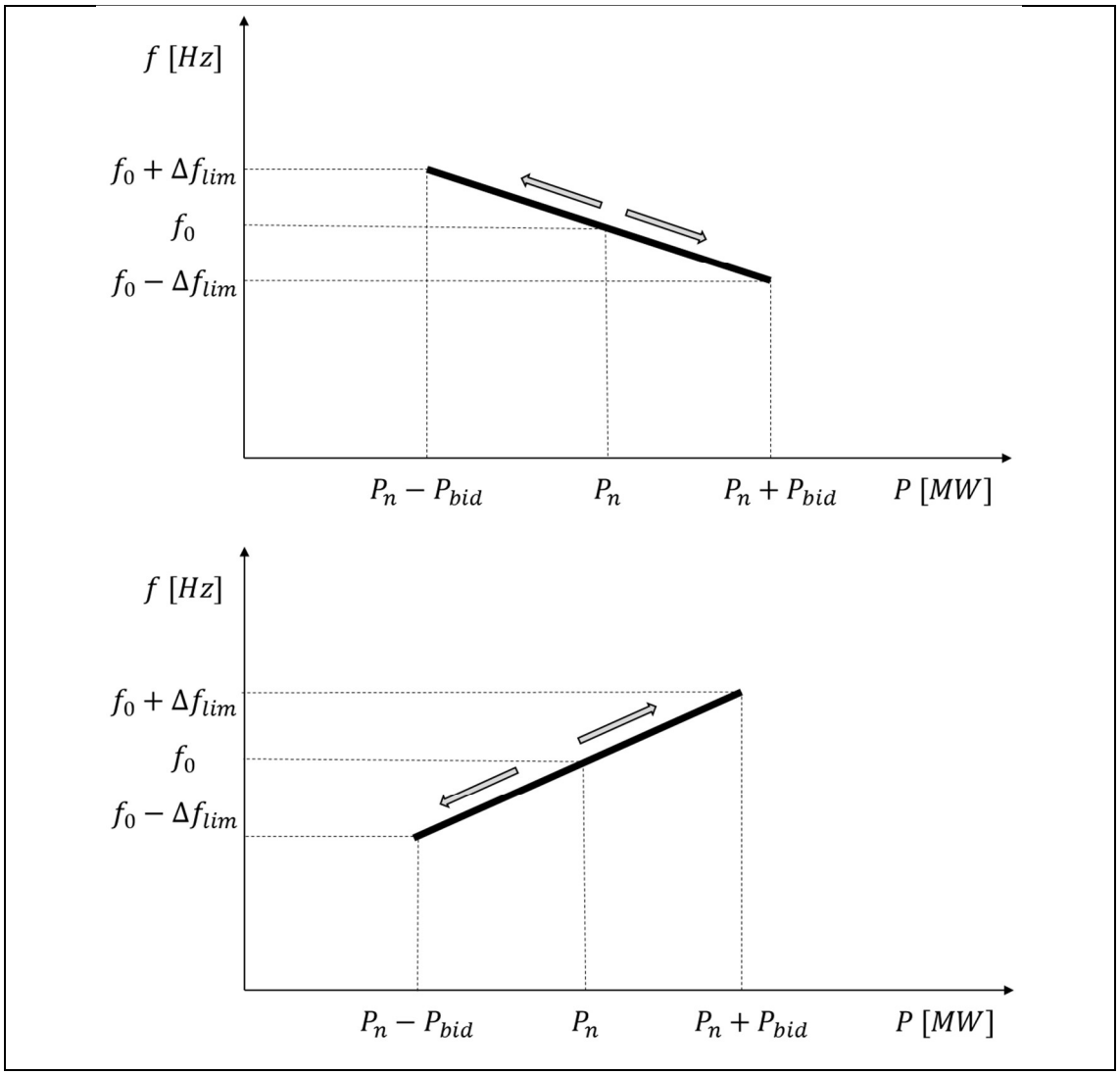

Figure 14 - Droop control diagram for a) negative droop and b) positive droop, representing the droop control behavior from the supply and from the demand side.

As already expressed, the action performed by the FCR reserve will be proportional to the frequency deviation, with B being the slope. The reserve action, the change in power, is thus calculated using equation 53, where Δf is the frequency deviation, B is the frequency bias and ΔP is the resulting power change action of the reserve.

$$\Delta P = B \Delta f \tag{53}$$

As grid frequency fluctuates a lot, constantly varying around the nominal frequency values, the response of reserves has a sensitivity deadband to limit continued and successive ramp ups and downs. In this way, as presented in Figure 15, for a negative frequency bias, the reserve's response will have a sensitivity window that, for each side, is defined between the deadband limit and the maximum deviation limit. The deadband window considered in the models used here is between -10 and $10\ mHz$, following the usual values set for this parameter.

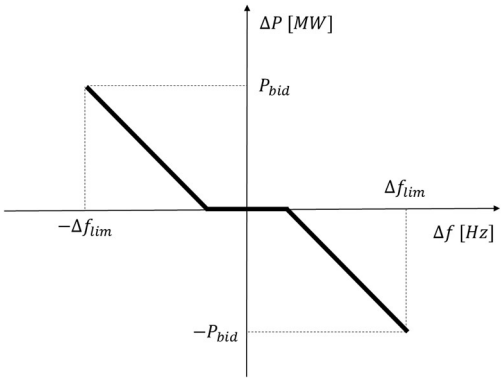

Figure 15 - Droop control output diagram for negative droop.

The droop mechanism was applied in the model using a feedback loop that connects the systems frequency to the power, either the synchronous generators, the electrolyzers or the fuel cells. The branch used is exemplified in Figure 16, including its deadband block which controls the sensitivity of the response, the frequency bias, B, and the saturation point of the bid, limiting the output of the reserves to their minimum and maximum, $-P_{bid}$ and P_{bid}. The remaining variables in the diagram are the instantaneous system frequency, f, the nominal system frequency, f_0, the corresponding frequency deviation, Δf, and the resulting power change ΔP.

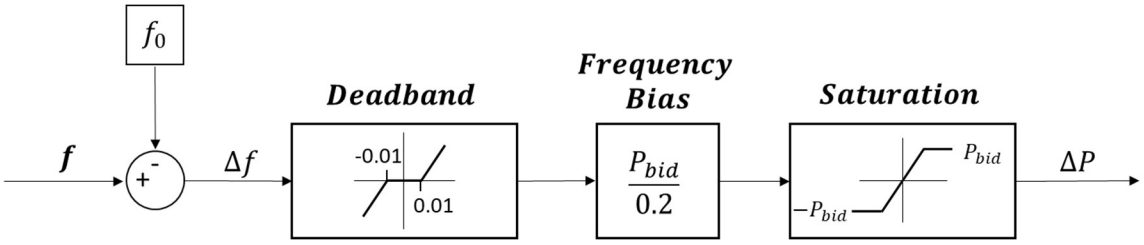

Figure 16 - Droop control diagram.

3.4. Grid Model

In this section the grid model that connects the many components described above is presented. The model design is similar for all the tests performed; a simple diagram of it is presented in Figure 17. As can be seen the loads and the power sources are summed up inside their groups and a balance is made between their total instantaneous values. The resulting imbalance of power, ΔP, will lead to a frequency deviation, Δf, that is calculated following the principles of the Equation of Motion. The frequency rate of change will drive the system frequency, f, away from its nominal value and the droop control loops will be used to adjust the power, through the system's reserves, and bring the system back into an equilibrium state.

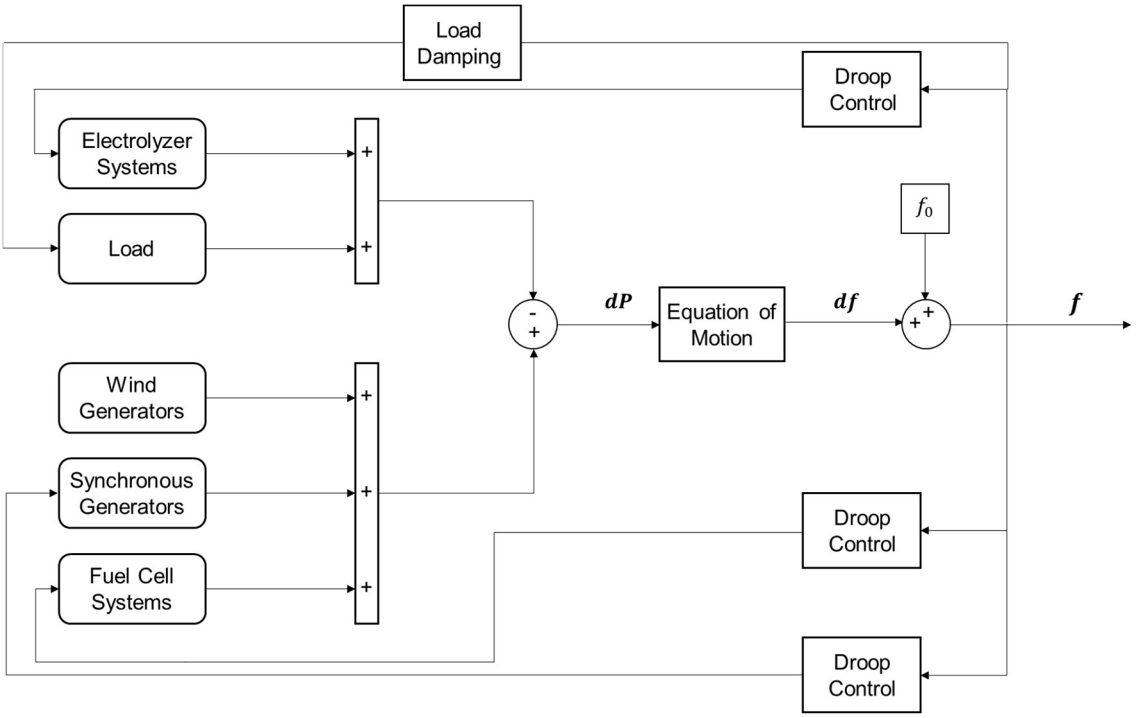

Figure 17 – Complete grid model diagram.

3.4.1. Model Limitations

This is a simplified model of an electric system and its frequency dynamics, created in Matlab/Simulink. In this model no controllers were included, leading to limitations in simulating the transitional periods of the power output of the reserves, which demonstrated overshoots followed by power oscillations before settling down. Despite of this the model is capable of correctly simulating the here focused behaviors of the system when responding to power imbalance, the initial power and frequency response, the performance of different parameters and the steady state reached after the system is stabilized.

3.4.2. Electrolyzer Equivalent Inertia

As presented in the beginning of this section the tests will be performed using different configurations of this model that range from not including any of the hydrogen systems, to including the electrolyzers or both the electrolyzer and the fuel cell systems. While these types of tests have been performed multiple times in research studies, to the authors knowledge there has not been any study that developed a metric connecting the results achieved by the presence of the hydrogen technologies and those achieved by increased inertia. With that purpose, one of the contributions of this work is to present the developed Electrolyzer Equivalent Inertia (EEI) metric.

This metric is calculated using the changes in frequency deviation, achieved by changes in the system's inertia and electrolyzer power, to estimate a relationship between the influences of each. The basis for this is the frequency deviation, Δf, calculated with equation 54, where f_0 stands for the nominal frequency and f for the frequency reached at the peak of a deviation.

$$\Delta f = f_0 - f \tag{54}$$

Changing the values of system inertia and electrolyzer power will have an effect on the variations achieved. The changes in Δf are calculated across levels of system inertia and electrolyzer power with the use of equations 55 and 56, respectively, with Δf_H and Δf_{Pel} being the frequency deviation changes caused by an increment in inertia constant and in electrolyzer power, respectively.

$$\Delta f_H = \Delta f(H_{i+1}) - \Delta f(H_i) \tag{55}$$

$$\Delta f_{Pel} = \Delta f(Pel_{i+1}) - \Delta f(Pel_i) \tag{56}$$

Using the average values of these frequency deviation improvements for each parameter a trend can be extrapolated between the size of frequency deviations and both, the system's inertia constant, and the hydrogen power in FCR. These averages were calculated using equations 57 and 58, where n is the number of reference points for each calculation. In equation 57, $\Delta f_{Pel_{avg}}$ refers to the average of Δf_{Pel}, the frequency deviation improvement caused by an increase in electrolyzer power in FCR. In equation 58, $\Delta f_{H_{avg}}$ refers to the average of Δf_H, the frequency deviation improvement caused by an increase in inertia constant.

$$\Delta f_{Pel_{avg}} = \frac{1}{n} \sum \Delta f_{Pel}(i) \tag{57}$$

$$\Delta f_{H_{avg}} = \frac{1}{n} \sum \Delta f_H(i) \tag{58}$$

The average improvement caused by an increase in system inertia and electrolyzer power can then be calculated with equations 59 and 60, which define the terms Impact of Electrolyzer Power (IEP) with the use of the average frequency deviation improvement cause by electrolyzer power, $\Delta f_{Pel_{avg}}$, and the correspondent electrolyzer power increment, ΔPel, and the Impact of Inertia Constant (IIC) with the use of the average frequency deviation improvement cause by increased inertia, $\Delta f_{H_{avg}}$, and the corresponding inertia increment, ΔH.

$$IEP = \frac{\Delta f_{Pel_{avg}}}{\Delta Pel} \tag{59}$$

$$IIC = \frac{\Delta f_{H_{avg}}}{\Delta H} \tag{60}$$

The Electrolyzer Equivalent Inertia, EEI, can then be calculated with the use of these two measurements using equation 61, representing, from the perspective of frequency deviations, the amount of system inertia that can be substituted by hydrogen technologies' power.

$$EEI = \frac{IEP}{IIC} \tag{61}$$

Chapter 4

Simulations and Results

Presentation and analysis of simulation results.

The model presented in Chapter 3 was used to perform simulations of multiple scenarios in an effort to evaluate the impact and benefits of changing the system's configuration. With that purpose two different sets of tests were performed to study the frequency response behavior of the system in two distinct situations. The first set of simulations covered the reaction of the system's frequency to a large disturbance while the second touched on the response to everyday steady-state imbalances. Each simulation set will reflect on different aspects of system stability. The first simulation set will cover the relevance of parameters related to the short-term frequency stability of the system, being tested here through its response to large disturbances. The second simulation set will evaluate the performance of frequency control along a day when the system must respond to steady-state imbalances caused by load and wind power forecast errors.

The simulations will be performed using the models presented in Chapter 3 in one of three different configurations: the simple configuration, used as the baseline, comprised of the island's load, the synchronous generators and the wind power generation; the electrolyzer configuration, which adds the electrolyzer systems to the simple configuration; and the electrolyzer and fuel cell configuration, which has the addition of the electrolyzer and fuel cell systems compared to the simple configuration. These three configurations are used to compare the frequency response of different systems to similar situations and analyze how the presence of additional technologies can be impactful for frequency stability. Additionally, these results will be a reflection of the model that was created, and for that reason part of the analysis will also touch on the limitations of this model.

4.1. Simulation set 1 – large disturbance response

Simulation set 1 is meant to evaluate the short-term frequency response of the system to a large disturbance, in particular the initial inertial response and the FCR response. Each simulation will have a duration of 30 seconds. At the beginning of each simulation the system will be at an equilibrium state with power generation and consumption sources having the same value. At second 5 a disturbance will be introduced and cause an imbalance between generation and consumption. The imbalance, as explained before, will cause a variation in system frequency that will be felt and answered by the system reserves.

The initial values for load, referring to the island's load without considering the electrolyzer systems, and generation, considering the synchronous generators and wind power generation without a fuel cell, were set to 30 MW and are not changed as the consulted research and additional simulations did not point to there being an effect caused by these parameters. The disturbance introduced was an increase in load of 5 MW which will lead to a decrease in frequency and force an increase in the power production side. No simulations from the opposite side, larger production than demand, will be presented as the results do not qualitatively differ from the ones of the situation represented here, due to the symmetric nature of the model, thus not adding to the analysis.

This set of tests is expected to clarify the influence of the system's inertia constant on the frequency stability. Additionally, it will also cover how the synchronous machines' ability to respond to power imbalances can be limited by their capacity to quickly change their power output. From there, the introduction of electrolyzers and fuel cells, with their shorter response times, will be considered. Their influence on stabilizing the system's frequency will be analyzed and put into question the possibility of replacing synchronous machines in the FCR.

Regarding the system's response to a large disturbance, after analyzing the results of the simulations presented, the answer to the following questions should be clear:

- What is the impact of inertia on frequency stability?
- Can hydrogen technologies have a considerable positive impact on frequency control?
- If so, how do they compare to synchronous generators in the provision of FCR services?
- Is there a way to quantify the potential benefits of hydrogen technologies on frequency control?
- What is the best configuration for frequency stability?

To measure the results of simulations this set of tests will use the frequency nadir (FN) and initial rate of change of frequency (RoCoF). The FN is defined as the frequency value where the absolute distance to the nominal frequency reaches its maximum after the disturbance, in this case, since the disturbance will cause a decrease in frequency, it will be determined as the minimum frequency after the disturbance. The RoCoF is defined here as the frequency change in the first 500 ms after the disturbance is introduced at second 5 [23], these are defined in equations 62 and 63.

$$FN = \min(f) \tag{62}$$

$$RoCoF = f(5.5) - f(5) \tag{63}$$

4.1.1. Simple Configuration

The starting point for this analysis is the current state of the Terceira island's grid, which is modeled here, as presented in Chapter 3, in the simple configuration. This section will reflect on the different aspects of this simple configuration covered in the simulations, presenting and analyzing its results, focusing in particular on the impact of the system's inertia constant on frequency stability, covering a range of values that represent its decrease and its possible improvements. Another focus is the considered ramp rate of synchronous generators, with test results showcasing the importance of correct definition of this parameter in research and consequential judgement of measures.

Inertia Constant

This work was developed as an effort to evaluate options to mitigate the degradation of system frequency stability based on the effects of lowered system inertia. The system's inertia constant is expected to decrease because of the transition from traditional synchronously connected generators to converter connected power sources. To evaluate the impact of this transition tests

were made considering a range of values for the inertia constant of the system, H. The range of values for these tests was chosen from the inertia constant values being considered in research studies [10, 20, 53], 54], and lay between 3 and 9 seconds.

These tests demonstrate the response to a 5 MW disturbance with a reserve capacity of 8 MW and a synchronous ramp rate of 3%. The system's power response to this imbalance is presented in Figure 18, including the variation of power output and load along time for an inertia constant value of 6 seconds. Firstly, it is important to highlight that these results display one of the weaknesses of the model, connected to its simplicity, and that is the lack of controllers to control the output of the reserves and avoid the pendular response displayed. Nevertheless, it is capable of correctly simulating the initial inertial reactions of the system, the initial response of the FCR systems and the final frequency and power outputs reached at the end of the FCR response, at multiple levels of inertia, as will be presented.

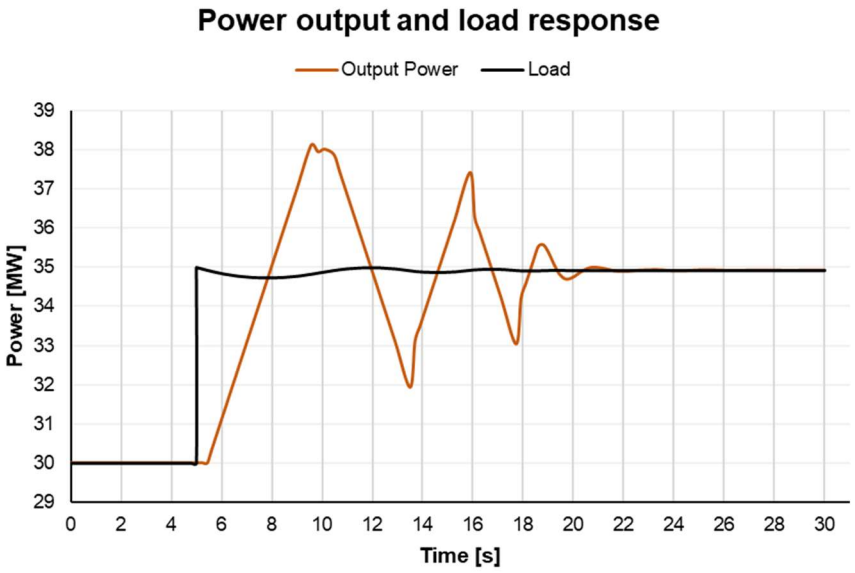

Figure 18 - Load and power output of the grid after a large disturbance for an inertia constant of 6, a ramp rate of 3% and a FCR of 8 MW of synchronous power

This time evolution demonstrates correctly the initial response of the FCR, increasing its power to match the increase in load. At the same time the load can be seen to slightly lower the power being demanded, which corresponds to the load damping effect explained in section 3.2.2

The frequency evolution during this period can be seen in Figure 19, together with the frequency evolutions for the studied range of inertia constant values. Additionally, Figure 20 displays the reached values of FN and RoCoF for each of the curves in Figure 19. These results display the clear relevance of system inertia and demonstrate its impact on the system's frequency. As can be seen in Figure 20 the values for FN and RoCoF change substantially with the decrease of inertia, having a considerably negative impact. Additionally, it has to be noted that the system's response does not have a linear relationship with the system's inertia, showcasing larger impact at the lower range of inertia values than at the higher range. Considering 6 seconds as the

reference point for the inertia constant it can be seen that a 50 percent decrease will lead to an 86.6 percent higher frequency deviation and a RoCoF that is 96.5 percent larger, while a 50 percent increase only results in a 68.7 percent smaller frequency deviation and a 46.4 percent smaller RoCoF, demonstrating the diminishing returns of increasing system inertia past a certain point.

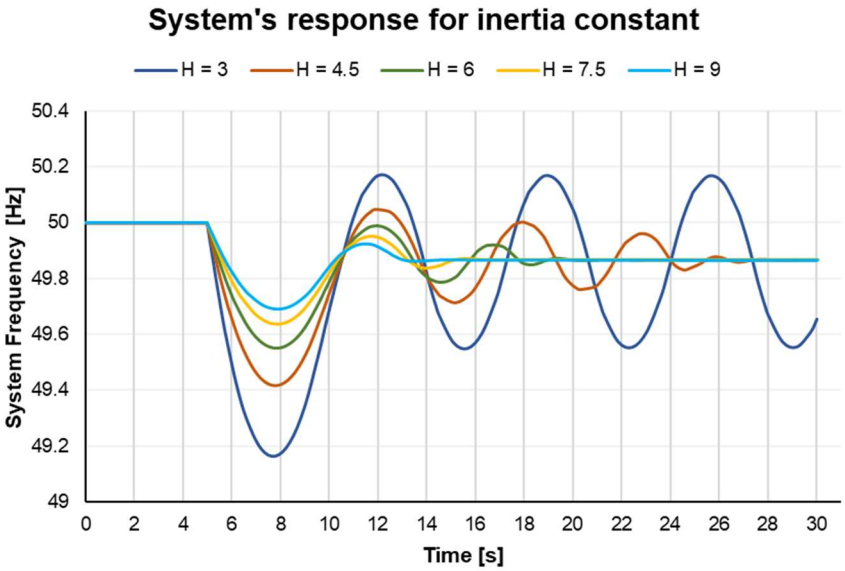

Figure 19 - Time evolution of the system's frequency after a large disturbance for multiple values of its inertia constant.

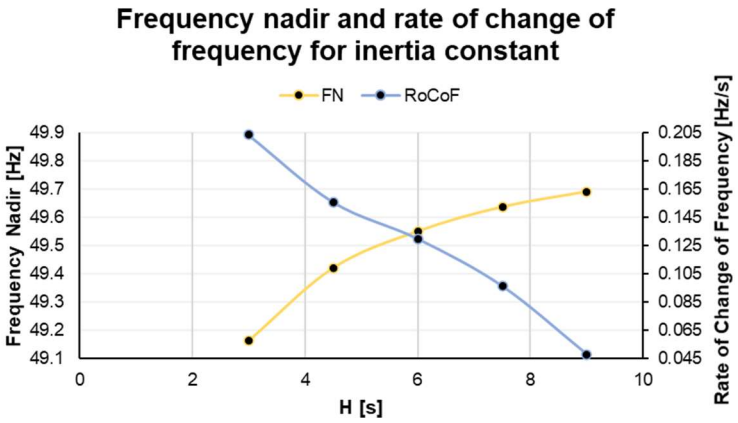

Figure 20 - Frequency nadir and rate of change of frequency values for multiple values of the system's inertia constant.

This first test confirms what has been described in this work, lowering system inertia has a negative impact on frequency stability. The dilution of this property has a direct and considerable impact on frequency stability that increases with its decline. The following tests will reflect on possible ways to mitigate these effects. These tests will use the reference value of the inertia constant, 6 seconds.

Synchronous generators ramp rate

When responding to large sudden imbalances the ability to alter power output quickly is one of the bottle necks that restricts machines' participation in frequency control services. Being capable of responding quickly to the disturbance, preventing the frequency deviation from escalating will limit its impact, dampen the RoCoF and avoid possible larger damages to the system. This is one of the expected benefits of the hydrogen technologies being considered. Their lower response times are expected to help the system's response in a more effective way than synchronous generators.

The simulation results presented in Figure 21 demonstrate the impact of having a higher response ramp capacity. In this figure are presented the responses of the system when considering a synchronous generator ramp rate of 3 percent and of 15 percent of the system's power capacity which, in the applied case of Terceira Island, would be equivalent to a rate of change of 1.9 MW/s and 9.7 MW/s, respectively. Looking at Figure 21 and Table 6 a noticeable difference in the FN reached is evident, with the lower ramp rate letting the frequency deviation reach almost two and a half times the size of the deviation achieved with the higher ramp rate. Despite in both cases the reserves having the ability to respond and contain the deviation, the lower FN reached with the 3 percent ramp rate, can be detrimental to the systems, in two ways: in the first place, reaching lower frequency values can either result in a cascade effect of complications or unnecessarily trigger additional security measures, and secondly, as can be seen in Figure 21, the settling time after an imbalance will be larger, resulting in more time under non-nominal conditions which could be a damaging factor for connected systems. On the other hand, this machine's parameter does not seem to impact the RoCoF in a significant way, which could indicate, together with the inertia constant tests presented above, an exclusive relationship between this specific system's response measurement and its inertia.

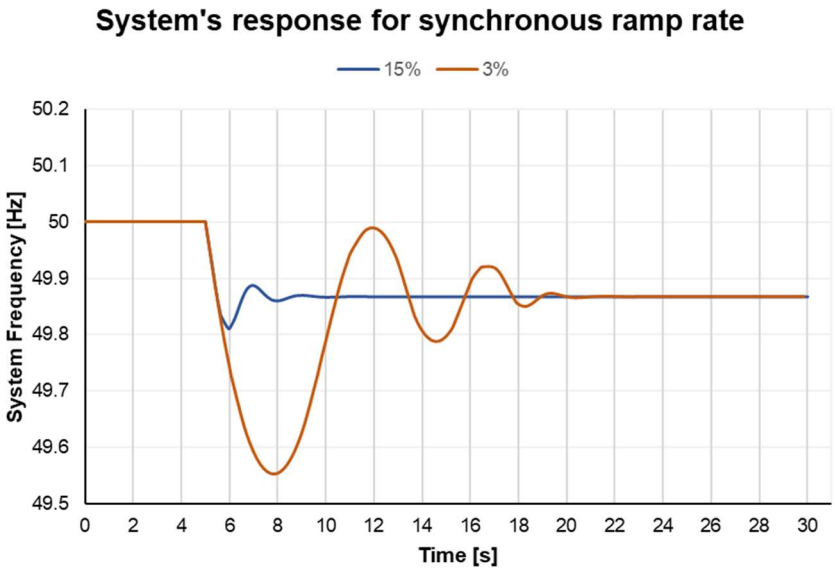

Figure 21 - Time evolution of the system's frequency after a large disturbance for two values of synchronous generator's ramp rate.

Table 6 - Frequency nadir and rate of change of frequency values for two ramp rate values of synchronous generators

Ramp Rate of Synchronous Generators	Frequency Nadir [Hz]	Rate of Change of Frequency [Hz/s]
15%	49.81	0.104
3%	49.55	0.103

The power output for these two cases is presented in Figure 22, showcasing the faster response of the synchronous machines in the FCR due to the ability to increase power output faster. It also highlights again how the time spent under a transitory condition would be smaller.

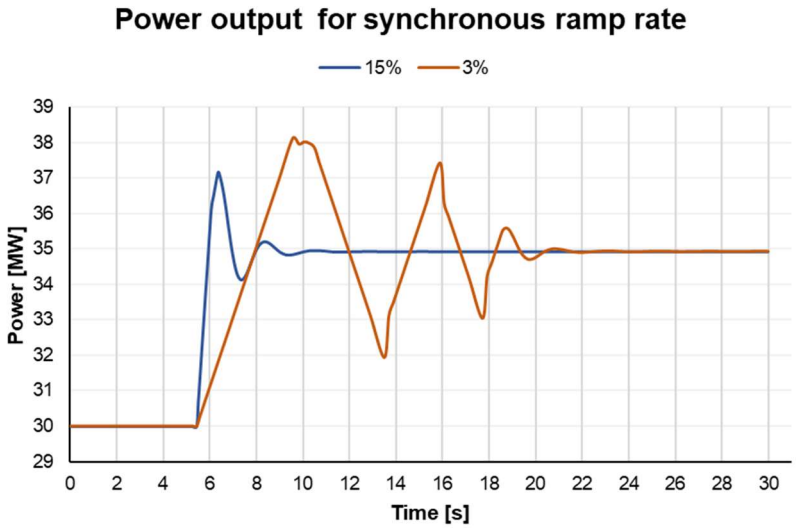

Figure 22 - Power output for two values of synchronous generator's ramp rate when responding to a large frequency disturbance.

4.1.2. Electrolyzer Configuration

The electrolyzer configuration consists of adding an electrolyzer system to the simple configuration already studied above. The addition of this hydrogen technology plans to take advantage of its faster response times to help improve the system's response. Here the electrolyzers and fuel cells are modeled to have a response time of 0.1 seconds, four times faster than the synchronous generators [34, 39]. The addition of the electrolyzer system is expected to have an impact particularly on the FN reached since it will be an equivalent to a faster system response while not having an impact on RoCoF as it is not an inertia providing technology.

For these simulations the same size of disturbance was considered, 5 MW, and the synchronous generators ramp rate was set to 3 percent. The FCR is shared by the synchronous generators, who initially provide 8 MW of power, and the electrolyzer system whose power will vary between simulations. At each of these simulations the electrolyzer will be set to function at a fraction of its maximum power so it has the ability to perform FCR services on both the supply and the demand side, lowering and increasing its power, respectively. The electrolyzer system will thus have two

parameters, its power and its FCR bid window, referring, respectively, to the electrolyzer's maximum power and the percentage of it that will be dedicated to the FCR. The window of FCR bid is given as a percentage value, for example, a 25 percent window indicates the electrolyzer will initially function at 75 percent of its maximum power and its bid to the FCR will be 25 percent of its maximum power, for both cases of frequency increase or decrease. In the case studied here, a frequency decrease, the electrolyzer is expected to lower its power consumption as a response, which for the example of a 25 percent bid window means it will be functioning between 75 and 50 percent of its maximum power. The use of this FCR bid window, despite not being covered here, is a common procedure in the design of these systems, to limit the participation in the FCR so not to hinder the production of hydrogen, and a topic of discussion in similar research projects [34]. From here forward, unless explicitly referred, the amounts of power presented refers to the electrolyzer's capacity bid to the FCR, 25 percent of what would be its nominal power.

The results from the simulations representing the addition of increasing amounts of power from the electrolyzer in the FCR are presented in Figure 23 and Figure 24. These results fit the initial expectations of lower frequency deviations. The impact of the electrolyzer system on the containment of frequency deviations is apparent and significant with each increment of electrolyzer power. As what was expected after seeing the previously displayed results, these technologies impact the FN, but their presence does not have a considerable effect on the RoCoF. From this data it can be said that the addition of an electrolyzer system with 1 MW of power and a bid window of 25 percent, which can be translated to an electrolyzer bid of 0.25 MW, will lead to a frequency deviation improvement of 0.0327 Hz, 7 percent of the total deviation. Additionally, from the points gathered, the improvements in FN seem to have a close to linear dependency on the electrolyzer power. These incremental improvements, as can be seen in Figure 23, not only avoid the system's frequency reaching lower values but also result in a lower settling time after the response to the deviation and a marginal improvement in the frequency reached after reaching a steady state.

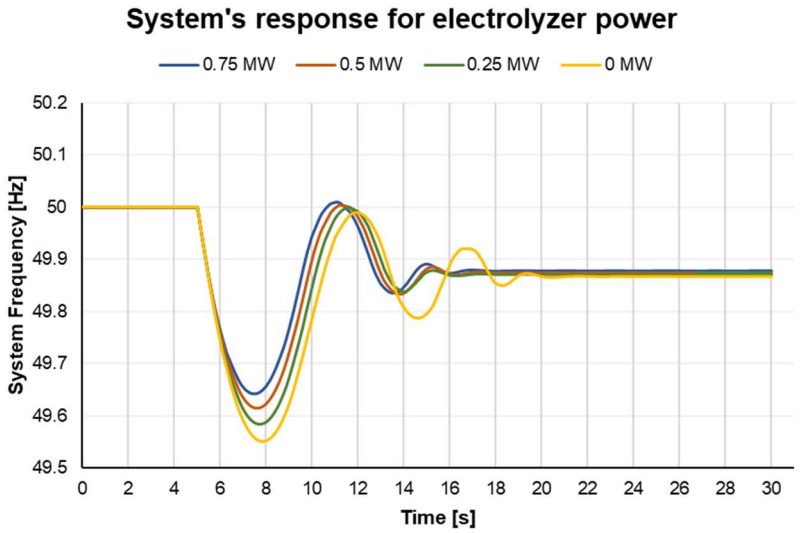

Figure 23 - Time evolution of the system's frequency after a large disturbance for multiple values of electrolyzer power.

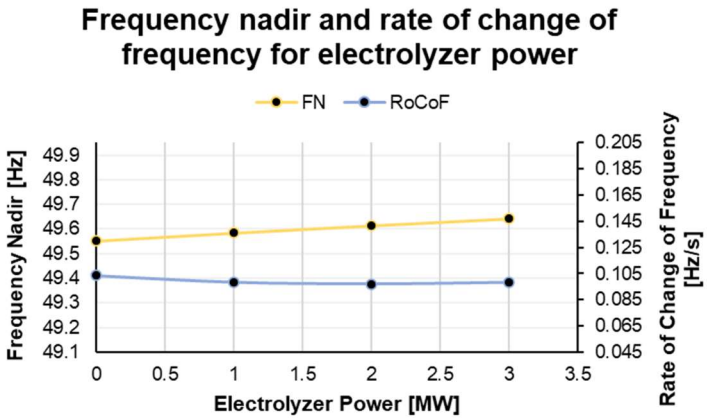

Figure 24 - Frequency nadir and frequency rate of change values for multiple values of electrolyzer power

An exemplary evolution of the electrolyzer power over time is presented in Figure 25 for an electrolyzer with approximately 1 MW maximum power and a 25 percent bid window. In this figure it can seen how the electrolyzer will lower its power demand to respond to the power imbalance. Additionally, it demonstrates this response being limited by the defined bid window, stopping the electrolyzer from going lower than 50 percent of its maximum power, and the power achieved at steady state, after the frequency is stabilized.

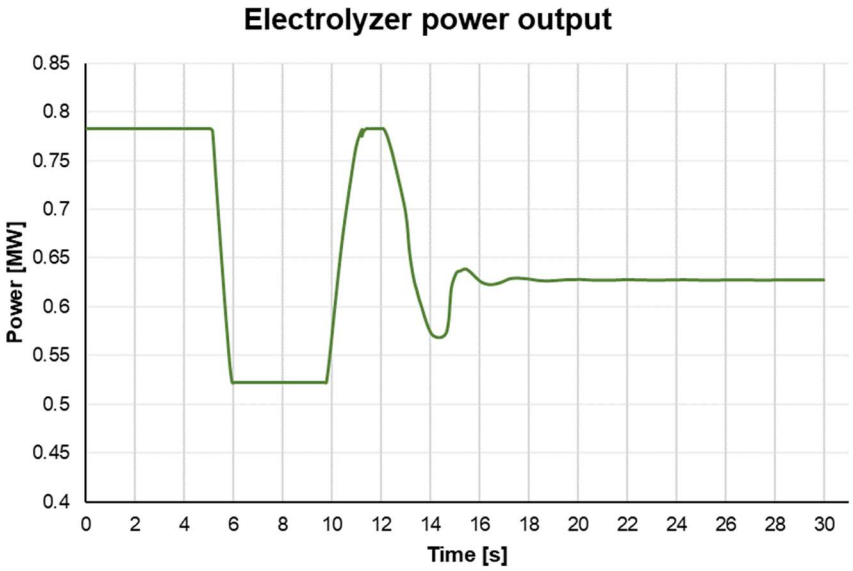

Figure 25 - Electrolyzer power output for a 25 percent bid window of a 1 MW electrolyzer, responding to a large power imbalance.

With these results an evaluation was done to determine a novel equivalence between the impact on the FN of the electrolyzer's power and the system's inertia. This was not done for the RoCoF due to the low contribution of these option for the improvement of this measurement.

Simulations across multiple values of H were performed for each of the considered electrolyzers powers. As was already demonstrated in the simulation results presented above the improvements in FN are linear in regard to the increase in electrolyzer power but not for the H.

The combination of these effects is made clear in Figure 26 which presents the FN results in function of multiple values of system inertia and electrolyzer power in FCR. From these results it is confirmed that the addition of an electrolyzer system is much more impactful to the FN at lower levels of inertia. Furthermore, it can be noted that, due to this difference in performance at various quantities of inertia, the growth of electrolyzer capacity can be considered to have a flattening effect on the impact of system inertia on FN, implying that a large enough electrolyzer system capacity dedicated to FCR could result in a system with no difference of frequency response at low or high levels of inertia constant, in terms of FN.

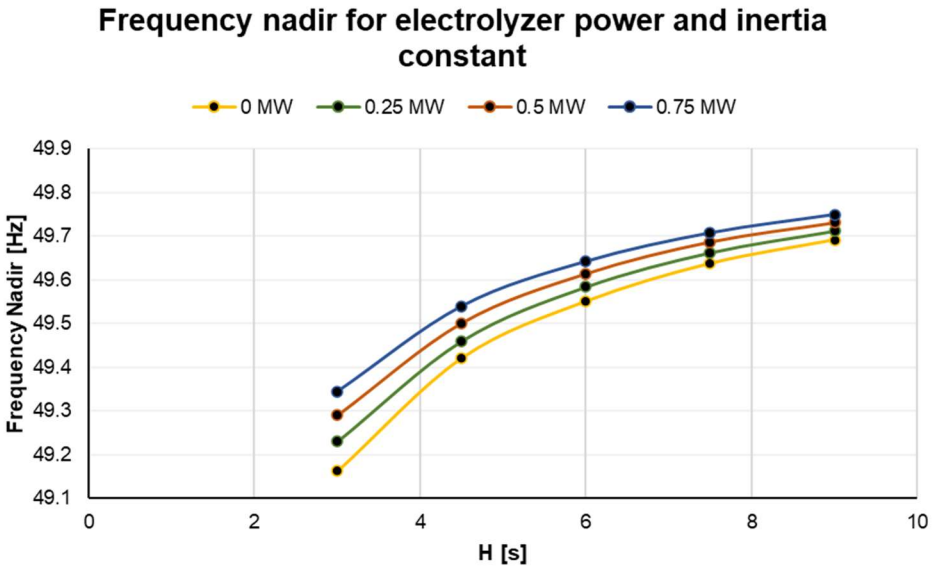

Figure 26 - Frequency nadir for multiple values of electrolyzer power and inertia constant.

These different relationships are also expressed separately in Figure 27 and Figure 28. Figure 27 presents the frequency deviation improvements caused by the inertia improvements across the different quantities of the electrolyzer power and Figure 28 presents the same from the perspective of the system's inertia with increments of the electrolyzer's power. To apply the Electrolyzer Equivalent Inertia metric, EIE, defined in Section 3.4.2, the frequency deviation is defined by equation XX, being the distance between the FN and the nominal frequency, f_0.

$$\Delta f = f_0 - FN \tag{64}$$

The changes in Δf are calculated across levels of system inertia or electrolyzer power with the use of equations 65 and 66, respectively, with Δf_H and Δf_{Pel} being the frequency deviation changes caused by an increment in inertia constant and in electrolyzer power, respectively.

$$\Delta f_H = \Delta f(H_{i+1.5}) - \Delta f(H_i) \quad i \in [3; 4.5; 7.5] \tag{65}$$

$$\Delta f_{Pel} = \Delta f(Pel_{i+0.25}) - \Delta f(Pel_i) \quad i \in [0; 0.25; 0.5] \tag{66}$$

At both figures each segment of a bar represents the improvement in frequency deviation achieved by an increase in the other parameter, with each total bar then being the improvement from one extreme to the other. In comparison with Figure 26, each section of the bar at Figure 27

is equivalent to jumping between points along a single line, and in Figure 28 it represents jumping between lines at the same inertia points.

It can be seen, as was already expressed, that in Figure 27, for each bar, its sections have different dimensions while in Figure 28 they have the same size, making explicit the difference in frequency deviation improvement between increasing inertia and increasing electrolyzer power in the FCR. Increments in inertia are more impactful for the FN at lower levels of inertia, while each increment in electrolyzer power results in a similar improvement. Likewise, these representations confirm again the statement made about the flattening of the curves in Figure 26, looking at the total size of each bar it can be seen that the improvements in inertia constant have a smaller relevance with higher levels of electrolyzer power, and similarly for the growth of electrolyzer power along the inertia levels.

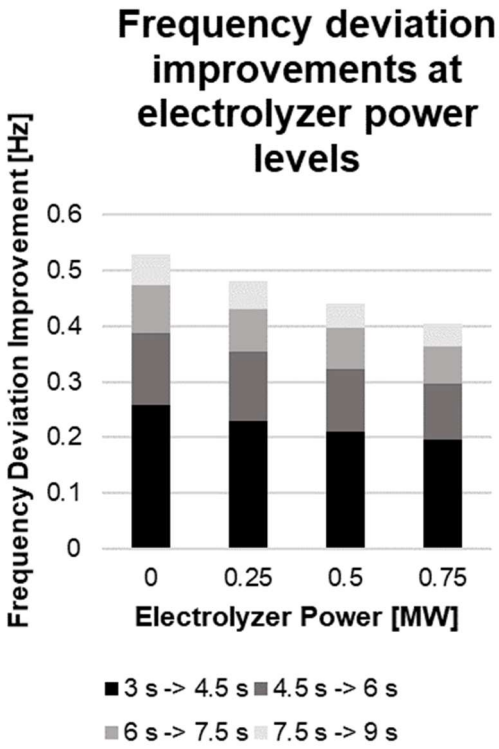

Figure 27 - Improvements in frequency deviation for increments of inertia constant across multiple values of electrolyzer power in FCR.

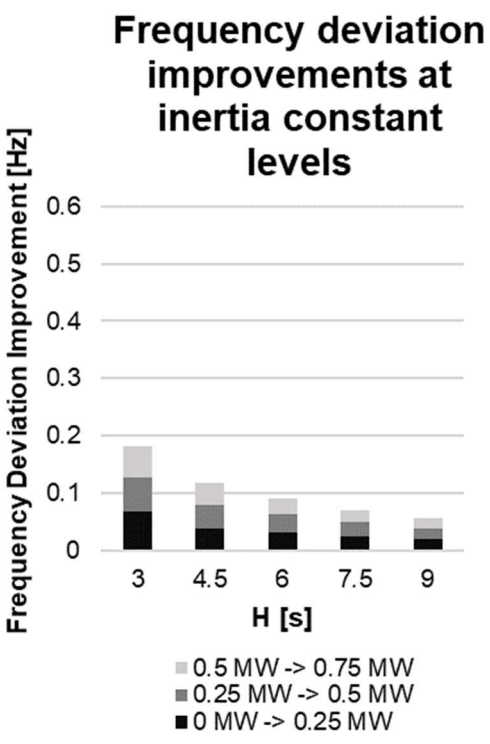

Figure 28 - Improvements in frequency deviation for increments of electrolyzer power in FCR at multiple values of inertia constant.

Due to the linearity of frequency deviation improvement with electrolyzer power the Impact of Electrolyzer Power, IEP, was considered constant across all values of electrolyzer power, but because of the large differences across inertia values, the calculation of the Impact of Inertia Constant, IIC, was separated in two ranges, one between 3 seconds and 6 seconds and the other between 6 seconds and 9 seconds. The values obtained from these indicate that an increase in 1 MW of electrolyzer will, on average, lead to an improvement in frequency deviation of 0.138 Hz, IEP, and the increase of system inertia will lead to an improvement of 0.114 Hz per second of additional inertia constant for low inertia levels and of 0.061 Hz for higher inertia levels, IIC. Using

equation 67 to determine the connection between these two measurements, referenced to as Electrolyzer Equivalent Inertia, EEI, it can be said that, in terms of its impact on frequency deviation, 1 MW of electrolyzer power in FCR is equivalent to 0.958 seconds of inertia constant at lower inertia levels and 2.262 seconds at the higher range.

$$EEI = \frac{IEP}{IIC} \tag{67}$$

The analysis until this point has shown the benefits and advantages gained by introducing electrolyzer systems to the current FCR and estimated its impact on stability through the improvement of frequency nadir. These last determined values of electrolyzer's bid equivalent inertia could be a metric used when considering the shutting down of plants with synchronous generators. The addition of electrolyzers could be a measure to counterbalance the substitution of those sources with others that do not provide inertia.

In that sense the electrolyzer systems can also be a substitute for synchronous capacity in the FCR. Figure 29 features the system's frequency response through time after a disturbance with a constant amount of FCR capacity but with different compositions. All simulations considered an FCR of 8 MW but each had a different capacity share of synchronous generators and electrolyzers. The subtitle in this figure indicates the share of electrolyzer power in the FCR. These results, as expected, are favorable for the FCR with higher shares of electrolyzer bids. The faster response of the electrolyzers leads the system's response to improvements in both FN and settling time, which are shown in detail in Figure 30.

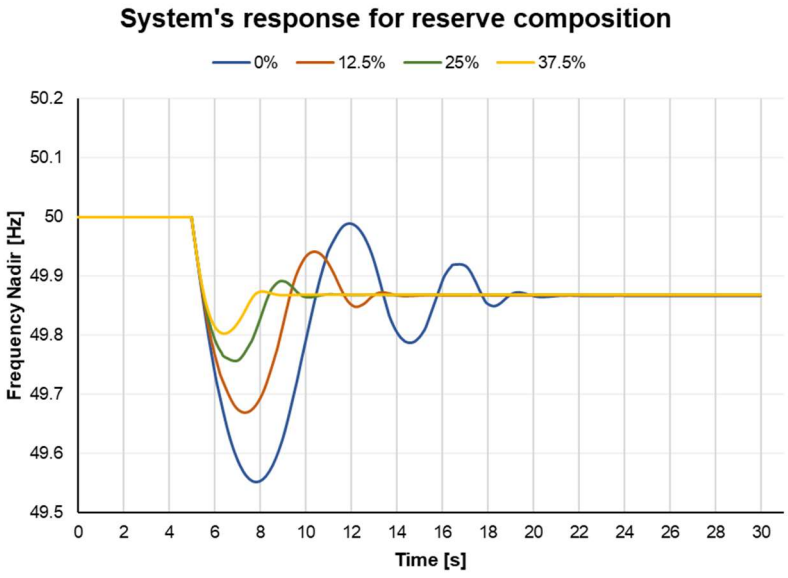

Figure 29 - System's response over time according to the share of electrolyzers' power in the FCR.

Figure 30 displays the FN and settling time improvement of the system's response according to the share of electrolyzer capacity in the FCR, for range of values presented in Figure 29, displaying the already analyzed behaviors of improvement and diminishing returns with the growth in electrolyzer capacity.

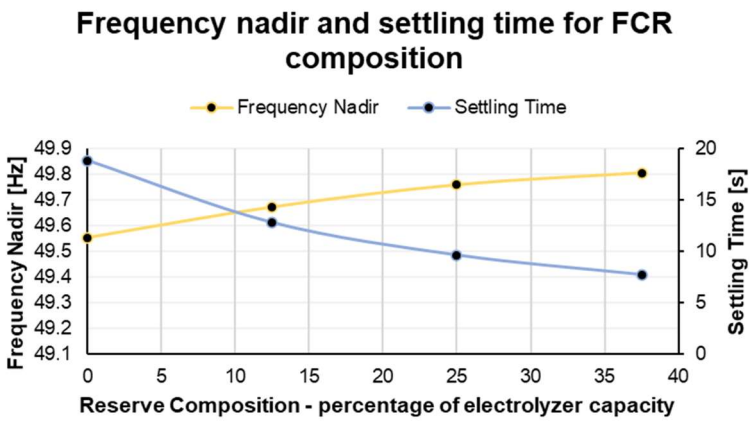

Figure 30 - Frequency nadir and settling time according to the FCR composition.

Using a similar thought process to the one used to calculate the equivalent inertia from electrolyzer's bid power, equations 68 and 69 were used to calculate the average Frequency Deviation Improvements per share of electrolyzer power in the FCR, FDI, and the Settling Time Improvements per share of electrolyzer power in FCR, STI. In these equations Δf_{ES} and ΔST represent the frequency deviation and the settling time improvements caused by an increased share of electrolyzer power in the FCR, and ΔES refers to the change in share of electrolyzer power.

$$FDI = \frac{\Delta f_{ES}}{\Delta ES} \tag{68}$$

$$STI = \frac{\Delta \mathrm{ST}}{\Delta ES} \tag{69}$$

The results show that the average improvement in frequency deviation per share of electrolyzer power in the FCR is - 0.674 Hz and the improvement in settling time is of - 29.215 seconds.

4.1.3. Fuel Cell and Electrolyzer Configuration

This configuration consists of adding fuel cells to the electrolyzer configuration. The addition of fuel cells is only considered together with the addition of electrolyzers given their need for hydrogen. By considering only the combination of these two technologies the dependency of imported hydrogen is avoided. For those reasons and due to the already displayed positive results obtained by the electrolyzer configuration, the performance of this configuration will be evaluated exclusively against that one. The functioning of the fuel cell applies a similar protocol to the electrolyzer's bid window, but while the impact of the electrolyzer is done by lowering or increasing its power demand, the fuel cell will only be used to increase its power output. In that sense the fuel cells are considered to be maintained at their minimum power, that being the minimum power inside the normal operation range, referred to as the standby power. The fuel cells cannot be turned off because of their higher start up times. Because of this the minimum power output of the fuel cell, the standby power, was set to 5 percent of its maximum power. The bid window for this technology is thus defined as the resulting 95 percent available capacity.

The simulations will cover the impact on frequency response of two possibilities, first, simply adding the fuel cells systems to the studied cases in the electrolyzer configuration, and second, substituting part of the electrolyzer capacity in the FCR with fuel cells, with the purpose of understanding, firstly, if the addition of these is beneficial and, secondly, if their share in the FCR has an impact of the system's frequency response. For these simulations the disturbance is of 5 MW, the synchronous ramp rate is set to 3 percent and the inertia constant has a value of 6 seconds.

Figure 31 presents the results of frequency response obtained by the addition of the fuel cells systems for a range of values of its bid to the FCR. From these results it can be said that adding fuel cells to the system will have a positive impact. In a similar way to the addition of electrolyzers this configuration will benefit the frequency nadir, avoiding large frequency deviations and bringing the system back to a steady state quicker.

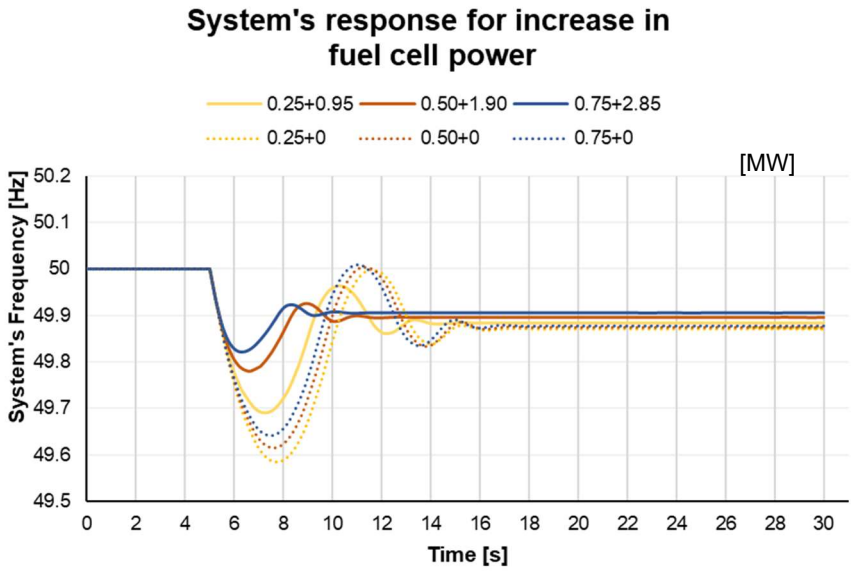

Figure 31 - System's response over time according to multiple combinations of fuel cell's and electrolyzer's powers, addition of fuel cells.

The results presented in Figure 31 show a non-linear relationship between increments in fuel cell power and the frequency nadir reached. The improved performance could be due to a benefit in the combination of electrolyzer and fuel cell systems. There could be an added benefit from their functioning from different sides of demand and supply or those results could simply be caused by the increase in FCR. The different behaviors in the response to the frequency deviation are presented in Figure 32, for a situation where both electrolyzer and fuel cell have 1 MW of maximum power. It exemplifies how the difference in bid window definition leads to the fuel cell having a larger range to respond to this deviation. Also displayed is the response to the same disturbance, in the same conditions, of the electrolyzer in the electrolyzer configuration, previously presented in Figure 25. Comparing the electrolyzer response in both configurations it can be noted how this configuration results in a modestly shorter settling time for the electrolyzer.

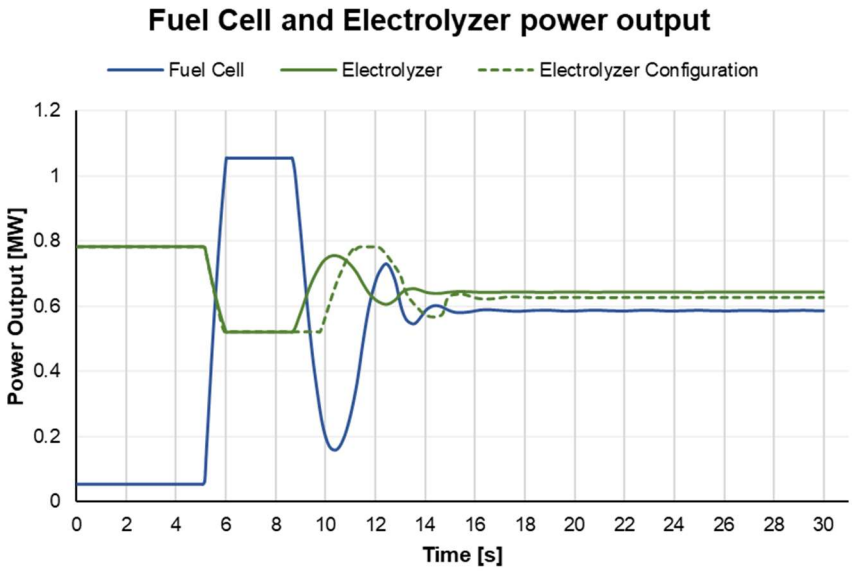

Figure 32 - Fuel cell and electrolyzer power outputs when responding to a large frequency deviation, for a 1 MW electrolyzer with a bid window of 25 percent, and a 1 MW fuel cell with a 95 percent bid window.

To better understand the impact on frequency response of the fuel cell configuration and verify if there is an added benefit to it, the simulations presented in Figure 33 were made to compare the system's frequency response when substituting part of the FCR with fuel cell capacity. Figure 33 also displays the results obtained with the electrolyzer configuration, where electrolyzers substituted part of the synchronous generators power in the FCR, precisely shown in Figure 29. As already explained, in all cases from both configurations the size of the FCR is the same, 8 MW. Each line in this figure represents a different share of electrolyzer and fuel cell power in the FCR, with the subtitles showing these shares as a sum of the electrolyzer's share and the fuel cell's share, from left to right.

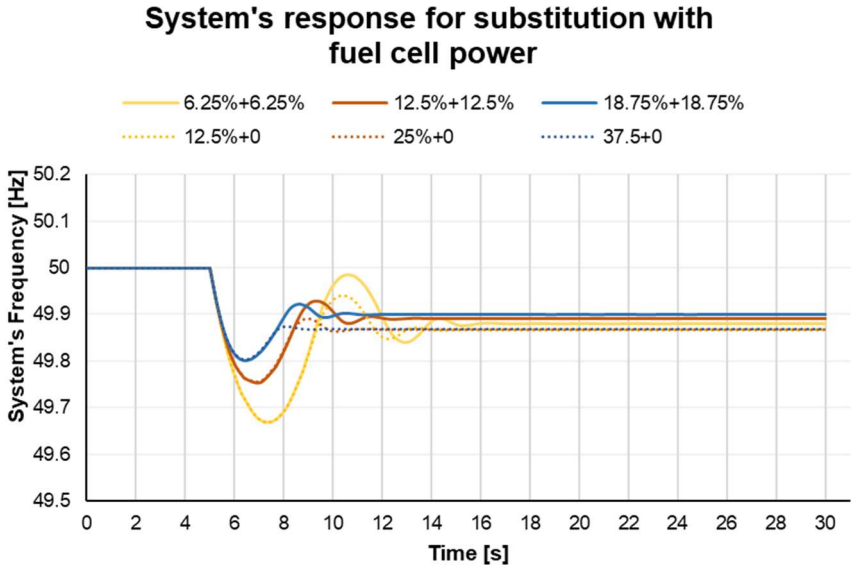

Figure 33 - System's response over time for multiple combinations of fuel cell's and electrolyzer's power to achieve equal participation in the Frequency Containment Reserve.

Comparing the results obtained between configurations no difference is noticeable in either the initial frequency response or the values of FN reached. There are however differences in the latter part of the frequency response. The fuel cell configuration seems to have more oscillations before reaching a steady state, consequently reaching it slightly later. Additionally, the addition of the fuel cell power sources led the system to stabilize at a higher frequency, which is beneficial for the stability of the system's frequency.

4.1.4. Answers

- **What is the impact of inertia on frequency stability?**

The quantity of inertia in the system, represented by the inertia constant, H, has a large effect on system frequency stability. The amount of inertia in the system is a determining factor in the size of the FN and RoCoF. From the studied elements, this was the only one considered to have an impact on the RoCoF. Additionally, for the simulated case of the Terceira Island, the benefits of increasing inertia are higher at lower levels of inertia than at higher levels.

- **Can hydrogen technologies have a considerable positive impact on frequency control?**

Simply, yes, they can. The results showed that both hydrogen technologies, electrolyzers and fuel cells, have a positive impact of the system's frequency control, expectedly due to their response times, here considered four times shorter. For the modeled case of the Terceira Island, they were noticed to decrease FN and frequency settling times. Unfortunately, the results did not show an impact on RoCoF.

- **If so, how do they compare to synchronous generators in the provision of FCR services?**

Through simulating the substitution of shares of synchronous generators in the FCR by electrolyzers and fuel cells, these demonstrated a better performance. The improvements were similar for both technologies, with the electrolyzer's impact on improving frequency deviation and settling time have been estimated to be - 0.674 Hz and -29.215 seconds, per share of electrolyzer power in the FCR.

- **Is there a way to quantify the potential benefits of hydrogen technologies on frequency control?**

A novel measurement was introduced to estimate the impact of electrolyzer power on system frequency stability. This was referred to as Electrolyzer Equivalent Inertia, EEI, representing, in terms of the FN improvements, the equivalent amount of inertia obtained from 1 MW of electrolyzer power, with values of 0.958 and 2.262 MW/s being calculated for low and high levels of inertia, respectively.

- **What is the best configuration for frequency stability?**

The electrolyzer and fuel cell configurations showed positive results for the improvement of FN and setting time after a large disturbance, showcasing how these are technologies that should be included in the FCR. While the fuel cell configuration added the benefit of a smaller frequency deviation after reaching steady state, the electrolyzer configuration might have the advantages of

more easily acting on both sides of the balancing services and producing hydrogen while doing it. The final choice between these two configurations would lie on a number of factors that are outside of the scope of this study as the economic balance of these technologies, hydrogen availability, the bid windows chosen and many others.

4.2. Simulation set 2 – steady-state imbalances

The second set of tests made, sets out to expand the scope of the frequency stability analysis from the short response to large disturbances, to the smaller power imbalances during the larger period of a day. Using load and wind speed data from specific days of the year 2012 at the Terceira Island, and the models presented in Chapter 3, simulations of the frequency evolution during a complete day were made to understand the influence of steady-state imbalances on the system's frequency and the impact of hydrogen technologies on its stability.

The method used to introduce steady-state imbalances was also presented Chapter 3, being considered as the relative difference between the load and wind power input used to create the synchronous power output forecast and that of the actual simulated day. This set will touch on the impact on frequency stability of the size of the steady-state imbalances, and on the performance of different configurations. The results between configurations will be compared to access the influence on frequency behavior. As the results from tests 1 pointed to no significant differences between the electrolyzer and the electrolyzer and fuel cell configurations, the simulations presented in this section will only consider the simple and the electrolyzer configurations. At the end of this chapter the following question should be answered:

- How do steady-state imbalances influence the frequency stability?
- Can hydrogen-based systems make a difference in responding to these smaller frequency deviations?
- What is the preferred configuration of the system for this frequency response application?

In the simulations presented the synchronous ramp rate used was of 3 percent. The system's reserve was kept, with 8 MW available, but it is considered that they were not used. Simulations were made to test the sensitivity of the frequency response results to these parameters, but no considerable differences were found, expectedly, due to the small size of imbalances. For simulations the inertia constant was set to 6 seconds.

4.2.1. Load Profiles

The loads data set contained measurements from various days along the year of 2012. It was then divided by seasons and by day of the week, having one example of a Wednesday, a Saturday and a Sunday, from May, August, October and December. The load profiles of each of theses days are present in Annex A. By looking at mean, maximum and minimum values of these load profiles the choice was to perform simulation with the profiles of a Wednesday and a Sunday from both August and December, because these were the ones with the most different load profiles, and representative of both days with large and small demands, as well as big and small load variability. The load profiles from these days are presented together in Figure 34. It can be seen

how in both seasons the weekday has a higher power demand and that in the summer days there is a larger difference in load than in the winter days.

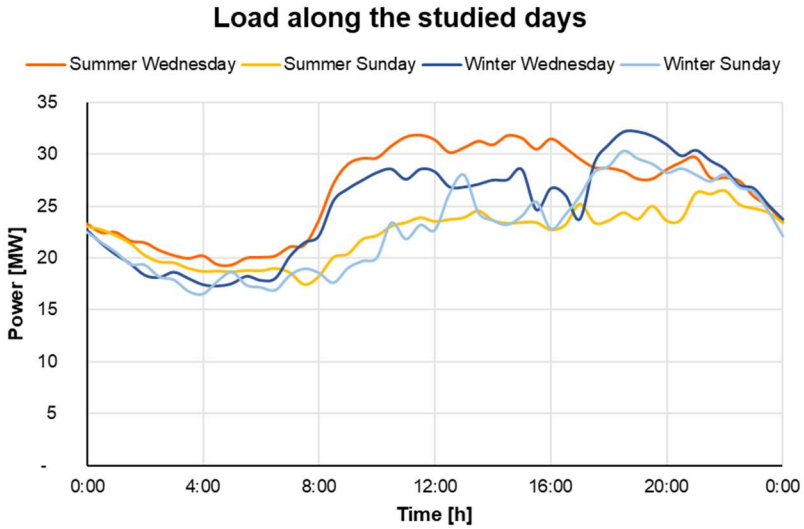

Figure 34 - Load profile of the studied days of the year 2012.

4.2.2. Steady-state imbalances

As presented in Chapter 3 the difference in load and wind power from their forecasted values, causes an imbalance of power, that, by nature, will have a considerably small size but will still lead to a frequency deviation that can escalate. Simulations were made to demonstrate the response of the system to these steady-state imbalances. Figure 35 presents the load and power profiles along the simulated Summer Wednesday, with a forecast error of 1 percent, meaning the possibility of each point of the load and wind power in the actual day being 1 percent higher or lower than its predicted value. The synchronous power at each moment is calculated by subtracting the wind power generated to the load, and during the simulation it is adjusted to accommodate the variations from the predicted values. This power adjustments by the synchronous power sources are included in the figure but not recognizable due to being comparably miniscule, smaller than 3kW.

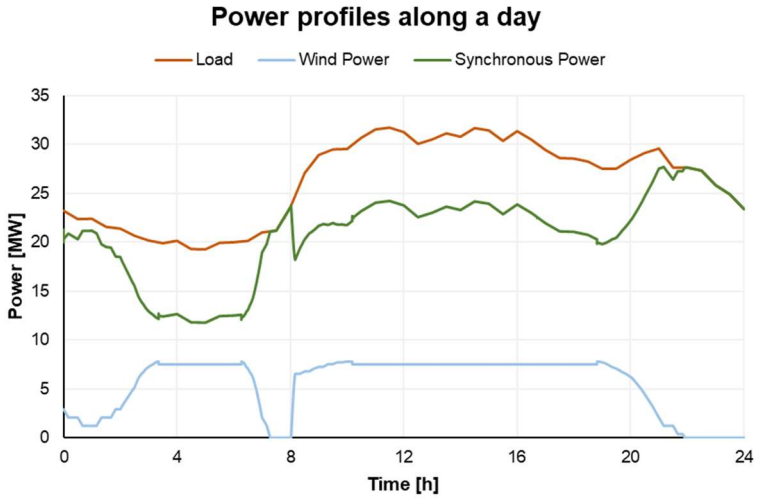

Figure 35 - Power profiles of load power demand, wind and synchronous power sources along the Summer Wednesday.

Figure 36 presents the simulated frequency along the same day. As can be seen there are certain point in the day where, due to larger changes in the wind power output, a considerably larger frequency change occurs. With the purpose of focusing the analysis on the response to the steady-state imbalances, under regular conditions, a choice was made to focus on a period of the day were there are no similar spikes. The period chosen was between 12:00 and 16:00, as presented in Figure 36. During this period, it is possible to analyze the impact on system frequency of larger steady-state imbalances and the addition of electrolyzers to the grid services.

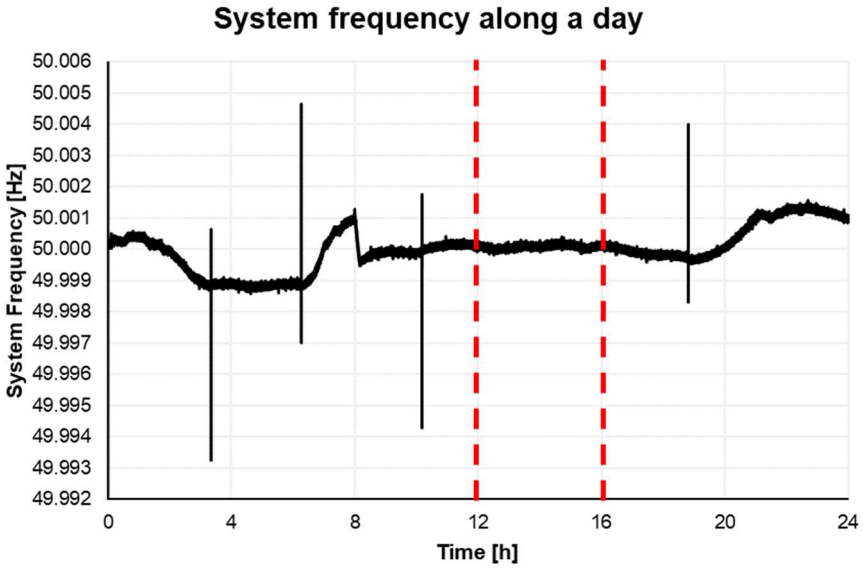

Figure 36 - System frequency along the Summer Wednesday with 1 percent steady-state imbalances.

Figure 37-40 present the frequency profiles between 12:00 and 16:00 of the Summer Wednesday for two considered steady-state imbalance values, 1 and 5 percent. The increased steady-state imbalances made it so the system's frequency had greater variations, causing the a larger band that also stepped considerably higher and lower than the nominal frequency. These results confirm how in in a scenario where load a wind power output cannot be predicted reliably, and thus there is a higher uncertainty, the system's frequency will reflect it.

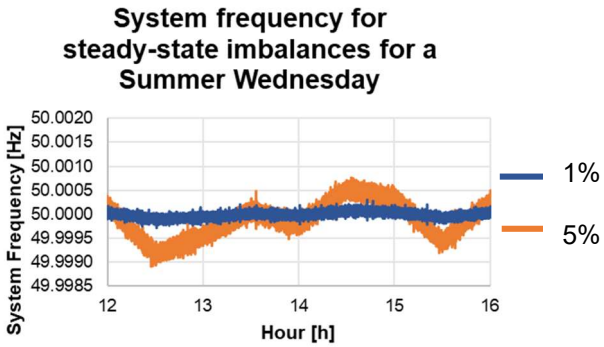

Figure 37 - System frequency for a Summer Wednesday during the 12:00 – 16:00 hour period, comparing the results with steady-state imbalances of 1 and 5 percent.

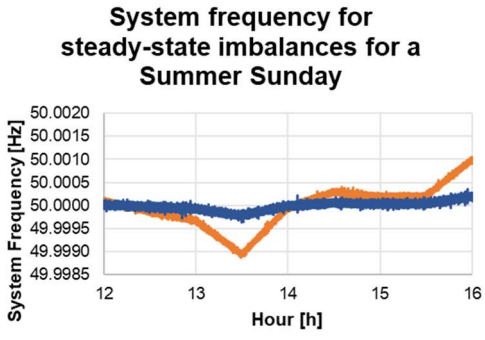

Figure 38 - System frequency for a Summer Sunday during the 12:00 – 16:00 hour period, comparing the results with steady-state imbalances of 1 and 5 percent.

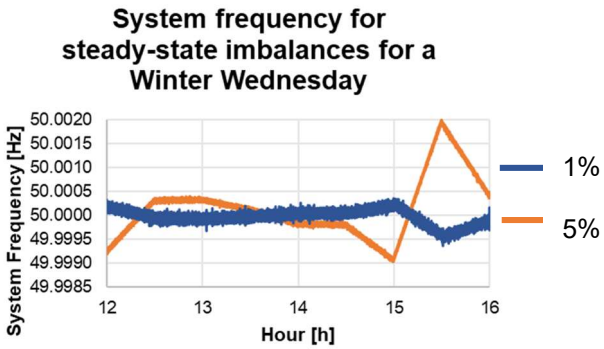

Figure 39 - System frequency for a Winter Wednesday during the 12:00 – 16:00 hour period, comparing the results with steady-state imbalances of 1 and 5 percent.

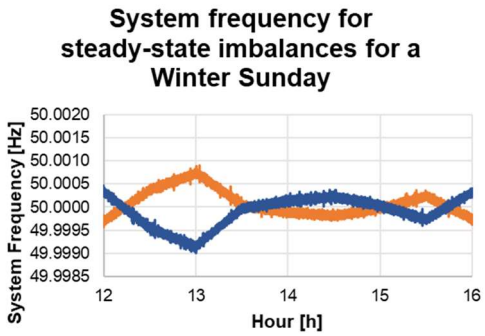

Figure 40 - System frequency for a Winter Sunday during the 12:00 – 16:00 hour period, comparing the results with steady-state imbalances of 1 and 5 percent.

4.2.3. Electrolyzer Configuration

The same window of time, 12:00 to 16:00 was maintained for the simulations performed in the hydrogen configuration, with a 1 MW hydrogen system, with a bid window of 25 percent and a deadband of 10 mHz. The simulations covered the system's frequency in each of the four selected days when the electrolyzer system is added and used to react to the steady-state imbalances, with the 1 percent value being applied. The results obtained are presented together in Figure *41*-44, with the results from the hydrogen configuration being displayed over the ones with the simple configurations. As can be seen in all the simulations presented the hydrogen configuration shows improved results in keeping the system's frequency inside a narrower interval. ´

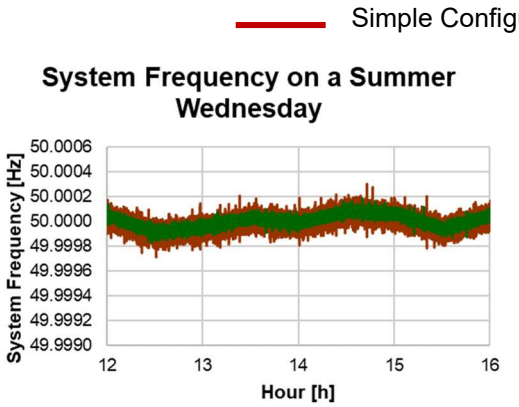

Figure 41 - System frequency for a Summer Wednesday along the 12:00-16:00 hour period for the simple and the electrolyzer configurations, for steady-state imbalances of 1 percent.

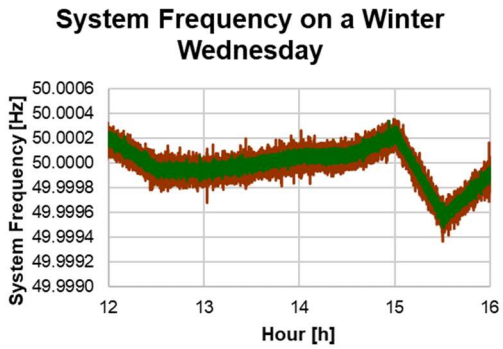

Figure 42- System frequency for a Winter Wednesday along the 12:00-16:00 hour period for the simple and the electrolyzer configurations, for steady-state imbalances of 1 percent.

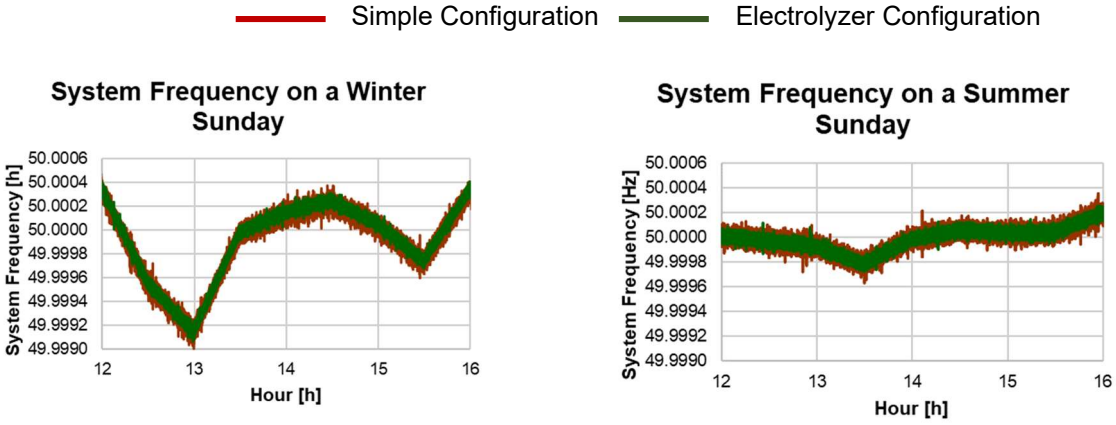

Figure 43- System frequency for a Winter Sunday along the 12:00-16:00 hour period for the simple and the electrolyzer configurations, for steady-state imbalances of 1 percent.

Figure 44- System frequency for a Summer Sunday along the 12:00-16:00 hour period for the simple and the electrolyzer configurations, for steady-state imbalances of 1 percent.

Figure 45 shows the absolute values of change in frequency deviation between the simple and the hydrogen configuration simulations presented in Figure 41-44, $FDAC$, calculated using equation 70, where f_{simple} refers to the frequency at that moment in the simple configuration, f_{el} to the equivalent but in the electrolyzer configurations and f_0 to the nominal system frequency. It is also notable how the Winter profiles have higher variations than the summer days and, in particular the Winter Sunday, showing larger differences between configurations. The mean values from these profiles are 4.37 μHz, 8.86 μHz, 38.53 μHz and 9.31 μHz, respectively for the Summer Sunday, the Summer Wednesday, the Winter Wednesday and the Winter Sunday, resulting in an average 5.73 μHz. These are very miniscule differences but the fact that all their means are positive indicates the improved frequency performance with the addition of the hydrogen configuration.

$$FDAC = |f_{simple} - f_0| - |f_{el} - f_0| \tag{70}$$

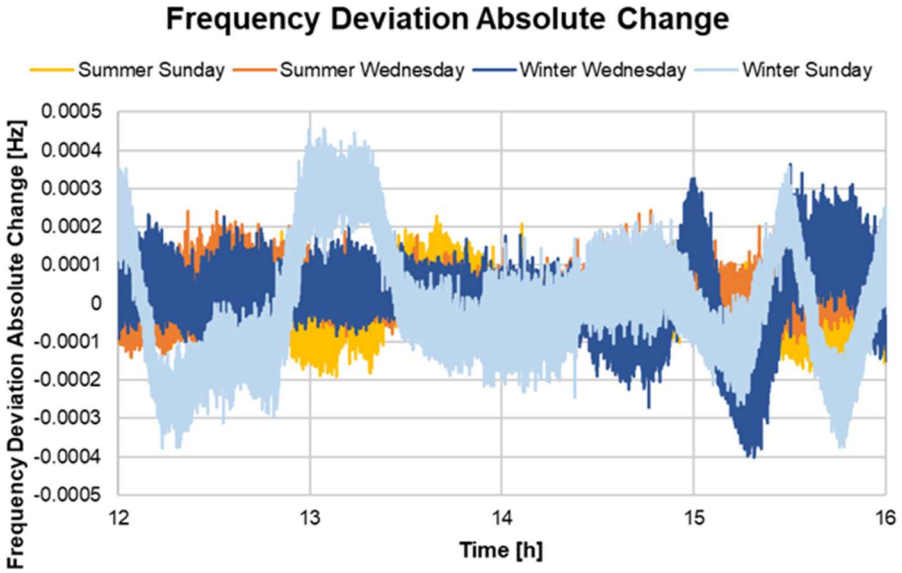

Figure 45 - Comparison of frequency deviation absolute values between the simple and the electrolyzer configurations for the studied days, calculated with equation 70.

A power profile of the electrolyzer system is presented in Figure 46, demonstrating the range of oscillations to which it is submitted. This power variations, despite small, can have a negative impact on the system's lifespan. It is then important to balance the benefits obtained from using these systems in frequency control, their longevity, and other possible purposes, as hydrogen production. This is one of the topics that must addressed when designing these systems, with the sensitivity window, defined by the set frequency dead band, being the parameter directly connected to it, limiting or expanding the filter of frequency deviations, a larger deadband for example would lead to small frequency deviation being ignored and thus resulting in less power oscillations by the electrolyzer system and in consequence an extended lifespan. On the other hand, as presented by the configurations comparison simulations, the system's frequency would not be kept inside a decreased range.

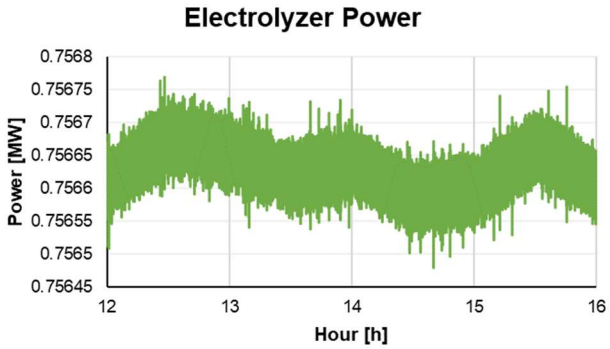

Figure 46 - Electrolyzer power profile along the simulated Summer Wednesday, for an electrolyzer of 1 MW with a 25 percent bid window, when responding to steady-state imbalances.

4.2.4. Answers

- **How do steady-state imbalances influence the frequency stability?**

This test set demonstrated how the size of steady-state imbalances can impact the systems frequency stability and by consequence the functioning of its machines. Large uncertainty will lead to larger and more frequent power imbalance that force the designated technologies to adapt their outputs. More precise forecasts can avoid frequency volatility and extend the lifespan of the system's machines.

- **Can hydrogen-based systems make a difference in responding to these smaller frequency deviations?**

The comparisons between the simple and the electrolyzer configurations showed consistent small frequency stability benefits in adding hydrogen technologies to the system of the modeled Terceira Island.

- **What is the preferred configuration of the system for this frequency response application?**

Despite the addition of hydrogen technologies being beneficial, the size of the difference is small, and thus it is important to weight the impact of the constant power changes on the lifespan of these technologies and other possibly conflicting interests. This can be designed through the adaptation of the frequency deviation deadband.

Chapter 5

Conclusions

This chapter finalises this work, summarising conclusions and pointing out aspects to be developed in future work.

In the work presented here a model of the electrical grid of the Terceira Island was developed. This model used load and wind speed data as inputs, together with developed models of synchronous generators and hydrogen-based technologies, electrolyzers and fuel cells. From there, based on the application of the equation of motion, the system's frequency behavior was simulated for situations of a large imbalances and steady-state imbalances, together with the system's response to that behavior, based on droop control mechanisms. The purpose was to understand the relevance of the system's inertia, the synchronous generator's ability to change their power output and of the size of steady-state imbalances, on the current configuration of the island. From there, additional simulations were performed with the addition of electrolyzers and fuel cell systems to measure and evaluate their impact on frequency stability.

The model used has limitations, particularly regarding the accurate evolution of power output when responding to a power imbalance, but it showed to be capable of simulating the initial systems' responses, the inertial frequency response, the frequency rates of change, the frequency nadir values and the expected settling times.

The first set of simulations, focused on the frequency containment reserve's response to large power disturbances. The frequency containment reserve is responsible for the initial response to power imbalances, acting to prevent the frequency deviations from escalating and returning the system back to a steady state. These reserves were initially only comprised of synchronous generators. The second set of simulations tackled the frequency control across a day without large disturbance but considering the presence of steady-state imbalances.

The amount of inertia in the system was shown to have an effect on both frequency nadir and the rate of change of frequency. As expected, lower levels of inertia result in larger frequency deviations and increased rates of frequency change. It was found that the variation of inertia at lower levels had a higher impact on the frequency nadir reached than at higher levels, demonstrating a non-linear relationship that points to the dangers of low inertia and the decreased benefits on increasing inertia. While changing the inertia constant between 9 seconds and 3 seconds caused the frequency nadir to be lowered by 0.529 Hz, 73 percent of that change occurred in the interval from 3 seconds to 6 seconds. This is an important revelation as it confirms the urgency to avoid low levels of inertia but also highlights how past a certain point the return received from increasing inertia diminishes. The rate of change of frequency was also greatly affected by the system's inertia, linearly decreasing 0.156 Hz/s between the inertia values of 3 seconds to 9 seconds. The system's inertia was the only parameter that had an influence on the initial rate of change of frequency.

The synchronous generator's ability to change power output quickly was also a topic covered, through their power ramp rate, with simulations being made for two levels, 3 and 5 percent of the synchronous total capacity, with the results showing large differences in frequency nadirs and settling times but not on rate of change of frequency, underlining the interest in correct estimation of this parameter and the ways of impacting the frequency's rate of change are limited.

The main focus of the study was to analyse the potential impact of hydrogen-based technologies on system frequency stability of cases similar to the Terceira Island.

For simulations set 1, simulations were made to compare the system's frequency behavior between configurations. The electrolyzer and fuel cell configurations showed considerable positive impacts on the frequency nadir, with a linear nature. By analysing the improvements in frequency deviation caused by both the growth of system inertia at multiple levels of electrolyzer power and vice-versa, a novel metric was presented to compare the frequency deviation results obtained through the growth of electrolyzer power and the increase of system inertia, it was called Electrolyzer Equivalent Inertia. This new metric indicates the amount of inertia that would be necessary to obtain the same benefits of a certain amount of electrolyzer power and it had the values of 0.958 s/MW for levels of inertia between 3 seconds and 6 seconds, and 2.262 s/MW for higher levels, between 6 seconds and 9 seconds. With the positive results obtained for the presence of these hydrogen-base systems, the hypothesis of substituting part of the frequency containment reserve was introduced. Assumed to initially only be comprised of synchronous generators, the frequency containment reserve benefited with the increasing shares of synchronous power being substituted by equal amounts of hydrogen-based power, with an improvement of -0.674Hz being estimated for each share of electrolyzer power in the frequency containment reserve. Additionally, the electrolyzer and fuel cell configurations showed identical results, leaving the choice between these configurations to be made according to additional factors.

Simulations set 2 expanded the time span studied, focusing on the frequency behavior along one entire day, and studied the influence steady-state imbalances caused by load and wind power forecasting errors, simulating the increase in uncertainty. Using data from four days of the year 2012, with distinct load profiles, no large differences in the system's frequency behavior were notices between those days. Performing simulations for two values of steady-state imbalances it could be seen how these have a negative impact of the system's frequency stability. The increase of the size of steady-state imbalances resulted in larger frequency deviations and a much more erratic frequency profile. The addition of electrolyzer systems proved to have a positive impact on the frequency profile of all the studied days. The power profile of the electrolyzer brought up the question of balancing the frequency stability benefits with the electrolyzers lifespan and other potential objectives. To avoid frequent unwanted ramping up and down of the electrolyzer but still benefit from its presence in the FCR, an appropriate deadband must be set.

With the work presented the initial research questions were answered

- What are the impacts on system frequency stability of system inertia, and power load and supply uncertainty?

System inertia is a fundamental element to be studied in the electric system. The level of inertia in the system is highly connected to the size of frequency deviations and the rate of change of frequency. While the rate of change of frequency varies linearly with the inertia constant, the size of frequency deviations is much more pronounced at lower levels of inertia constant values, for the case of the Terceira Island.

An increase in supply and load uncertainty showed a frequency profile with much more pronounced and frequent deviations, additionally it led to an increase in demand of ramping up and down of the machines involved in the frequency response, which can have damaging effects.

- Can hydrogen technologies provide benefits to the frequency stability? If so, how can we measure them?

The addition and even the substitution of part of the frequency containment reserves with hydrogen-based power, showed positive results to both the response to large imbalances and the handling of steady-state imbalances, for the case of the Terceira Island. The simulations performed reflected those benefits and allowed the development of new measures to easily estimate the frequency control benefits achieved by the presence of hydrogen technologies. The most relevant being the Electrolyzer System Inertia, but also the frequency deviation improvements on frequency nadir according to the share of hydrogen-based power on the frequency containment reserves.

5.1. Further steps

Following the work presented here, there are possible steps to progress the topics discussed. While the technical side of this analysis has been studied multiple times, other parallel spheres have yet to be extensively explored, as the economic benefits for the hydrogen technology provider of providing grid services, the mechanisms that can be developed to make their introduction more feasible, as well as the environmental impacts of the substitution of synchronous carbon-based power sources in the frequency containment reserves with hydrogen-based alternatives. Another direction of research is to clearly define, from the perspective of the hydrogen technologies, what are the potential benefits of each competing application, as, for example, the production of hydrogen, the storage of curtailed renewable energy and the provision of grid services.

Annexe A

Load profiles of exemplary 2012 days

Figures of all the load data points available.

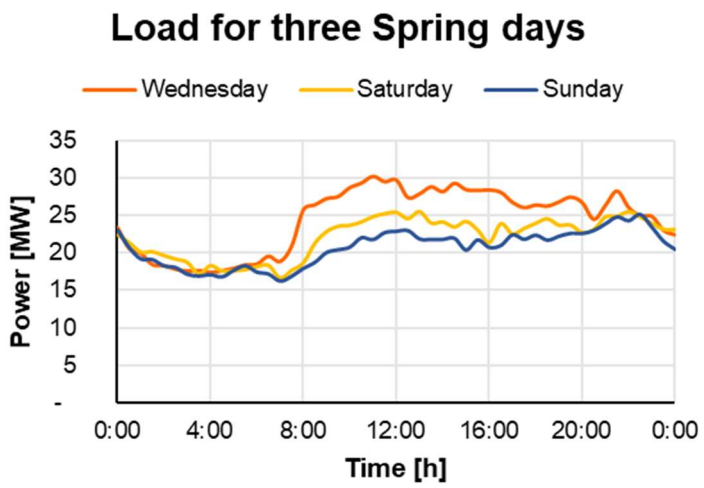

Annexe A.Figure 47 - Terceira's load of three Spring days in 2012

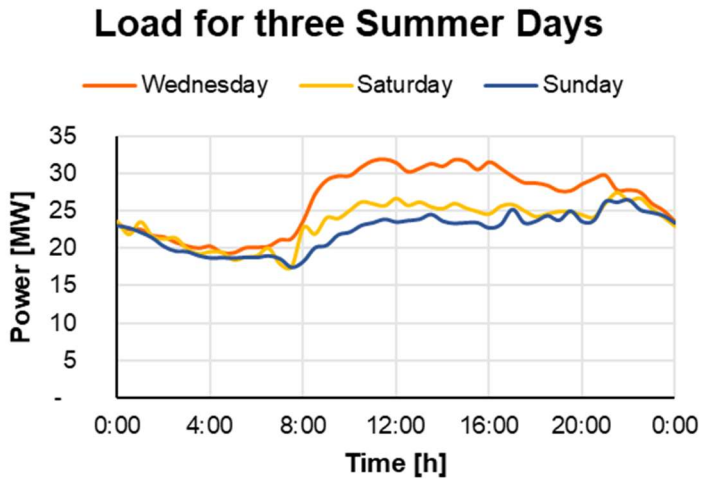

Annexe A.Figure 48 - Terceira's load of three Summer days in 2012

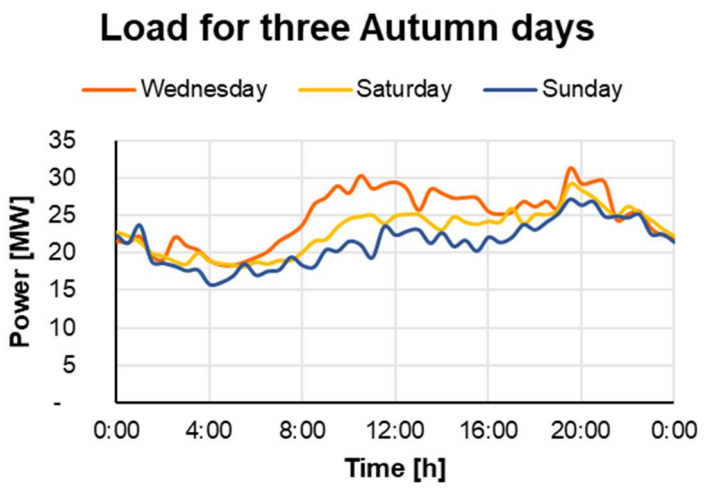

Annexe A.Figure 49 - Terceira's load of three Autumn days in 2012

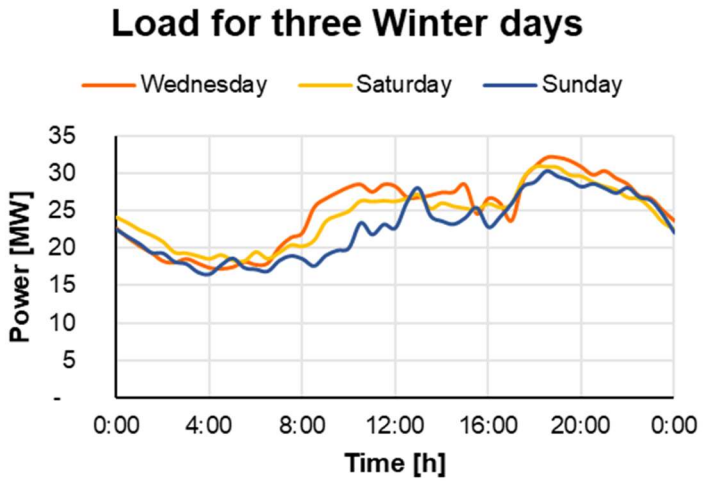

Annexe A.Figure 50 - Terceira's load of three Winter days in 2012

References

[1] Carreiro, A. M., Oliveira e Silva, G., Vasconcelos, J. V., (2020). Estratégia Açoriana para a Energia 2030, Diração Regional da Energia - Governo Regional dos Açores.

[2] J. Widén *et al.*, “Variability assessment and forecasting of renewables: A review for solar, wind, wave and tidal resources,” *Renewable and Sustainable Energy Reviews*, vol. 44. Elsevier Ltd, pp. 356–375, Apr. 01, 2015, doi: 10.1016/j.rser.2014.12.019.

[3] S. Simoes, J. Seixas, P. Fortes, L. Dias, J. Gouveia, and B. Mauricio, “The Medium to Long-Term Role of Renewable Energy Sources in Climate Change Mitigation in Portugal,” in *Proceedings of the World Renewable Energy Congress – Sweden, 8–13 May, 2011, Linköping, Sweden*, Nov. 2011, vol. 57, pp. 724–731, doi: 10.3384/ecp11057724.

[4] N. Bañol Arias, S. Hashemi, P. B. Andersen, C. Træholt, and R. Romero, “Assessment of economic benefits for EV owners participating in the primary frequency regulation markets,” *Int. J. Electr. Power Energy Syst.*, vol. 120, p. 105985, Sep. 2020, doi: 10.1016/J.IJEPES.2020.105985.

[5] I. Staffell and S. Pfenninger, “The increasing impact of weather on electricity supply and demand,” *Energy*, vol. 145, pp. 65–78, Feb. 2018, doi: 10.1016/j.energy.2017.12.051.

[6] K. Veum and D. Bauknecht, “How to reach the EU renewables target by 2030? An analysis of the governance framework,” *Energy Policy*, vol. 127, pp. 299–307, Apr. 2019, doi: 10.1016/J.ENPOL.2018.12.013.

[7] L. V. Villamor, V. Avagyan, and H. Chalmers, “Opportunities for reducing curtailment of wind energy in the future electricity systems: Insights from modelling analysis of Great Britain,” *Energy*, vol. 195, p. 116777, Mar. 2020, doi: 10.1016/J.ENERGY.2019.116777.

[8] S. Strunz, P. Lehmann, and E. Gawel, “Analyzing the ambitions of renewable energy policy in the EU and its Member States,” *Energy Policy*, vol. 156, p. 112447, Sep. 2021, doi: 10.1016/J.ENPOL.2021.112447.

[9] M. Joos and I. Staffell, “Short-term integration costs of variable renewable energy: Wind curtailment and balancing in Britain and Germany,” *Renew. Sustain. Energy Rev.*, vol. 86, pp. 45–65, Apr. 2018, doi: 10.1016/J.RSER.2018.01.009.

[10] P. Makolo, R. Zamora, and T. T. Lie, “The role of inertia for grid flexibility under high penetration of variable renewables - A review of challenges and solutions,” *Renew. Sustain. Energy Rev.*, vol. 147, p. 111223, Sep. 2021, doi: 10.1016/J.RSER.2021.111223.

[11] M. Koller, T. Borsche, A. Ulbig, and G. Andersson, “Review of grid applications with the Zurich 1 MW battery energy storage system,” *Electr. Power Syst. Res.*, vol. 120, pp. 128–135, Mar. 2015, doi: 10.1016/j.epsr.2014.06.023.

[12] C. Chen, Y. Lu, and L. Xing, “Levelling renewable power output using hydrogen-based storage systems: A techno-economic analysis,” *J. Energy Storage*, vol. 37, p. 102413, May 2021, doi: 10.1016/J.EST.2021.102413.

[13] A. A. Solomon, D. M. Kammen, and D. Callaway, “Investigating the impact of wind-solar complementarities on energy storage requirement and the corresponding supply reliability criteria,” *Appl. Energy*, vol. 168, pp. 130–145, Apr. 2016, doi: 10.1016/j.apenergy.2016.01.070.

[14] A. Daniela and P. Ejnar, *E Rapport 2016*. 2016.

[15] S. Homan, N. Mac Dowell, and S. Brown, “Grid frequency volatility in future low inertia scenarios: Challenges and mitigation options,” *Appl. Energy*, vol. 290, no. September 2020, p. 116723, May 2021, doi: 10.1016/j.apenergy.2021.116723.

[16] F. Alshehri, V. G. Suárez, J. L. Rueda Torres, A. Perilla, and M. A. M. M. van der Meijden, “Modelling and evaluation of PEM hydrogen technologies for frequency ancillary services in future multi-energy sustainable power systems,” *Heliyon*, vol. 5, no. 4, 2019, doi: 10.1016/j.heliyon.2019.e01396.

[17] H. Bevrani, H. Golpîra, A. R. Messina, N. Hatziargyriou, F. Milano, and T. Ise, “Power system frequency control: An updated review of current solutions and new challenges,” *Electr. Power Syst. Res.*, vol. 194, p. 107114, May 2021, doi: 10.1016/j.epsr.2021.107114.

[18] A. Ulbig, T. S. Borsche, and G. Andersson, “Impact of low rotational inertia on power system stability and operation,” *IFAC Proc. Vol.*, vol. 19, pp. 7290–7297, 2014.

[19] R. Eriksson, N. Modig, and K. Elkington, “Synthetic inertia versus fast frequency response: A definition,” in *IET Renewable Power Generation*, Apr. 2018, vol. 12, no. 5, pp. 507–514, doi: 10.1049/iet-rpg.2017.0370.

[20] P. Tielens and D. Van Hertem, “The relevance of inertia in power systems,” *Renew. Sustain. Energy Rev.*, vol. 55, pp. 999–1009, Mar. 2016, doi: 10.1016/J.RSER.2015.11.016.

[21] J. Morren, S. W. H. De Haan, and J. A. Ferreira, “Primary power/frequency control with wind turbines and fuel cells,” *2006 IEEE Power Eng. Soc. Gen. Meet. PES*, pp. 1–8, 2006, doi: 10.1109/pes.2006.1709074.

[22] E. Lobato Miguélez, I. Egido Cortés, L. Rouco Rodríguez, and G. López Camino, “An overview of ancillary services in Spain,” *Electric Power Systems Research*, vol. 78, no. 3. Elsevier, pp. 515–523, Mar. 01, 2008, doi: 10.1016/j.epsr.2007.03.009.

[23] F. Alshehri, “Ancillary services from Hydrogen Based Technologies to Support Power System Frequency Stability.”

[24] M. J. Brear, “Thoughts on the Prospects of Renewable Hydrogen,” *Engineering*, vol. 6, no. 12, pp. 1343–1345, 2020, doi: 10.1016/j.eng.2020.09.008.

[25] P. G. Hartley and V. Au, “Towards a Large-Scale Hydrogen Industry for Australia,” *Engineering*, vol. 6, no. 12, pp. 1346–1348, Dec. 2020, doi: 10.1016/j.eng.2020.05.024.

[26] R. Bhandari, C. A. Trudewind, and P. Zapp, “Life cycle assessment of hydrogen production via electrolysis - A review,” *J. Clean. Prod.*, vol. 85, pp. 151–163, 2014, doi: 10.1016/j.jclepro.2013.07.048.

[27] M. Shaygan, M. A. Ehyaei, A. Ahmadi, M. E. H. Assad, and J. L. Silveira, “Energy, exergy, advanced exergy and economic analyses of hybrid polymer electrolyte membrane (PEM) fuel cell and photovoltaic cells to produce hydrogen and electricity,” *J. Clean. Prod.*, vol. 234, pp. 1082–1093, Oct. 2019, doi: 10.1016/j.jclepro.2019.06.298.

[28] P. Nikolaidis and A. Poullikkas, “A comparative overview of hydrogen production processes,” *Renewable and Sustainable Energy Reviews*, vol. 67. Elsevier Ltd, pp. 597–611, Jan. 01, 2017, doi: 10.1016/j.rser.2016.09.044.

[29] M. El-Shafie, S. Kambara, and Y. Hayakawa, “Hydrogen Production Technologies Overview,” *J. Power Energy Eng.*, vol. 07, no. 01, pp. 107–154, 2019, doi: 10.4236/jpee.2019.71007.

[30] J. Chi and H. Yu, “Water electrolysis based on renewable energy for hydrogen production,” *Cuihua Xuebao/Chinese Journal of Catalysis*, vol. 39, no. 3. Science Press, pp. 390–394, Mar. 01, 2018, doi: 10.1016/S1872-2067(17)62949-8.

[31] O. Schmidt, A. Gambhir, I. Staffell, A. Hawkes, J. Nelson, and S. Few, “ScienceDirect Future cost and performance of water electrolysis : An expert elicitation study,” *Int. J. Hydrogen Energy*, vol. 42, no. 52, pp. 30470–30492, 2017, doi: 10.1016/j.ijhydene.2017.10.045.

[32] D. Akinyele, E. Olabode, and A. Amole, “Review of fuel cell technologies and applications for sustainable microgrid systems,” *Inventions*, vol. 5, no. 3, pp. 1–35, 2020, doi: 10.3390/inventions5030042.

[33] R. Madurai Elavarasan, S. Leoponraj, A. Dheeraj, M. Irfan, G. Gangaram Sundar, and G. K. Mahesh, “PV-Diesel-Hydrogen fuel cell based grid connected configurations for an institutional building using BWM framework and cost optimization algorithm,” *Sustain. Energy Technol. Assessments*, vol. 43, no. November 2020, p. 100934, 2021, doi: 10.1016/j.seta.2020.100934.

[34] M. Virji, G. Randolf, M. Ewan, and R. Rocheleau, “Analyses of hydrogen energy system as a grid management tool for the Hawaiian Isles,” *Int. J. Hydrogen Energy*, vol. 45, no. 15, pp. 8052–8066, 2020, doi: 10.1016/j.ijhydene.2020.01.070.

[35] M. İnci and Ö. Türksoy, “Review of fuel cells to grid interface: Configurations, technical challenges and trends,” *J. Clean. Prod.*, vol. 213, pp. 1353–1370, 2019, doi: 10.1016/j.jclepro.2018.12.281.

[36] P. Daly, D. Flynn, and N. Cunniffe, “Inertia considerations within unit commitment and economic dispatch for systems with high non-synchronous penetrations,” *2015 IEEE Eindhoven PowerTech, PowerTech 2015*, 2015, doi: 10.1109/PTC.2015.7232567.

[37] B. Guinot, F. Montignac, B. Champel, and D. Vannucci, “Profitability of an electrolysis based hydrogen production plant providing grid balancing services,” *Int. J. Hydrogen Energy*, vol. 40, no. 29, pp. 8778–8787, Aug. 2015, doi: 10.1016/J.IJHYDENE.2015.05.033.

[38] G. Matute, J. M. Yusta, and L. C. Correas, “Techno-economic modelling of water electrolysers in the range of several MW to provide grid services while generating hydrogen for different applications: A case study in Spain applied to mobility with FCEVs,” *Int. J. Hydrogen Energy*, vol. 44, no. 33, pp. 17431–17442, Jul. 2019, doi: 10.1016/j.ijhydene.2019.05.092.

[39] D. S. Falcão and A. M. F. R. Pinto, “A review on PEM electrolyzer modelling: Guidelines for beginners,” *Journal of Cleaner Production*, vol. 261. Elsevier Ltd, p. 121184, Jul. 10, 2020, doi: 10.1016/j.jclepro.2020.121184.

[40] H. W. Wu, “A review of recent development: Transport and performance modeling of PEM fuel cells,” *Applied Energy*, vol. 165. Elsevier Ltd, pp. 81–106, Mar. 01, 2016, doi: 10.1016/j.apenergy.2015.12.075.

[41] T. E. Springer, T. A. Zawodzinski, and S. Gottesfeld, “Polymer Electrolyte Fuel Cell Model,” *J. Electrochem. Soc.*, vol. 138, no. 8, pp. 2334–2342, Aug. 1991, doi: 10.1149/1.2085971.

[42] A. Rowe and X. Li, “Mathematical modeling of proton exchange membrane fuel cells,” *J. Power Sources*, vol. 102, no. 1–2, pp. 82–96, Dec. 2001, doi: 10.1016/S0378-7753(01)00798-4.

[43] M. Blal, A. Benatiallah, A. NeÇaibia, S. Lachtar, N. Sahouane, and A. Belasri, “Contribution and investigation to compare models parameters of (PEMFC), comprehensives review of fuel cell models and their degradation,” *Energy*, vol. 168, pp. 182–199, Feb. 2019, doi: 10.1016/j.energy.2018.11.095.

[44] V. Liso, G. Savoia, S. S. Araya, G. Cinti, and S. K. Kær, “Modelling and experimental analysis of a polymer electrolyte membrane water electrolysis cell at different operating temperatures,” *Energies*, vol. 11, no. 12, p. 3273, Dec. 2018, doi: 10.3390/en11123273.

[45] D. Guilbert, “Experimental Validation of an Equivalent Dynamic Electrical Model for a Proton Exchange Membrane Electrolyzer,” pp. 7–12, 2018.

[46] Z. Abdin, C. J. Webb, and E. M. Gray, “Modelling and simulation of a proton exchange membrane (PEM) electrolyser cell,” *Int. J. Hydrogen Energy*, vol. 40, no. 39, pp. 13243–13257, Oct. 2015, doi: 10.1016/j.ijhydene.2015.07.129.

[47] Á. Hernández-Gómez, V. Ramirez, and D. Guilbert, “Investigation of PEM electrolyzer modeling: Electrical domain, efficiency, and specific energy consumption,” *International Journal of Hydrogen Energy*, vol. 45, no. 29. Elsevier Ltd, pp. 14625–14639, May 26, 2020, doi: 10.1016/j.ijhydene.2020.03.195.

[48] A. Heydari, M. Majidi Nezhad, E. Pirshayan, D. Astiaso Garcia, F. Keynia, and L. De Santoli, “Short-term electricity price and load forecasting in isolated power grids based on composite neural network and gravitational search optimization algorithm,” *Appl. Energy*, vol. 277, p. 115503, Nov. 2020, doi: 10.1016/J.APENERGY.2020.115503.

[49] J. Xiao, Y. Jia, B. Jia, Z. Li, Y. Pan, and Y. Wang, “An inertial droop control based on comparisons between virtual synchronous generator and droop control in inverter-based distributed generators,” *Energy Reports*, vol. 6, pp. 104–112, Dec. 2020, doi: 10.1016/j.egyr.2020.12.003.

[50] Z. Abdin, C. J. Webb, and E. M. A. Gray, “PEM fuel cell model and simulation in Matlab–Simulink based on physical parameters,” *Energy*, vol. 116, pp. 1131–1144, Dec. 2016, doi: 10.1016/j.energy.2016.10.033.

[51] R. García-Valverde, N. Espinosa, and A. Urbina, “Simple PEM water electrolyser model and experimental validation,” in *International Journal of Hydrogen Energy*, Jan. 2012, vol. 37, no. 2, pp. 1927–1938, doi: 10.1016/j.ijhydene.2011.09.027.

[52] A. Ulbig, T. S. Borsche, and G. Andersson, “Analyzing Rotational Inertia, Grid Topology and their Role for Power System Stability,” *IFAC-PapersOnLine*, vol. 48, no. 30, pp. 541–547, Jan. 2015, doi: 10.1016/j.ifacol.2015.12.436.

[53] B. C. Ummels, “Power System Operation with Large-Scale Wind Power in Liberalised Environments,” pp. 1–193, 2009.

[54] Y. Cheng, R. Azizipanah-Abarghooee, S. Azizi, L. Ding, and V. Terzija, “Smart frequency control in low inertia energy systems based on frequency response techniques: A review,” *Appl. Energy*,

vol. 279, p. 115798, Dec. 2020, doi: 10.1016/j.apenergy.2020.115798.

[55] https://ec.europa.eu/clima/policies/strategies/2030_en#tab-0-0.

[56] IEA (2020), Tracking Power 2020, IEA, Paris https://www.iea.org/reports/tracking-power-2020.

[57] IEA (2019), Renewables 2019, IEA, Paris https://www.iea.org/reports/renewables-2019

[58] IEA (2020), Renewable Power, IEA, Paris https://www.iea.org/reports/renewable-power

[59] Energy Live News, June 2021, https://tinyurl.com/krswvpdm

[60] P. Kundur *et al.*, "Definition and classification of power system stability," *IEEE Trans. Power Syst.*, vol. 19, no. 3, pp. 1387–1401, Aug. 2004, doi: 10.1109/TPWRS.2004.825981.

[61] Ministry of Environment and Climate Action, National Strategy for Hydrogen, 2020, May, Portuguese Republic.

[62] Federal Ministry of Economy and Energy, National Hydrogen Strategy, 2019, June, German Federal Government.

[63] J. Milewski, J. Kupecki, A. Szczęśniak, and N. Uzunow, "Hydrogen production in solid oxide electrolyzers coupled with nuclear reactors," *Int. J. Hydrogen Energy*, vol. 46, no. 72, pp. 35765–35776, Oct. 2021, doi: 10.1016/J.IJHYDENE.2020.11.217..

[64] SOLCAST, May 2021, https://solcast.com/

[65] Wind Turbine Models, May 2021, https://en.wind-turbine-models.com/turbines/531-enercon-e-44

[66] Guzzi, F., 2016, Development of a modelling and planning tool for renewable microgrids: The case study of Terceira Island, Master Thesis, Instituto Superior Técnico, Lisbon

[67] EDA, Produção de Energia Elétrica (POEE) 2012, May 2021, https://www.eda.pt/Mediateca/Publicacoes/Producao/Paginas/Produ%C3%A7%C3%A3o-de-Energia-El%C3%A9trica.aspx

[68] EDA, EDA informa - julho a dezembro 2017, nº164, https://www.eda.pt/Mediateca/Publicacoes/Lists/EDAINFORMA/Attachments/157/EDA_INFORMA_164_JUL_DEZ%202017.pdf